THE FUNDAMENTAL INTERACTIONS BETWEEN DEPOSITS AND SURFACES AT NANOSCALE USING ATOMIC FORCE MICROSCOPY.

by

NOREEN RAZAQ AKHTAR

A thesis submitted to

The University of Birmingham

for the degree of

DOCTOR OF PHILOSOPHY

School of Chemical Engineering

University of Birmingham

June 2010

ABSTRACT

The objective of this research was to investigate adhesion of different fouling deposits with different contact surfaces using atomic force microscopy (AFM). In this thesis, AFM has been employed to measure:

(i) The adhesive interactions between a colloidal silica microparticle and stainless steel, PTFE-coated stainless steel, glass and ceramic surfaces, in the presence of a number of solutions and suspensions of ingredients found in commercially available toothpaste.

(ii) To compare the measurements from the AFM and micromanipulation to see the differences and similarities. The micromanipulation technique was developed to measure the adhesive strength of different deposits. The method uses a T-shaped probe made of stainless steel chip, dimension 30 x 6 x 1 mm connected to the output aperture of a transducer (Model BG-1000, Kulite Semiconductor, Leonia, NJ. USA) which was itself mounted on a three dimensional micromanipulator (MicroInstruments, Oxon, UK). The two measurement methods are capable of giving quantitative results for the strength of the forces involved in adhesion; fast moving consumer goods (FMCG) deposits, toothpaste and confectionary stimulant deposits have been studied, and their interactions with stainless steel, glass and PTFE surfaces measured.

(iii) Further investigation of AFM adhesion measurements, with caramel, whey protein and sweet condensed milk (SCM) deposits after heating at 30ºC, 50ºC, 70ºC, and 90ºC. The two selected spherical microparticles used were stainless steel and PTFE, which were attached to the end of an AFM tip.

The data shows that, for removal in all cases using micromanipulation, the pulling energy increases with increasing height above the surface and the slope of the lines of pulling energy versus thickness is similar. Stainless steel shows the highest pulling energy with slightly higher energies than glass and PTFE, whilst PTFE show the lowest interaction. For the AFM data, PTFE again gives much lower adhesion forces. This is due to the different molecular interactions between different surfaces and caramel. There is thus partial agreement between the two methods. The micromanipulation method measures a range of parameters – such as the deformation and flow of the deposits, and so it might not be expected that there would be complete agreement. Here stainless steel and glass show very similar behaviour, as opposed to the differences seen using AFM; the different surface roughness of the two materials might also be expected to have an effect.

At different temperatures the results from the different contact positions on the deposits; with an approach speed to the deposits for all experiments was 3µm/s, then a 5 second pause on the deposit and then the rate of retract was 0.25µm/s. Significant (more than an order of magnitude) differences are seen between forces for the same and different deposits, and between different surfaces for the same deposits. Lower forces are seen at 90ºC in all cases; at the higher temperature, the force between surface and deposit is less. To design systems to resist fouling, these results suggest that measurements at different process temperatures are needed; data at room temperature has overpredicted the interactions.

The results suggest that the AFM force curve measurement technique could be used to study a variety of food deposits that have undergone different processing conditions. The method can help in optimising removal of food deposits in terms of food cleaning protocols. AFM

could be a valuable technique in measuring surface properties, and in relating behaviour to surfaces.

The capability of the AFM to provide better understanding of materials structure, surface characteristics and the interactive forces at the meso- and nanoscale level. The AFM will enhance the understanding of large-scale engineering processes, especially as materials are increasingly being designed down to the submicrometre level.

Presented in conference:

EFFoST/EHEDG Joint conference 2007, Practical application of research results 14-16 November 2007, Lisbon, Portugal. Investigating the fundamental interactions between industrially relevant materials and the ingredients of toothpaste using atomic force microscopy. N.R. Akhtar, J.Bowen, P.J.Fryer, university of Birmingham.

ACKNOWLEDGEMENTS

I would like to take this opportunity to express my gratitude to the University of Birmingham and the School of Chemical Engineering in completing my thesis.

A massive thank you to Professor Peter Jonathan Fryer and Dr. Milla Shah, for their encouragement, support and personal guidance.

A special thanks to Dr. James Bowen and Dr. Konstantia Asteriodiou for their stimulating suggestions and help during the PhD.

The financial support of the Zeal project is gratefully acknowledged. Thank to the Zeal project group for all their help, support, interest and valuable hints.

I would also like to thank all students, researchers, and academics who have given me so much support and motivation throughout the duration of this project.

I would like to thank my Husband, Nassar Hussain, my parents, and all of our family.

I couldn't have done it without you…….

TABLE OF CONTENTS

LIST OF FIGURES

Figure 4-1: AFM topographic scans of the four surfaces (100µm by 100µm Scan). The ceramic and stainless steel are rougher than PTFE and glass. This is seen by the imperfections in the images.

Figure 4-2: SEM images of the microstructure of the four surfaces of interest at 50µm scan size. Ceramic and stainless steel show increased roughness compared to PTFE and glass.

Figure 4-3: Goniometer used for contact angle experiments.

Figure 4-4 (a): Contact angles on the four surfaces with water and sorbitol, repeated least five times.

Figure 4-4 (b): Surface energies of sorbitol and water on the four surfaces, calculated from Young's equation.

Figure 4-5: Images of water drops on the four surfaces, showing typical contact angles:

Figure 4-5 (a): Water drop on ceramic

Figure 4-5 (b): Water drop on glass

Figure 4-5 (c): Water drop on PTFE

Figure 4-5 (d): Water drop on stainless steel

Figure 4-6: AFM force plots.

Figure 4-6 (a): Example of a retract plot recorded in Zinc citrate solution in the presence of a glass surface using an AFM cantilever modified with a SiO_2 microparticle. Zero is no deflection.

Figure 4-6 (b): Example of retract plot recorded during water in the presence of a stainless steel surface using an AFM cantilever modified with a SiO_2 microparticle. This is a typical ''hydrophobic effect'' curve.

Figure 4-6(c): Example of retract plot recorded in sorbitol solution in the presence of a stainless steel surface using an AFM cantilever modified with a SiO_2 microparticle.

Figure 4-6(d): Example of retract plot recorded in sorbitol solution in the presence of PTFE surface using an AFM cantilever modified with a SiO_2 microparticle.

Figure 4-6(e): Example of retract plot recorded in water in the presence of PTFE surface using an AFM cantilever modified with a SiO_2 microparticle.

Figure 4-7 (a): Example of retract plot recorded in saccharin solution in the presence of a ceramic surface using an AFM cantilever modified with a SiO_2 microparticle. (Velocity of 2000 nm s^{-1}).

Figure 4-7 (c): Example of retract plot recorded during saccharin solution in the presence of a ceramic surface using an AFM cantilever modified with a SiO_2 microparticle. (Velocity of 14000 nm s^{-1}).

Figure 5-1: Removal of toothpaste from stainless steel using the micromanipulation rig, at a cut height of 20 µm. On the left is a stainless steel disc fully covered with toothpaste. The middle is partially removed toothpaste. On the right is the surface after passage of the probe. The probe was moved at 1.1 mm/s over a displacement of 1.5 mm.

Figure 5.2-1: Interaction between stainless steel microparticles and caramel, measured using the AFM. Data shows local variation of 5 points at each of the 5 regions on the caramel deposit; error bar shows the equipment error per measurement.

Figure 5.2-2: AFM force measurements of Stainless steel, glass and PTFE microparticles immersed in caramel (spread out between 50µm to 60µm thick on a glass slide) and then retracted. Data shows results from five different contact positions on the caramel deposit. Error bars represent the global variation of the mean of five experiments. The approach speed for all experiments was 3µm/s, and then a 5 second pause on deposit and 0.25µm/s retract.

Figure 5-3: AFM force measurements of Stainless steel, glass and PTFE microparticles were immersed in SCM and then retracted off the deposit. SCM was spread out between 50µm to 60µm thick on a glass slide. The approach speed for all experiments was 3µm/s, and then a 5 second pause on deposit and 0.25µm/s retract. Data shows the mean of five experiments at each of five.

Figure 5-4: AFM force measurements of Stainless steel, glass and PTFE microparticles were immersed in Turkish delight and then retracted off the deposit. Turkish delight was spread out between 50µm to 60µm thick on a glass slide. The approach speed for all experiments was 3µm/s, and then a 5 second pause on deposit and 0.25µm/s retract. Data shows the mean of five experiments at each of five different contact positions on the Turkish delight deposit.

Figure 5-5: AFM force measurements of Stainless steel, glass and PTFE microparticles were immersed in Toothpaste and then retracted off the deposit. Toothpaste was spread out between 50µm to 60µm thick on a glass slide. The approach speed for all experiments was 3µm/s, and then a 5 second pause on deposit and 0.25µm/s retract. Data shows the mean of five experiments at each of five different contact positions on the Toothpaste deposit.

Figure 5-6: Summary of the forces measured by AFM for the different microparticles and all four deposits.

Figure 5-7: Pulling energy for removal of caramel deposit using the micromanipulation probe. The gap between probe and substrate was kept at 20, 100, 200, 300 and 400µm, the surfaces used were stainless steel, glass and PTFE.

Figure 5-8: Pulling energy for removal of SCM deposit using the micromanipulation probe. The gap between probe and substrate was kept at 20, 100, 200, 300 and 400µm, the surfaces used were stainless steel, glass and PTFE.

Figure 5-9: Pulling energy for removal of Turkish delight deposit using the micromanipulation probe. The gap between probe and substrate was kept at 20, 100, 200, 300 and 400µm, the surfaces used were stainless steel, glass and PTFE.

Figure 5.-10: Pulling energy for removal of Toothpaste deposit using the micromanipulation probe. The gap between probe and substrate was kept at 20, 100, 200, 300 and 400 µm, the surfaces used were stainless steel, glass and PTFE.

Figure 5-11: Summary of Micromanipulation experiments at 20µm thickness of caramel, SCM, Turkish delight and toothpaste on glass, stainless steel and PTFE.

Figure 6-1: The Nanowizard II (JPK) adapted with a heating stage (JPK).

Figures 6.2.1: Force measurements of Stainless steel microparticle immersed in caramel and then retracted off the deposit. Caramel was spread out between 50µm to 60µm thick on a glass slide, then the caramel was heated for 5 minutes at each temperature and the temperature was monitored and controlled at required temperature. Data shows results from five different contact positions on the caramel deposit. The approach speed for all experiments was 3µm/s, then a 5 second pause on deposit and rate of retract was 0.25µm/s. The data shows variation of the mean of the five experiments. (The error bars show the average of five experiments)

Figure 6-2-2: Force measurements of Stainless steel microparticle immersed in caramel and then retracted off the deposit, at variable rates. The deposit was spread out between 50µm to 60µm thick on a glass slide, then the caramel was heated for 5 minutes at each temperature and the temperature was monitored and controlled at the required temperature. The retract speed for all experiments was 0.25, 0.75, 1.00, 1.5, 3 and 5µm/s. The tip was held on the deposit for 5 seconds before retraction.

Figure 6-2-3: Force measurements of Stainless steel microparticle immersed in caramel and then retracted off the deposit, at variable times on caramel. The deposit was spread out between 50µm to 60µm thick on a glass slide, then the caramel was heated for 5 minutes at each temperature and the temperature was monitored and controlled at the required temperature. The waiting times on the deposits for the experiments were 0, 0.5, 1.0, 5.0 and 10 seconds. The approach speed for all experiments was 3µm/s and a rate of retract was 0.25µm/s.

Figure 6-3-1: Force measurements of PTFE microparticle immersed in caramel and then retracted off the deposit. Caramel was spread out between 50µm to 60µm thick on a glass slide, then the caramel was heated for 5 minutes at each temperature and the temperature was monitored and controlled at required temperature. Data shows results from five different contact positions on the caramel deposit. The approach speed for all experiments was 3µm/s, then a 5 second pause

on deposit and rate of retract was 0.25µm/s. The data shows a global variation of the mean of the five experiments.

Figure 6-3-2: Force measurements of PTFE microparticle immersed in caramel and then retracted off the deposit, at variable rates on caramel. The deposit was spread out between 50µm to 60µm thick on a glass slide, then the caramel was heated for 5 minutes at each temperature and the temperature was monitored and controlled at the required temperature. The retract speed for all experiments was 0.25, 0.75, 1.00, 1.5, 3 and 5µm/s. The tip was held on deposit for 5 seconds.

Figure 6-3-3: Force measurements of PTFE microparticle immersed in caramel and then retracted off the deposit, at variable times on caramel. The deposit was spread out between 50µm to 60µm thick on a glass slide, then the caramel was heated for 5 minutes at each temperature and the temperature was monitored and controlled at the required temperature. The waiting times on the deposits for the experiments were 0, 0.5, 1.0, 5.0 and 10 seconds. The approach speed for all experiments was 3µm/s and a rate of retract was 0.25µm/s.

Figure 6-4-1: Force measurements of stainless steel microparticle immersed in SCM and then retracted off the deposit. SCM was spread out between 50µm to 60µm thick on a glass slide, then the SCM was heated for 5 minutes at each temperature and the temperature was monitored and controlled at required temperature. Data shows results from five different contact positions on the SCM deposit. The approach speed for all experiments was 3µm/s, then a 5 second pause on deposit and rate of retract was 0.25µm/s. The data shows a global variation of the mean of the five experiments.

Figure 6-4-2: Force measurements of stainless steel microparticle immersed in SCM and then retracted off the deposit, at variable rates on SCM. The deposit was spread out between 50µm to 60µm thick on a glass slide, then the SCM was heated for 5 minutes at each temperature and the temperature was monitored and controlled at the required temperature. The retract speed for al experiments was 0.25, 0.75, 1.00, 1.5, 3 and 5µm/s. The tip was held on deposit for 5 seconds.

Figure 6-4-3: Force measurements of stainless steel microparticle immersed in SCM and then retracted off the deposit, at variable times on SCM. The deposit was spread out between 50µm to 60µm thick on a glass slide, then the SCM was heated for 5 minutes at each temperature and the temperature was monitored and controlled at the required temperature. The waiting times on the deposits for the experiments were 0, 0.5, 1.0, 5.0, 10 and 60 seconds. The approach speed for all experiments was 3µm/s and a rate of retract was 0.25µm/s.

Figure 6-5-1: Force measurements of PTFE microparticle immersed in SCM and then retracted off the deposit. SCM was spread out between 50µm to 60µm thick on a glass slide, then the SCM was heated for 5 minutes at each temperature and the temperature was monitored and controlled at required temperature. Data shows results from five different contact positions on the SCM deposit. The approach speed for all experiments was 3µm/s, then a 5 second pause on deposit and rate of retract was 0.25µm/s. The data shows a global variation of the mean of the five experiments.

Figure 6-5-2: Force measurements of PTFE microparticle immersed in SCM and then retracted off the deposit, at variable rates on SCM. The deposit was spread out between 50µm to 60µm thick o a glass slide, then the SCM was heated for 5 minutes at each temperature and the temperature was monitored and controlled at the required temperature. .

Figure 6-5-3: Force measurements of PTFE microparticle immersed in SCM and then retracted off the deposit, at variable times on SCM. The deposit was spread out between 50µm to 60µm thick on a glass slide, then the SCM was heated for 5 minutes at each temperature and the temperature was monitored and controlled at the required temperature. The waiting times on the deposits for the experiments were 0, 0.5, 1.0, 5.0, 10, 20 and 60 seconds. The approach speed for all experiments was 3µm/s and a rate of retract was 0.25µm/s.

Figure 6-6-1: Force measurements of stainless steel microparticle immersed in whey protein and then retracted off the deposit. Whey protein was spread out between 50µm to 60µm thick on a slide, then the whey protein was heated for 5 minutes at each temperature and the temperature was monitored and controlled at required temperature. Data shows results from five different contact positions on the whey protein deposit. The approach speed for all experiments was 3µm/s, then a 5 second pause on deposit and rate of retract was 0.25µm/s. The data shows a global variation of the mean of the five experiments.

Figure 6-6-2: Force measurements of stainless steel microparticle immersed in whey protein and then retracted off the deposit, at variable rates on whey protein. The deposit was spread out 50µm to 60µm thick on a glass slide, then the whey protein was heated for 5 minutes at each temperature and the temperature was monitored and controlled at the required temperature. The retract speed for all experiments was 0.25, 0.75, 1.00, 1.5, 3 and 5µm/s. The tip was held on deposit for 5 seconds.

Figure 6-6-3: Force measurements of stainless steel microparticle immersed in whey protein and then retracted off the deposit, at variable times on whey protein. The deposit was spread out between 50µm to 60µm thick on a glass slide, then the whey protein was heated for 5 minutes

at each temperature and the temperature was monitored and controlled at the required temperature.

Figure 6-7-1: Force measurements of PTFE microparticle immersed in whey protein and then retracted off the deposit. Whey protein was spread out between 50µm to 60µm thick on a glass slide, then the whey protein was heated for 5 minutes at each temperature and the temperature was monitored and controlled at required temperature. Data shows results from five different contact positions on the whey protein deposit. The approach speed for all experiments was 3µm/s, then a 5 second pause on deposit and rate of retract was 0.25µm/s. The data shows a global variation of the mean of the five experiments.

Figure 6-7-2: Force measurements of PTFE microparticle immersed in whey protein and then retracted off the deposit, at variable rates on whey protein. The deposit was spread out between 50µm to 60µm thick on a glass slide, then the whey protein was heated for 5 minutes at each temperature and the temperature was monitored and controlled at the required temperature. The retract speed for all experiments was 0.25, 0.75, 1.00, 1.5, 3 and 5µm/s. The tip was held on deposit for 5 seconds.

Figure 6-7-3: Force measurements of PTFE microparticle immersed in whey protein and then retracted off the deposit, at variable times on whey protein. The deposit was spread out between 50µm to 60µm thick on a glass slide, then the whey protein was heated for 5 minutes at each temperature and the temperature was monitored and controlled at the required temperature. The waiting times on the deposits for the experiments were 0, 0.5, 1.0, 5.0, 10, 20 and 60 seconds.

Figure 6-7-4: Summary of Log force measurements of stainless steel and PTFE microparticle immersed in caramel, SCM and whey protein. Data shows results from different contact positions on the deposits. The approach speed for all experiments was 3µm/s, then a 5 second pause on deposit and rate of retract was 0.25µm/s at 30ºC and 90°C.

LIST OF TABLES

NOMENCLATURE

Abbreviations

AFM	Atomic Force Microscopy
AES	Auger electron spectroscopy
CVD	Chemical vapour deposition
CIP	Cleaning in practice
DLC	Diamond- like carbon
EELS	High-resolution electron energy-loss spectroscopy
EDS	Energy-dispersive X-ray
FMCG	Fast moving consumer goods
FT Raman	Fourier transformation Raman spectroscopy
LSM	Light microscopy
HRTEM	High- resolution transmission electron microscopy
LEED	Low-energy electron diffraction
Ni-P-PTFE	Nickel-Phosphorous-Polytetrafluoroethylene
PTFE	Polytetrafluoroethylene
RMS	Root Mean
SCM	Sweet condensed milk
STM	Scanning tunnelling microscopy
TEM	Transmission Electron Microscopy
UV/Vis	UV-Visible spectroscopy
VASE	Variable angle spectroscopic ellipsometry
WPC	Whey Protein Concentrate
XPS	X-ray photoelectron spectroscopy
XRD	X-ray diffraction
F/R	Force/radius
Hookes law, F= -kz	F is the force k is the stiffness of the lever z is the distance the lever bent

Symbols:

β-l_g	β-lactoglobulin
R_q	Known as the root mean square
R_a	Mean roughness
R_z	Standard deviation of the z height value
R_a	Roughness parameter
χ	Deposit initial thickness
θ	Contact angle
λ	Thermal conductivity
ν	Velocity
τ	Surface shear stress
γ	Surface free energy

CHAPTER 1: INTRODUCTION

Much work has been done in order to reduce the formation of fouling deposits. In food production, it is often not possible to change product ingredients and process conditions to reduce fouling. As a result, recent works by Wilson, *et al.* [2006], Müller-Steinhagen, *et al.* [2005] and Watkinson, *et al.* [2003 have focussed on effective cleaning methods].

To understand any cleaning process, it is imperative to determine how soil deposits are removed from process surfaces. Additionally it is necessary to measure the forces required to remove these soils and their sensitivity to process variables such as temperature and flow velocity, this could help to reduce effluent and energy used in cleaning. This data could then be used as a basis for modelling and control of industrial cleaning processes.

Cleaning of fast moving consumer goods (FMCG) in the food industry is still poorly understood. This chapter outlines how fouling research has benefited from the use of a simplified classification of mechanisms. Parallel classifications for cleaning problems have been proposed; one based on soil type and the other focused on cleaning mechanism. The aim of the classification is firstly to allow results from different cleaning problems to be compared and secondly to aid in the development of solutions that can be effectively transferred to the food industry.

A set of deposits have been selected that are representative of different types of industrial cleaning problems. These deposits: toothpaste, caramel, Turkish delight, sweet condensed milk and whey protein, are then studied in the rest of the thesis.

1.1.1 Fouling problems.

Cleaning is required to remove deposit layers which are known as fouling and which form on the surface of industrial plants by deposition of material from the surrounding fluids during production. The issue of fouling problems have been known since the first heat exchangers were used until about 1920, empirical methods were devised to overcome the problem of fouling, during this period scientific knowledge of the mechanisms involved was limited [Somerscales, *et al.* 1988]. Many researchers have since used a scientific approach to study fouling such as Somerscales, *et al.* [1988], Changani, *et al.* [1997] and Verran, *et al.* [2002]. Fouling mechanisms have been identified and are described below:

- *Reaction fouling:* where the fouling deposit results from the reaction of some component of the fluid. This occurs in areas as diverse as milk and protein denaturation, (see Changani, *et al.* [1997]) and petroleum engineering (see Yun-ren Qiu, *et al.* [2009]).
- *Biological fouling*: this can occur across several length scales, from the adhesion of single organisms to the growth of biofilms (see Verran, *et al.* [2002]; Boulangé-Petermann, *et al*. [2006]).
- *Crystallisation or precipitation fouling:* here some component of the fluid is deposited when its solubility limit is exceeded, such as calcium carbonate from boiling water or

calcium phosphate (whose solubility decreases with increasing temperature). A special case of this is described in Helalizadeh *et al.* [2000].

- *Particulate fouling:* the adhesion of particles which are transferred from the bulk onto the surface, such as the deposition of magnetite particles from cooling water, dust from air, or protein aggregates onto surfaces (see Simmons, *et al.* [2007]).
- *Corrosion fouling:* fouling resulting from the corrosion of the surface. This can be in situ, from the surface itself, or ex situ, via deposition of corrosion products formed elsewhere (although this occurs via a particulate fouling mechanism).

These are the main types, but another type can be found, especially in processing of highly viscous food and personal care products, *Solidification fouling:* the solidification of the fluid or components of the fluid onto the surface (Sharma, *et al.* [1982]; Fernandez-Torres, *et al.* [2001]), for example solidification of ice from water, starch from a food fluid, or, as in personal care product processing, deposition of waxes in cosmetics.

1.1.2 Fouling Mechanisms

The processes of fouling can be further classified as a 5x5 matrix, Epstein [1983] in that fouling from the five mechanisms involves 5 stages;

(i) *Initiation:* there may be some time before significant fouling starts, usually felt to be due to some surface conditioning process,

(ii) *Transport* of fouling species to the surface,

(iii) *Attachment* of fouling material,

(iv) *Removal* – the fouling process is often modelled as a balance between deposition and removal and,

(v) *Ageing;* in which the native deposit changes in structure and properties, for example the browning and hardening of food deposits. This is the most difficult step to predict and model;

It is also clear that repeated exposure to fouling and cleaning cycles changes the surface and its fouling/cleaning properties [Jullien, *et al.* 2008].

1.1.3 Definition of Cleaning.

Cleaning can be described as the removal of unwanted deposits to return a system to its original state after fouling occurs. The cleaning requirement of a system depends on the process. Different classifications for the extent of cleaning are possible, outlined below:

- *physically*: no physical measurement of the deposit is possible;
- *chemically*: absence of substances that may interfere with product processing;
- *biologically* (or sterile): free of microorganisms.

Fast moving consumer goods (FMCG) industries clean using a process called 'cleaning-in-place' (CIP). Here, an automated system provides a set of programs to rinse and recirculate cleaning solutions through the equipment.

CIP regimes generally involve a number of cycles (Adnan Tamime, [2008]):

- *pre-rinse*- circulation of water to remove loosely bound substances from the surface and bulk,
- *detergent cycle*- action of the cleaning chemical (typically acid or alkali) to release the deposit from the surface. The resulting components are held in solution and removed

with the fluid flow. The majority of cleaning takes place during this cycle, and sometimes a recycle,

- *post rinse*- all traces of deposit and cleaning chemical are removed from the system by circulation of water,
- *sanitization*- using disinfection and surface conditioning,
- *final rinse*- circulation of water prior to product processing. This could also been done at a different temperature to give sterility.

CIP still requires development to increase efficiency: if it were possible to increase the time between cleaning regimes or decrease CIP cycle time this would in effect increase production times. Different chemicals are circulated to remove deposits; alternatively surfaces can be subjected to sprays or jets of the cleaning chemicals. These processes have become highly developed and automated, but are rarely fully optimised. Cleaning regimes have a number of environmental impacts. Use of chemicals, water, steam and energy causes an increase in the carbon footprint.

1.1.4 Economics: Cost of fouling and cleaning.

The direct costs of fouling and cleaning have been categorised by Gillham [1997]:

- Loss of production: reduced process efficiency and the need to shut down to clean;
- Maintenance costs: due to the necessity to install complex cleaning processes;
- Fuel costs: increased heating and pumping power to maintain process conditions;
- Capital expenditure: overestimating heat exchanger area and installation of extra pump capacity to allow for fouling.

- *Environmental effects:* are of increasingly importance. There are increasing global concerns to reduce the amount of waste from food production and lessen $C0_2$ emissions.

1.1.5 Understanding cleaning.

If fouling did not occur the process of cleaning would not be required, but we still would require cleaning after a product change over. However, extensive research has not yet found a prevention method thus cleaning must still take place. Understanding cleaning requires knowledge of the following aspects:

- *Deposit removal*; understanding of how the deposit is removed will allow the process to be improved.
- *Cleaning process parameters*; these include cleaning fluid, temperature, chemical type, chemical concentration and flow rate.
- *Process plant design*; i.e. reduce the 'dead legs' within the system and construction of the plant to use material that is easily cleaned and maintained.
- *Cleaning regime*; such as the order and duration of circulation of cleaning chemicals and rinse waters. Knowledge of a regime to ensure cleaning in the shortest time and with the lowest use of chemicals and water is desirable.
- *Monitoring the extent of cleaning*; all of the above factors could be optimised if the level of cleaning throughout the plant is sensitively and accurately known.

1.1.6 Cleaning Mechanisms.

Regular cleaning in-place can be very expensive in terms of downtime and materials [Changani, *et al.* 1997]. To optimise the time for cleaning, it is essential to understand the

removal mechanism and to gain some knowledge of material behaviour during cleaning. This can decrease maintenance cost and production losses; furthermore a better understanding of cleaning could reduce contamination and breakdowns. ClP to remove deposit from process equipment is often not a simple task, due to the highly complex chemistry of the processes that give rise to deposition [Changani, *et al.* 1997]. The rate and extent of food fouling is a function of many variables. Three layers within the process are involved during cleaning of the food deposit:

- **A solid layer**: the surfaces of process equipment in FMCG factories that are cleaned such as pipes, valves, filters, vessels, and plate heat exchangers. The soiled surface materials that may need to be cleaned may include: stainless steel (plant surfaces and valves), copper (heat exchanger), and metal alloys. The civil construction surfaces of factories are made of ceramics, plastics and glass.
- **An adherent deposit layer:** The severity of the fouling deposit differs depending on the material properties:
    - *low viscosity fluids*: here the fluid forming the 'deposit' is water or has properties close to water; examples are the emptying of pipes and tanks containing milk or beer between process runs,
    - *high viscosity fluids*: here the deposit is a highly viscous (perhaps viscoelastic) fluid, such as layers of toothpaste or shampoo left on the walls of process equipment in personal product processing, or starch from food sauces. The viscosity of these fluids may be several thousand times that of water,
    - *cohesive solids*: here the fouling deposit behaves as a solid; different deposits have very different material properties, ranging from the soft protein gel films formed from

milk or other food fluids to the very hard solid scales generated by precipitated minerals, (Figure 1.1: Produced by the Zeal Project part of the University of Birmingham, Chemical Engineering).

- **A liquid**: The cleaning fluids that are used include caustic detergents, (e.g 0.3% NaOH(aq) which predominates in FMCG factories, rinse water and acid detergents. The physical and chemicals properties of the deposit control the type of chemical needed.
    - *cold water:* some soils are sufficiently weakly bound to the surface that they can be removed by rinsing with cold water alone.
    - *hot water*: in personal products processing it is common to clean by circulation of hot water – product removed may then be able to be recycled.
    - *hot cleaning fluid*: many deposits are either impossible to remove by water alone or removal would take an unacceptable amount of time; cleaning chemicals (based around acid or alkali) are thus used to speed the cleaning process. Obviously the environmental impact of these fluids is potentially much greater.

A wide variety of fouling deposits are formed which require different cleaning conditions. Figure 1.1 shows cleaning problems classified in a two-dimensional plot. The two axes are type of cleaning fluid against the soil complexity.

Figure 1.1 shows a range of cleaning issues from the food and personal product industries, demonstrating that clusters of similar problems are found. A cross-section of cleaning problems are shown in the shaded area; three types of soil can be defined:

Type 1: cleaning of highly viscous or viscoelastic fluids by water. In personal products, the fouling film (such as toothpaste, shampoo, and creams) is often the same as the process fluid, and so forms by solidification. Similar problems are found with viscous foods such as starch-based sauces and confectionary fluids. However, these materials can be removed by the action of water alone.

- *hard cohesive*: these include proteinaceous soils as well as mineral scales formed from dissolved salts in the fluid. These form solid and adhesive deposits that have to be removed using hot cleaning chemical.

Type 2: cleaning and sterlisation of biofilms. Although it is possible to remove some biofilms with water alone more usually some biocide is used to kill adhered organisms which changes the removal characteristics (such as in Burfoot and Middleton, [2008])

- *biofilms*; layers of bacteria and/or yeasts which adhere and grow on surfaces. These are less adhesive than the solid soils and are removed with hot biocidal solution.

Type 3: cleaning of solid deposits by chemical action: formed by components of the process fluid as a result of one or more of the fouling mechanisms and which require cleaning chemicals for efficient deposit removal. The nature of the deposit will determine the type of cleaning chemical used; such as sodium hydroxide to remove organic films and acids to remove mineral scales.

- *complex fluids*: these include many home and personal care fluids, such as toothpastes, shampoos and detergents, which form deposits that are essentially composed of the product. These are commonly removed by hot water in a rinsing step.

1.1.7 Surface interfacial parameters.

In the food industry a hygienic surface needs to be smooth, easy to clean, able to resist wear and must retain its hygienic qualities. Stainless steel is the most common food contact material used in industry being stable at a variety of temperatures, inert, relatively resistant to corrosion, and it may be treated mechanically or electrolytically to obtain surfaces which are easy to clean. It is able to maintain this surface through many operating cycles [Boulange-Petermann, 1996].

Most surfaces have a complex structure; the properties depend on the nature of the solid and the method of surface processing. The surface parameters arise from the interactions of the surface and foulant, and the interaction between the surface and the environment. The properties of the surface are crucial because they affect the real area of contact, the friction, the wear, and the lubrication [Liang, 2004]. Interfacial parameters play a vital role in fouling and cleaning.

Surface modification has often been proposed as a solution to the surface interfacial fouling problem [such as Woo *et al.* 2009 and Nermen Maximous *et al.* 2009]. The move towards surface modification promises to provide a revolution in fouling and cleaning studies. The criteria for the success of modified surfaces are their ability to reduce the amount of fouling formed, or the rate of formation and lengthen the induction period before fouling is significant. Surface modification is an alteration of the surface of substrate material (normally metal) to transform it to a new surface which has much better functions (e.g. chemical resistance, corrosion resistance, abrasive wear resistance, electrical properties and non-stick).

This modification can be done by coating the surface or inclusion of certain elements on the surface. Surface modification has been proposed as one solution to the fouling problem [Muller-Steinhagen *et al.* 2000].

The interaction between the heat transfer surface and the process fluid is obviously critical in fouling. Surface free energy, for instance, is one of the surface properties that may affect both the fouling and cleaning rates. Adhesion forces are when two materials interact to join. The strongest joins are where atoms of the two materials swap (ionic bonding) or share (covalent bonding) outer electrons. Cohesive forces are the intermolecular attraction between like molecules. The higher the surface energy, the more easily fouling is formed whilst lower surface energy can reduce the fouling amount and weaken the adhesion force (Rankin & Adamson, [1973]; Baier, [1970]). Corrieu [1981] reported that adhesive forces of a proteinaceous deposit to a stainless steel surface are stronger than cohesive forces.

Britten *et al.* [1988] studied the effect of coatings (polymethylacrylate, nylon and cellulose acetate) on fouling. The results showed that coating the heating surface could affect the strength of adhesion to the surface, but not the amount of deposit. The interfacial energy of the surface appeared to be the main factor affecting the adhesive strength. The higher the surface energy the more easily fouling is formed. A number of authors have proposed modifying the surface energy of stainless steel. Britten *et al.* [1988] and Yoon and Lund [1994] altered the surface of equipment and found that PTFE (Poly-Tetra Fluoro Ethylene) has lower surface energy than stainless steel. An alteration of surface energy reduces polarity and fouling.

Different studies have been done to attempt to create anti-fouling surfaces by coatings, with ceramic, PTFE and other polymer layers. Yoon and Lund [1994] investigated electropolished stainless steel plates, Teflon-coated plates and polysiloxane coated plates. Implantation of the stainless steel heat transfer surface with silicone and fluorine reduced surface energy and $CaSO_4$ scale formation [Zettler *et al.* 1999]. Muller-Steinhagen *et al.* [2000] concluded that the effect of surface energy is much more significant than the effect of surface roughness.

1.1.8 Aims of the Thesis.

The aim of this thesis is to contribute to industrial objectives, to develop new technological approaches to the measurement, modelling, monitoring and control of cleaning in FMCG plant which will result in significant reduction in environmental impact:

- deliver innovative solutions for minimising cleaning waste from FMCG factories;
- create FMCG processes which are inherently less wasteful and more resource efficient;
- Generate new knowledge for plant, process and control system design, increasing manufacturer profitability as well as that of their chemical, equipment and design suppliers.

The response of surfaces to different foulant materials tested by AFM in force mode will show how surfaces/foulants interact and aid in the specification of possible fouling-resistant surfaces.

To increase understanding of how interactions between surfaces and deposits may control the cleaning process. The thesis concentrates on surface interactions between different food deposits using Atomic Force Microscopy (AFM), to investigate the responses of different surfaces to different foulant materials using the AFM in force mode. This work will help to understand the effects of interfacial surface parameters on the cleaning of different foulant deposits.

Previous work on different fouling deposits and the AFM include Parbhu [2002, 2006], Rosmaninho [2003], Verran [2006] and Whitehead [2006]. However there is very little work done on AFM force measurements and food deposits. This work will provide a better understanding of the AFM force measurements, to help understand the interactions which may occur between the aqueous environments and different FMCG deposits. In order to understand adhesion in food systems it is important to have an understanding of the medium in which interactions occur. Studies using the micromanipulation technique developed at Birmingham to quantify the forces involved in deposit removal [Liu, *et al.* [2007]; Liu, *et al.* [2006]; Liu, *et al.* [2002]] , will be used as a bases of comparison to the AFM . [See chapter 3].

This project is part of a larger programme involving a group of industries such as Unilever, GSK, Cadburys, S&N Breweries, Alfa Laval, Ecolab, GEA and Bruker Optics. The commonality between the industrial members of the consortium was the need to resolve the cleaning problems which are common across the industry sectors represented within the consortium, so that the technical programme could be focused as much as possible.

The cleaning problems of these industries included are illustrated in Figure 1.1: The horizontal axis shows the increasing complexity of the soil, from attached films of low viscosity fluid, through attached films of complex non-Newtonian rheology, to adhered films with significant microstructure. The vertical axis represents the energy and environmental costs of cleaning, from water at ambient temperature, through hot water to the use of hot cleaning chemical. In practice, the wish is to use the minimum level of cleaning that ensures that cleaning times are economically short: the aim is to move to less environmentally damaging methods.

The soils were chosen to represent major problems for the manufacturing industry:

(1) Hard cohesive soils: this study uses sweetened condensed milk (SCM), caramel/Turkish delight and whey proteins, which are problems for the confectionary and milk processing industries. The deposits which form tend to be gels which adhere to the surface strongly.
(2) Complex fluid: toothpaste. Toothpaste processing is a large industry, in which rinsing of toothpaste from the surfaces – for examples of tanks and pipes - is necessary either to ensure process sterility or at changeover.
(3) Surfaces: stainless steel, glass and Polytetrafluoroethylene (PTFE) have been identified by industrial interest. Stainless steel is the basis of most process plant – PTFE is obviously widely used in non-stick surfaces. Glasses and ceramics are the basis for many food process hall surfaces.

1.1.9 Structure of Thesis.

Chapter 2 reviews the work on cleaning, based on the surface interactions that happen during the process. It reports studies on modified surfaces and introduces AFM and Micromanipulation.

Chapter 3 describes the methods and procedures followed and used to perform AFM force experiments. The methods used to modify the AFM tips with the surface particles are discussed in this chapter. The experimental procedures for micromanipulation results are discussed. Summary of all the different types of AFM used to produce results are discussed in chapter 4, 5 and 6.

Chapter 4 studies how different components of fluids might affect adhesion; this might be useful in defining ways of varying the composition of formulation to minimize fouling or aid cleaning.

Chapter 5 studies if AFM data can be related to micromanipulation data, to also see if nano and micro-scale measurements can be related.

Chapter 6 studies the effects of temperature on fouling and cleaning from a range of materials which are known to be thermally labile; cleaning rates are known to be temperature-dependent.

Chapter 7 summarises and conclude the findings of the results and research of each chapter. Future work is also suggested.

Chapter One Figures:

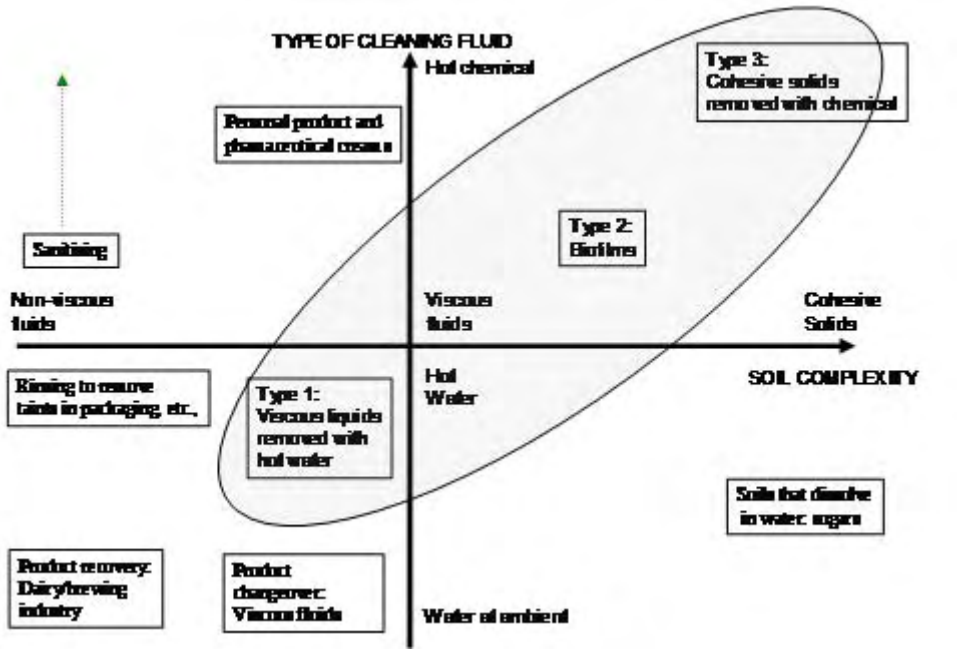

Figure 1.1 Cleaning map: shows a range of cleaning issues from the food and personal product industries, demonstrating that clusters of similar problems are found. A cross-section of cleaning problems are shown in the shaded area. It can thus be define to three types of soil that are most difficult to clean. (Produced by the Zeal Project part of University of Birmingham).

CHAPTER 2: A REVIEW OF SURFACES IN CLEANING INVESTIGATIONS AND AFM APPLICATIONS.

Chapter 1 has introduced the concerns and needs of cleaning process plants. The contamination of surfaces by fouling and micro-organisms (particularly pathogenic ones) are a cause of serious concern within the food industry. The levels of cleanability of material should be addressed when choosing the materials for process line equipment, along with their mechanical and anticorrosive properties.

This Chapter will discuss food fouling and associated cleaning problems. In addition it will discuss how various surfaces have been used in different anti-fouling situations. A detailed description of AFM uses and AFM studies conducted on fouling will be discussed.

Here, the factors that need to be taken into account in the design of industrial processing plants will be discussed. These are normally specified by knowledge and experience of running a plant or process to simulate dirt accumulation on the heat transfer surfaces, but if not defined carefully they can totally negate any benefits generated by skilful design

2.1 Fouling mechanisms.

The mechanisms of fouling are as follows [Fryer and Asteriadou, 2009]:

Chemical reaction fouling: when chemical changes within the fluid cause a fouling layer to be deposited onto the surface. This can be, for example, reactions of proteins which generate insoluble aggregates which form the majority of the fouled layer in milk pasteurisers.

Crystallisation fouling: a common example of this phenomenon is scaling in a kettle or boiler caused by 'hardness' salts depositing onto the heating elements as the solubility of the salts reduce with increasing temperature.

Biological fouling: this is caused either by the growth of organisms within the fluid which deposits out onto the surfaces of the heat exchanger, or by surface growth of organisms. When this type of fouling occurs it is normally removed by either chemical treatment or mechanical brushing processes.

Deposition fouling: this is when particles contained within the fluid settle out onto the surface when the fluid velocity falls below a critical level. When this type of fouling occurs it can be removed by mechanical brushing processes.

Corrosion fouling: this is when a layer of corrosion products build up on the surfaces forming an extra layer of, usually, highly thermally resistance material. By careful choice of materials the effects can be minimised as a wide range of corrosion resistant materials based on stainless steel and other nickel based alloys are now available.

Fouling is taken account of in practice in heat exchange design in terms of a fouling resistance R_f, defined as:

$$\frac{1}{U} = \frac{1}{U_0} + R_f \qquad \textbf{(2.1)}$$

Where U_0 is the clean heat transfer coefficient (W/m^2K), U is the heat transfer coefficient after fouling and R_f is the fouling resistance. Models for fouling attempt to predict both the magnitude of R_f and the rate of change.

2.2 Deposit-wall interaction

It is vital to know how the fouling deposit is formed, the structure of the fouling deposit and its response towards the surfaces of equipment. Here the discussion will concentrate on milk fouling, as it is a well defined fouling deposit on which many studies have been done.

Epstein [1983] and Burton [1988] described the stages involved in fouling. In the dairy industry it is believed that proteins will be first transported to the stainless steel surface (Belmar-Beiny & Fryer, [1992]). This is due to the fact that proteins have amphoteric (acid and base criterion) and amphipathic (has hydrophobic, hydrophilic and charged side chains) nature and high molecular weight, so they tend to move to interfaces reducing the interfacial tension.

In contrast Green *et al.* [1988] studied milk fouling at high temperatures, and found that the first layer of fouling was mostly calcium phosphate. Although a homogeneous protein layer was observed in the first 40 seconds, after one hour, the layer near to the stainless steel surface consisted of a high mineral content [Belmar-Beiny & Fryer, 1992]. However Foster & Green [1990] suggested that minerals and protein layers are built simultaneously (studied with milk fouling onto the stainless steel surface at wall temperature, 140°C). This suggests that the structure of the deposit changes during fouling and initial adsorption will both alter surface physical properties and might possibly encourage more adhesion.

During the period of rapid fouling from milk, aggregation of β-lactoglobulin (β-lg) in the bulk fluid leads to rapid fouling [Gotham *et al.* 1989; Gotham, 1990] . This is caused by the interaction between denatured or aggregated proteins. In denaturation, reactive groups inside the proteins are exposed, accelerating the rate of reaction and causing protein to aggregate, so that protein heated in the bulk fluid will react and adhere faster.

Protein-wall interactions are complicated and it is clear that many factors will determine the structure of fouling deposits. Electrostatic and Van der Waals forces on the stainless steel surface are known to affect the adsorption of β-lg onto the stainless steel surface so changes in surface chemistry will affect adhesion [Sakiyama *et al.* 1996]. Complicated deposit formation on the surfaces is expected for real food products.

2.3 Deposit-fluid interactions

The area of deposit-fluid interactions is critical in cleaning. If the deposit and fluid phases are not contacted, cleaning reactions are unlikely.

- **Fluid actions:** Cleaning solution and fluid flow play an important role in cleaning both in chemical action and physical action [Grassoff, 1997] . In general, fluid is needed both as a medium to transport the chemical to the deposit and to provide mixing and shear. Once chemical solution is in contact with the deposit, reaction will occur to modify or deform the deposit structure. Dissolution may also occur at the same time. In addition to any reactions of the cleaning solution with the deposit, the structure of the deposit will keep changing with time, this is known as ageing.

- **Cleaning fluids:** Cleaning is a complex process involving interaction between the cleaning components and the deposit. Cleaning begins with the deformation of the fouling by the reaction of cleaning detergent [Grassoff, 1997] . This is agreed by Karlsson *et al.* [1998] who concluded that cleaning is strongly influenced by deposit and surface characteristics together with the choice of cleaning agent.

For economic cleaning, it is essential to choose the correct detergents or chemical solution. Thus knowledge of fouling deposits is crucial. If proteins are the main component, alkali based detergent is the best to apply; alkali cleaning is often used in industries that process protein and fat containing foods. Alkalis react with proteins through hydrolysis of the peptide bonds and solubilisation while with fat through saponification. For milk fouling, cleaning of processing equipment starts with a hot water rinse to melt the fats and thus enhance the chemical solution contact with the deposit [Alfa -Laval, 1987] . Around 1 wt% concentration of alkali is normally used in the food industry. For food deposit that mainly consists of minerals, acid solution is the best since most minerals are acid soluble [Jeurnink & Brinkman, 1994; Grassoff, 1997] . Nitric acid or phosphoric acid is usually used for acid wash and the typical concentration applied is 0.5 to 1.0 % [Kane & Middlemiss, 1985; Timperley & Smeulders, 1987] .

Nevertheless, alkali and acid solution alone may be insufficient to clean the surface completely. Timperley & Smeulders [1987] discovered that the deposit contained 25% w/w protein on the surface after the alkaline cleaning stage and once the cleaning stages were completed, residual calcium phosphate was still detected. Jennings *et al.* [1957]

found that removal of milk deposit improved drastically when all the cleaning agents were mixed: alkaline cleaners, sequestering agent and wetting agent. Sequestering agents and surfactants (surface-active agents) are the major components in formulated detergents that can enhance the removal process. Sequestering agents both prevent the precipitation of salts and may prevent redeposition of fouling deposit [Kane & Middlemiss, 1985; IDF, 1993].

2.4 Methods for surface analysis

A variety of methods are available to characterise surfaces. These include:

- Atomic force microscopy (AFM), Scanning tunnelling microscopy (STM), Transmission electron microscopy (TEM), Scanning electron microscopy (SEM), Scanning transmission electron microscopy (STEM), Variable angle spectroscopic ellipsometry (VASE) and light microscopy (LSM). Table 2.1 summarises the techniques that can image, and take quantitative measurements of film thickness.

Elemental composition and chemical state measurement can be determined by the following techniques:

- Auger electron spectroscopy (AES), Energy-dispersive X-ray (EDS), X-ray photoelectron spectroscopy (XPS), High-resolution electron energy-loss spectroscopy (EELS), Fourier transformation Raman spectroscopy (FT Raman) and UV-Visible spectroscopy (UV/Vis). Table 2.2 shows a summary of the techniques, in which it shows detailed information of a surface layer helps diagnose unwanted deposits on surfaces.

Microstructure, crystallography, and defects (unwanted matter or damage of surface) measurements can be determined by the following techniques:

- High- resolution transmission electron microscopy (HRTEM), Low-energy electron diffraction (LEED) and X-ray diffraction (XRD). Table 2.3 shows a summary of the techniques that can show different defects on a surface which is useful to check if a surface is clean or has some contamination on it.

The above experimental methods, can contribute to innovative cleaning methods and solution, by using the techniques in conjunction with each other, giving a bigger and accurate picture. These techniques will help to generate new information for plants, processes and designs. In this study, both AFM and SEM have been used.

2.5 Surface modification.

The physical properties of the deposit and the surface will affect removal. Fouling deposits form as a result of adhesion of species to the surface and cohesion between elements of the material. Cohesion is defined as the internal strength of an adhesive as a result of a variety of interactions within the adhesive. Adhesion is the bonding of one material to another, namely an adhesive to a substrate. The forces between elements of the deposit depend on the nature of the material; deposits may be covalently bonded (for example reacted egg or milk proteins) or held together physically (such as gelled biopolymers). Understanding of the interaction between deposits and surfaces is clearly critical in cleaning. On a nanoscale, atomic force microscopy (AFM) has been used to characterise surfaces and fouling (such as Parbhu *et al*, 2002; Weiss *et al*, 2002). Low-adhesion coatings (Muller-Steinhagen and Zhao, 1997) have been shown to reduce fouling in some situations such as mineral scales.

Modifying the properties of processing surfaces, which are typically stainless steel in food applications, may be one way of achieving a reduction in initial fouling rate or of enhancing cleaning, Parbhu, *et al.* [2006]. This is due to the highly complex chemistry of the processes that give rise to deposition of milk proteins occurring on the equipment surfaces, [Changani, *et al.* 1997]. Surface modification has often been proposed as a solution to the fouling problem; Rosmaninho, Rizzo, Müller-Steinhagen and Melo, [2005] have dedicated time into researching antifouling surfaces and found that they show interesting results in fouling and cleaning studies. Rosmaninho, *et al.* [2006] investigated different modified stainless steels. The surface modification techniques were: direct and turbulent ion implantation (with SiF_3^+ and MoS_2^{+2} ions); sputtering (thin diamond- like carbon (DLC) films); plasma chemical vapour deposition (CVD) (thin films of DLC, SiO_x, and DLC– Si–O) and an autocatalytic Ni–P–PTFE coating.

(1) **Direct and turbulent ion implantation:** Here the surfaces were bombarded with highly accelerated SiF_3^+ ions with an average energy of 200 keV, achieving an ion concentration of 5 x 10^{16} ions/cm^2. In this reported case, the ions were directly implanted into the metal material, forming a surface alloy of approximately 0.2 μm in depth. MoS_2 ions were implanted in the stainless steel surfaces by turbulent ion implantation. The atoms impacting the surface of the substrate had such a high energy that they could penetrate into the interior of the material, since molecules hitting the surface could push already deposited molecules further inside the substrate, leading to implantation depths of up to 10μm and resulting in modified surface layers of 2–5 μm thickness.

(2) **Sputtering and plasma CVD technique**: Sputter coating as well as plasma CVD coating are plasma processes, which take place at sub-atmospheric pressures. The advantages of the sputter coatings are the hardness and the good adherence of the films produced while the main disadvantages of plasma CVD coatings are their reduced density and weaker adherence to the substrate material. The DLC sputter coating used in this work was a multilayer coating with a TiN sublayer, followed by a TiC film and finally a DLC coating. The DLC–Si–O surface was produced by Plasma CVD using CxHx as precursor for the DLC film and Hexamethyldisiloxan (HMDSO) for the addition of silicon and oxygen. In addition, a plasma CVD SiOx film was produced using HMDSO as precursor.

(3) **Autocatalytic Ni–P–PTFE coating**: The Ni–P– PTFE coating was produced by an autocatalytic plating process. In this process the stainless steel surface went through five steps: (1) an alkaline cleaning bath; (2) a pickling process; (3) activation by the galvanic deposition of nickel and (4) an autocatalytic reaction in which Ni–P plating is deposited. After the Ni–P plating had reached a certain thickness, PTFE particles were added to the coating bath, to be incorporated in the Ni–P matrix. In order to be effective in reducing fouling, the outer surface of the Ni–P–PTFE plating should contain a high percentage of homogenously distributed PTFE particles.

(4) **Silica coating**: Silica coated (SiOx) surfaces were prepared by a sol–gel process, where metal alkoxide compounds are typically used as raw ingredients. The process started with the hydrolysis of such compounds in the presence of water and condensation to form M–O–M bonds (‘‘M’’ being elements like Si, Ti, Zr). After the hydrolysis and condensation have

proceeded to a certain degree (sol formation), a coating could be applied on the substrates by, for example, dip- or spin-coating; dip-coating, under well controlled conditions was used. The coating structure was then consolidated by high temperature annealing in order to oxidize and remove any residual organic molecules. Sols were prepared from methyl triethoxysilane (MTES): H2O (molar ratio 1:3) solutions in ethanol at various dilutions (1:10–1:4), and annealed at temperatures in the range of 200–500ºC.

Different fouling materials used were: (i) Calcium phosphate, where deposition was from Simulated Milk Ultra Filtrate (SMUF), was studied; this is an aqueous solution that simulates the mineral composition of milk (Jenness and Koops, 1965). (ii) the β-Lactoglobulin solution preparation method and its gross chemical composition were as described by Holt *et al.* (1999). The protein was dissolved in phosphate-buffered saline. The cleaning efficiency of each surface is here defined as the percentage of deposit mass removed for each surface after the cleaning process. It was concluded that Ni–P–PTFE coating was the easiest material to clean. Conversely, SiO_x, DLC, MoS_2, and Silica coating did not show any advantage over standard stainless steel.

The Ni–P–PTFE coating seems to be the most appropriate surface treatment to minimize milk fouling effects. This conclusion is supported by the fact that the characteristics of the Ni–P–PTFE surface modification method were systematically different from the other methods: (i) Ni–P–PTFE was the most hydrophobic surface of them all, the others being essentially hydrophilic; (ii) a polar component (London–van der Waals) of the surface energy of Ni–P–PTFE was lowest among all surfaces, (iii) the electron donor component (polar) of the surface energy had the lowest value for the Ni–P–PTFE material.

The use of Ni-P-PTFE coating in fouling studies has shown remarkable results. Ni-P-PTFE is significantly improved by graded technique (in which the PTFE content is gradually increased from the substrate to the top surface); and the fouling formation of $CaSO_4$ deposits on heat exchanger surfaces are reduced [Zhao *et al.* 2002] . Zhao & Liu [2005] found that the graded technique of Ni-P-PTFE coatings give corrosion-resistant coatings. Zhao [2004] used graded Ni-P-PTFE surfaces and found the attachment of thermophilic streptococci reduced by 82-97%. In addition, Zhao & Liu *et al*, [2006] showed that the attachment of biofouling on Ni-P-PTFE surfaces reduced by 87.7-92.8% compared to stainless steel 304.

To evaluate the importance of surface modification on the formation of mineral deposits, calcium phosphate fouling was studied using stainless steel surfaces modified by TiN sputtering. [Rosmaninho, Rocha, Rizzo, Müller-Steinhagen, & Melo, 2007]. The importance of this work is the importance of the surface energy of the substrate, particularly its electron-donor (γ^-) component, on the fouling behaviour of calcium phosphate from a simulated milk mineral solution.

Many researchers such as Rosmaninho *et al.* [2004] have used surface modifications to characterized chemical composition, roughness, topography and wettability. Variety of surface modifications methods have been studied SiF_3^+ and MoS_2^{2+} ion implantation; diamond-like carbon (DLC) sputtering; DLC, DLC–Si–O and SiO_x plasma enhanced chemical vapor deposition (PECVD); autocatalytic Ni–P–PTFE and silica coating.

2.6 Surface Roughness.

Quantifying the degree of roughness can be complex, but a quantitative description of surface roughness is critical in order to assess the effects of surface roughness in the food industry [Round *et al.* 2001]. The topography of any surface will take the form of a series of peaks and valleys which may vary in both height and spacing. Surface roughness exists in two principal planes [Round *et al.* 2001] one perpendicular to the surface, described as height deviation, and the second in the plane of the surface, described by spatial parameters and identified as texture [Round *et al.* 2001]. There are a number of amplitude parameters, for example R_a known as arithmetic average height parameter; R_q, known as the root mean square; the standard deviation of the *z* height value and R_z, the difference in height between the averages. R_a is the most universally used roughness parameter for general quality control [Verran *et al.* 2006].

2.7 Atomic force microscopy (AFM).

The atomic force microscope (AFM) was invented in 1986 by Binnig, Quate and Gerber, [Martin *et al*, 1987]. The AFM collects information at the nanoscale by using a sharp probe (5 - 10 nm), which moves a few nanometers (<10nm) over the surface of a sample in a raster scan. The AFM probe is a tip on the end of a cantilever (<125μm), which bends in response to the force between the tip and the sample. The cantilever flexes, the light from the laser is reflected onto the photo-diode. Changes in the bending of the cantilever can be measured by this method. The cantilever obeys Hooke's Law, F = -kz, for small displacements, and so the interaction force between the tip and the sample can be found, where F is the force, k is the stiffness of the lever, and z is the distance the lever is bent. The movement of the tip or

sample is performed by precise positioning devices made from piezo-electric ceramics in the form of a scanner, (Figure 2.2). The scanner is capable of sub-angstrom resolution in x-, y- and z-directions. The z-axis is conventionally perpendicular to the sample. Most AFMs use a laser beam deflection system, introduced by Meyer and Amer, (Veeco AFM manual) where a laser is reflected from the back of the reflective AFM lever and onto a position-sensitive detector. AFM tips and cantilevers are microfabricated from Si or Si_3N_4. Typical tip radius is from a few to 10nm. (Veeco AFM manual).

AFM provides a method for detecting nanoscale information on surfaces. The AFM has been used by many researchers such as Lent, *et al.* [1998], Adams, *et al.* [2003], Nakao, *et al.*, [2005] and Round, *et al.* [2001], for the analysis of surface topography, electrostatic forces, adhesion forces, etching, tribological properties and material properties.

The AFM has the capability to make measurements on a single particle and to measure forces, and hence interactions energies, with respect to intersurface distances. A number of different interactions can be measured, either separately or simultaneously, including long-term forces such as van der Waals and electrical double layer forces, hydrophobic interactions, salvation forces, steric interactions, hydrodynamic drag forces as well as adhesion.

A measurement of the van der Waals interactions between different materials in different media is possible using the AFM. By changing the sharp probes with a colloidal particle, a wide range of different interactions can be measured. The possibility of forces other than van der Waals interactions may be present, such as double layer interactions and hydrodynamic effects. The magnitude of the adhesion between two surfaces is dependent upon the contact

area at the junction between the surfaces as well as the interaction forces themselves. The contact area will depend upon the mechanical deformation of the material due to the applied force and material properties. [Hilal *et al.* 2009].

The AFM has been used to measure adhesive forces between particles and process surfaces. Adhesion between particles, inorganic colloidal particles, bacterial cells and filtration membranes. This interaction is of great importance when considering the fouling and biofouling of such surfaces. Particles adhere to the process membrane and reduce flow through the membrane, greatly reducing filtration, the efficiency and working lifetime of the membranes. The quantification of adhesion forces between colloids and membranes can provide an important contribution to developing the theoretical prediction and optimisation and control of many engineering separation processes.

There are a number of models that have been developed to account for the effect of the surface roughness on measured adhesion when trying to infer various properties of interactions from adhesion forces. These generally use some measures of roughness, such as the root mean square (RMS) roughness of the surface, or value of mean asperity size to account for the reduced contact areas due to the presence of asperities. As well as serving to keep the two surfaces separated, the angle at which asperities on the particle surfaces approach each other may also affect the effective contact area and thus the measured adhesion. [Hilal *et al.* 2009].

AFM Surface tip modifications.

The number of materials used to make the AFM tips is limited to silicon (which is in ambient conditions oxidized to silica) and silicon nitride (which is also oxidized). These tips can be coated with various metals and diamond (commercially available from the AFM tips suppliers [Veeco,UK]). Direct measurements of forces involving such particles can therefore be very useful from both fundamental and practical points of view. Direct attachment, gluing of spherical multi-micron size particles to the AFM cantilevers was demonstrated first in 1991 [Drucker *et al.* 1991], and has been broadly used to study to molecular forces and mechanics of biological cells [Sokolov, 2006, Berdyyeva, 2006 and Park, 2005]. Chemical functionalization of AFM tips with various molecules has demonstrated its great importance for studying molecular interactions, force spectroscopy, detection, etc.

The problems with attachment and functionalization of AFM tips with nanoparticles are:

- To attach a single particle to the cantilever, it has to be visible under an optical microscope. This is not the case for nano-sized particles.
- The smaller the particle, the easier for epoxy to engulf it. Because the layer of epoxy deposited on the cantilever is at least several cubic microns, it is quite tricky to avoid coating of the particles with the epoxy.

To overcome these issues, Sokolov *et al.* [2006] suggested the following solutions:

- gluing not a single nanoparticle but a large amount of nano-sized particles at once,
- gluing not to the cantilever but to a standard Si_3N_4 pyramidal tip,
- depositing nanoparticles to the epoxy coated tip not immediately, but after the epoxy being semi-rigidified, becoming viscous enough to avoid engulfing the particles

before complete curing. The suggested method can be used for attachment of virtually any solid nanoparticles.

AFM is a powerful tool as it collects data for images by feeling and touching rather than looking [Morris, *et al.* 1999]. AFM is a useful tool used in investigating the fine structure information of food materials. AFM is capable of imaging both conductive and insulating materials, a clear advantage over the scanning tunnelling microscope (STM), which works only with conductors or semiconductors.

A number of researchers have used the AFM in fouling and cleaning, such as Boulange-Petermann, [1997], Boyd, [2000], Allen, [1997] and Verran [2000]. To measure topographic images and surface adhesion, the AFM can also provide much more information than just surface imaging. The AFM has been used to measure the topography of worn surfaces, and of surfaces of new materials used in the food industry. The problem in this area is a lack of good correlation between roughness measurements and parameters such as cleanability, and microbial adhesion and retention on surfaces (Boulange- Petermann, 1996; Garry *et al.* 1995; Langeveld *et al.* 1972; Masurovsky and Jordan, 1958; Taylor et al. 1998b, Verran and Maryan, 1997; Verran *et al.* 1991). Roughness measurements, particularly R_a, are statistical values describing a surface, and thus are only truly representative if there is a regular topography, as for polished and brushed stainless steel, but not for worn surfaces whose abrasions tend to be of a random nature. This feature is also of importance if the area examined is considered, since defects may be included or excluded depending on the sampling method and area. If wear occurs on a microbiological scale, then only the AFM would be able to both measure and visualise the relevant topographic features, and potentially

relate surface features to fouling and cleanability. Surface roughness can play a key role of attachment of fouling deposit to surfaces [Verran *et al*, 2002].

The AFM can record the amount of force felt by the cantilever as the probe tip is brought close to and even indented into a sample surface and then pulled away (Figure 2.3). This technique can be used to measure the long range attractive or repulsive forces between the probe tip and the sample surface, elucidating local chemical and mechanical properties like adhesion and elasticity. Topographic imaging of a sample can be performed using contact mode AFM or tapping mode AFM:

(1) In contact mode: the cantilever tip is in direct contact with the surface, and as the tip moves across the surface the change in cantilever deflection is monitored via the change in the position of the laser beam on the photodiode. A feedback control system is used to maintain contact at a prescribed force between the cantilever and the surface. This mode is suitable for smooth surfaces; in this mode rough samples could damage the tip, [Verran, 2000].

(2) In tapping mode: AFM imaging the cantilever is vibrated close to its resonant frequency at a short distance above the surface. When the tip and surface move relative to each other in the vertical direction, the amplitude of oscillation of the cantilever is monitored using a feedback loop, affording a topographic image of the surface. This mode is ideal for rougher surfaces such as a ceramic, [Verran, 2000].

Force measurements can be performed in air, liquid, vapour or vacuum environments, using a standard pyramidal Si_3N_4 AFM cantilever tip or with a variety of specially chosen probes

attached to the apex of an AFM cantilever. e.g. a microparticle. Force curves (force-versus-distance curve) typically show the deflection of the free end of the AFM cantilever as the fixed end of the cantilever is brought vertically towards and then away from the sample surface. Experimentally, this is done by applying a triangle waveform voltage pattern to the electrodes for the z-axis scanner. This causes the scanner to expand and then contract in the vertical direction, generating relative motion between the cantilever and sample. The deflection of the free end of the cantilever is measured and plotted at many points as the z-axis scanner extends the cantilever towards the surface and then retracts it again. By controlling the amplitude and frequency of the triangle waveform voltage pattern, it is possible to vary the distance and speed that the AFM cantilever tip travels during the force measurement.

2.8 Studies of AFM in fouling and cleaning:

The following studies demonstrate how the AFM has been used for surface measurements in different applications such as: biofilms, hygiene, and microbes in biofouling and surface modifications. The studies show that the AFM is a very helpful tool in determining surface characteristics.

Verran, *et al.* [2000] investigated the wear of food contact surfaces using the AFM for measuring surface roughness and wear on the nanometer scale, in order to produce realistic models for in vitro testing. This was achieved by (i) comparing R_a values for a range of smooth surfaces obtained from solid and laser stylus profilometers and the AFM; (ii) using the AFM to visualise and measure the roughness of stainless steel surfaces in situ in food processing factories either directly, or indirectly using dental impression materials; (iii)

producing abraded stainless-steel surfaces in vitro which reproduced the typically worn surface of real food contacts.

Worn food contact surfaces in a food processing factory were sampled. Flat, horizontal surfaces representing a range of food contact surfaces were identified e.g. polypropylene, polymethylmethacrylate, polished and unpolished 316L stainless steel, and glass and porcelain materials.

Verran, *et al.* [2000], wiped the surfaces with 95% ethanol or detergent if greasy and placed them on the test surface. The two components of a high-resolution impression material were pipetted and mixed for 45 seconds in a weighing boat (working time 5 min) and then poured into the frame. After 30 min of setting time, the material was peeled from the surface and the top surface was attached to the lid of a Petri dish so that the contact surface was protected. The surface was then examined via incident light optical microscopy, and also by AFM for visualisation, and R_a measurement.

The samples of worn stainless steel surfaces, a range of R_a values were obtained, either at or below the 0.8 μm hygiene levels. The information enabled the production of a range of worn stainless steel surfaces, produced in a reproducible and controlled manner via the use of silicon carbide paper and quartz grit with a known and constant load, to give surface topographies mirroring those found in situ. These surfaces were then used for soil and microbial fouling and cleanability studies, by Boyd, *et al.*, [2000], Verran, *et al*, [1999].

The above studies showed that an increase in substratum surface roughness increases the retention of microrganisms on that surface, An increase in roughness R_a (from 0.02 to 1.24

μm) had a significant effect on cell retention. Profilometric methods used to obtain R_a values were relatively crude, and did not facilitate discrimination of surfaces differing only slightly in R_a value. R_a values for the smooth test surfaces varied considerably. For the solid stylus profilometer, the highly polished surfaces were not measurable in terms of R_a values. The laser profilometer was able to provide a measurement for these surfaces, but it was the same value in each case. The AFM was able to differentiate between all surfaces in terms of R_a values on the nanometer scale. The R_a values increase with decreasing probe size, reacting greater resolving ability of the laser and AFM probes. Both SEM and AFM were used to visualise the surface. AFM found the ceramic surfaces to be to rough for the depth of field. However, for the smooth surfaces, the AFM provided images which gave more detail of surface features than the SEM and also required less sample preparation.

The AFM was used to measure the topography of the worn surfaces, and of surfaces of the new materials used in the food industry, providing data and information. These studies give an insight into what problems that AFM encountered with the different surfaces and helps to prove that more information can be obtained compared to other techniques.

The applications of AFM in interfacial science are too numerous to list. The following studies illustrate some applications in different areas of research which have some relevance to fouling and cleaning. All surfaces will become fouled eventually under adverse conditions, Wu, *et al*. [2008], employ a robust defouling method to remove adsorbed protein in order to maintain surfaces free of proteins. They found that nanobubbles can inhibit protein adsorption on a variety of surfaces, but to make use of this, control over the production of nanobubbles is required.

The ethanol–water exchange method for the production of nanobubbles depends upon the nucleation of supersaturated gas, which is inherently difficult to regulate. Therefore the coverage and size of nanobubbles cannot be controlled. In contrast, electrochemical formation and growth of nanobubbles was found to be relatively easy to control. Nanobubbles are formed on the surface with a regular density and their size can be controlled by the applied current. Wu and Zhang [2008] demonstrated that the area density of nanobubbles on highly oriented pyrolytic graphite (HOPG) surfaces can be controlled electrochemically. It was demonstrated that the presence of nanobubbles on a surface decreases the adsorption of protein dramatically, that is the nanobubbles act as antifouling agents. Wu, *et al*. [2008], demonstrate that nanobubbles cannot only be used to prevent the nonspecific adsorption of protein but also can be used to remove protein that is already adsorbed and therefore might be used as cleaning (or defouling) agents.

The AFM was used for samples that had electrochemical treatment applied to using a battery (1.5 V) electrically connected between the HOPG substrate (cathode) and a copper electrode (anode) within the buffer solution for 20 to 50 seconds. Antifouling nanobubbles were first formed on the HOPG surface electrochemically, and then a drop of bovine serum albumin (BSA) solution (20 μg/ml, 200 μl) was deposited onto the HOPG and allowed to stand for 5 minutes. Then pure water was used to wash away any remaining BSA. For defouling experiments, the BSA was applied in the same manner to the HOPG surface. Then the surface was washed with a large quantity of pure water before nanobubbles were produced electrochemically. The surface was then washed again with a large quantity of pure water. The samples were dried using compressed air before AFM observation.

BSA solution (10 μg/ml, 4 ml) was injected into the fluid cell, and allowed to adsorb for 30 min. Then four millilitres of pure water was injected to rinse excess protein from the surface. The sample was imaged by tapping mode AFM 10 min later. After imaging the BSA film, a voltage of 1.5 V was applied for 30s to produce nanobubbles. Then the same region of the BSA film was again imaged by tapping mode AFM.

Wu, *et al*. [2008] thus demonstrated using AFM that nanobubbles could desorb protein from HOPG surfaces. This provides a means for control of protein adsorption and therefore, may also be used to control cell and bacterial adsorption at interfaces on any conducting substrate. Therefore, this approach may be used to control biocompatibility of materials or for the regeneration of filters that have been clogged with adsorbed materials.

The AFM was used by Hankinso *et al.* [1968] to estimate the difference in adhesion strength between the dissolved and suspended solids in milk samples and on glass surfaces. The influence of the liquid phase of the milk products was minimized by a washing and drying procedure which left a microscopic size film on the substrate. AFM can produce high resolution images of the surface topography of organic/inorganic films and biological materials [Raghavan *et al.,* 2001; Herrmann *et al.* 2004], and has been used to study the molecular structure of various food items [such as by Morris *et al.* 2001; Hodge and Rousseau, 2002; Morris, 2004]. This imaging is achieved by scanning the surface using the pointed tip attached to a cantilever, and the AFM can be operated in the contact and tapping modes. In the contact mode, a predetermined dimension of the residual milk films can be removed from the glass surface. This is sometimes referred to as the scratching AFM mode [Schmutz and Frankel, 1998, 1999]. The tapping mode, on the other hand, provides high resolution 3-D topographic images of the milk films before and after the scratch. This

combination can determine the thicknesses of residual milk samples on glass surfaces. Thus, milk samples with deeper thicknesses represent those that are more difficult to be removed during washing. The objective was to measure and compare the adhesion strength of different milk products on glass surfaces before and after manual washing protocols using contact angle, surface tension and atomic force microscopy analyses.

Schmidt [1997] showed that food proteins are one of the most difficult soils to be removed from food contact surfaces. Handojo *et al.* [2009] used the atomic force microscope to determine the thickness of a thin film of milk left on a drinking glass after a washing protocol. The thickness of this film could be used to estimate the strength of the adhesion and by extension, the difficulty of removing milk from glasses. This study demonstrated that the whole and chocolate milk had the strongest adhesion force on the glass surface. Therefore, in worst case scenarios during washing protocols when milk products are selected to soil drinking glasses, chocolate and/or whole milk should be chosen. In summary, the combination of contact angle, surface tension and AFM could be used to predict the difficulty in removing various milk-based products from the surface of glasses.

2.9 Micromanipulation to quantify the effects of cleaning.

Significant work has been done at Birmingham and elsewhere to study and quantify cleaning processes. The flows within process plant can be predicted using methods such as Computational Fluid Dynamics (CFD) which has been used to predict surface shear stress and thus cleanability, [Jensen and Friis, 2002, Christian and Fryer, 2004]. CFD predictions give reasonable agreement with experimental results, and offer the possibility of being able to design cleanable equipment. CFD does however have the problems that it does not take

account of the physical properties of deposits; if the deposit is cohesive, then the force required to remove it will depend on factors other than fluid shear, such as the thickness and fracture behaviour of the material.

Cleaning processes are difficult to optimize, because of the lack of understanding of the ways in which surfaces clean. Visual observation of cleaning of food deposits, starches and whey proteins [Christian and Fryer, 2004; Christian, 2004] shows, removal of deposit in large chunks with adhesive failure occurring between deposit and the surface, and removal of deposit in small chunks from the surface, with cohesive failure between elements of the deposit. If it was possible to initiate fracture in deposits, for example, by surface modification or fluid shear, then cleaning rates might be increased. Understanding how deposits fracture and clean is thus valuable.

The micromanipulation technique was developed to measure the adhesive strength of different deposits. The method uses a T-shaped probe made of stainless steel chip, dimension 30 x 6 x 1 mm connected to the output aperture of a transducer (Model BG-1000, Kulite Semiconductor, Leonia, NJ. USA) which was itself mounted on a three dimensional micromanipulator (MicroInstruments, Oxon, UK). A schematic of the T-shaped probe, fouling sample and stainless steel disc is shown in Figure 2.4. The gap between the edge of T-shape probe and the substrate can be adjusted from 20 μm to several mm depending on the thickness of deposits and the measurements that are to be taken (Figure 2.5).

The force required to remove the deposit can be measured by drawing the micromanipulation arm across the surface of the deposit, as shown in the video stills of Figure 2.6. A typical curve showing the measured force versus the sampling time is shown in Figure 2.7. The

sample can be pulled horizontally from the initial contact points A, B and C at the centre of the disc and the final edge respectively [Liu, *et al.* 2005]. As shown in Figure 2.7, during pulling, the force measured by the transducer first increases to a maximum (A to B), corresponding to the maximum width of the deposit and then decreases (B to C). The saw-tooth shape of the force curve can be attributed to a series of interactions between the deposit and the surface, i.e. to successive waves of sample deformation and detachment during pulling. The diagram shows typical deposit removal; the deposit was pulled from the surface in one piece. Once the sample is pulled away from the surface, no significant forces are imposed on the probe as shown by C to D in Figure 2.7.

The total work, W (J) done by the applied force, F(t), to remove the deposit may be calculated as the integral of

$$dW = Fdx \qquad \textbf{(2.1)}$$

where the distance dx is vdt, so that

$$W = \frac{d}{(t_C - t_A)} \int_{t_A}^{t_C} F dt \qquad \textbf{(2.2)}$$

where d is the diameter of the circular disc, and t_A and t_C the first and last times at which the probe touched the fouled surface. The apparent adhesive strength of a fouling sample, σ (J/m^2), defined as the work required to remove the sample per unit area from the surface to which it is attached, is then given by:

$$\sigma = \frac{W}{\alpha A} \qquad \textbf{(2.3)}$$

where A (m^2) is the disc surface area of the surface being tested, and α is the fraction of that area covered by the sample measured by image analysis. The relationship between σ and the actual adhesive strength between the surface and the deposit is not clear, as the measured force not only removes the deposit from the surface but also deforms it significantly, as shown in Figure 2.6. The probe speed can vary from 167 μm/s – 2.5 mm/s based on the requirement of the experiment.

Micromanipulation has been used to quantify the forces required to disrupt and remove a baked tomato paste deposit representative of cleaning problems in the food industry [Liu et al, 2006]. Two types of removal behaviour were seen, depending on the height, x, at which the probe is passed above the surface:

- At low height x, the material fractures away from the surface; the force required to remove the deposit increases with cut height and is a function of the surface properties.
- At high x the material fails by deposit–deposit breakage, leaving a layer of material on the surface; here the force required to remove the surface decreases with cut height and is not a function of surface conditions.

Variation in adhesive strength could be measured, and the effects of sample heating time, sample hydration time, surface roughness, medium temperature and the thickness of sample identified. At room temperature, the adhesive strength of tomato paste is smaller than the cohesive strength: this is supported by observations of 'flow cleaning at low temperature, in which the whole of the deposit is removed from the surface at once' [Liu *et al*, 2005].

Tomato paste deposits are removed by (primarily) adhesive failure between deposit and surface. Modifying the surface might thus be expected to have a significant effect on the cleanability of the material. Experiments studied the total removal of tomato paste, baked and unbaked onto modified surfaces which had surface energy values ranging from 15 – 40 mN/m. Figure 2.8(a) shows data for baked and unbaked pastes. In both cases there is a minimum adhesive strength between the surface energies of 20 and 25 mN/m, with an increase in the adhesive strength on either side. The data is scattered, but the minimum is clear in both cases; the change in adhesive strength for the unbaked material with free energy is smoother.

The force measured by the micromanipulation probe is a composite of the cohesive forces between deposit elements and the adhesion to the surface. This is shown explicitly by Figure 2.8(b), which shows data for different thicknesses of unbaked paste. It can be seen:

- As the thickness increases, the total energy required to remove the deposit increases. The increase reflects the need to overcome the cohesive forces between elements of the deposit and to force the deposit to break and flow with the probe away from the sample surface; as the thickness increases, so does this force.
- A similar minimum to that found in Figure 2.8(a), in similar regions of surface energy. However, the minimum becomes more difficult to identify as the thickness of deposit increases, reflecting the decreased contribution of the surface forces to the removal of the deposits as the thickness increases. At the highest thicknesses used, there is no measurable minimum; the curve simply flattens out at the lowest surface energies.

Estimation of cohesive and adhesive contribution.

Figure 2.8 shows that the thickness of deposits has impact on the overall apparent adhesive strength when surfaces with a range of surface energies are employed. The force measured by the probe is a combination of that required to overcome the forces between surface and deposit and that required to disrupt the deposit-deposit bonds. The simplest model for the relationship between the measured work (W) required to remove a deposit of volume (V) from a surface of area (A) is:

$$W = \omega_s A + \psi_v V \qquad \textbf{(2.4)}$$

i.e. the measured W is the sum of the work required to overcome the surface-deposit bonds and the deposit-deposit bonds, where ω_s represents the work (per unit area) needed to overcome the surface bonds and ψ_v is the work per unit volume required to overcome the deposit-deposit bonds. This implies that (i) all of the deposit is removed, and (ii) that all of the deposit is equally deformed (ψ_v is analogous to a plastic work of failure of a material). This equation can be transformed into one that relates the apparent adhesive strength and the deposit thickness

$$\sigma = \omega_s + \psi_v \frac{V}{A} = \omega_s + \psi_v x \qquad \textbf{(2.5)}$$

Figure 2.9(a) and (b) replot the data of Figure 2.8(b) as a function of thickness rather than surface energy. The graphs show that:

- for some data sets, such as those for surfaces of surface energy 20-25.5 mN/m shown in Figure 2.9(a), the data all lie on single straight lines, with a slope of 240 kJ/m^3 and an intercept of 540 mJ/m^2;

- however, where the surface energy exceeds 28 mN/m, shown in Figure 2.9(b), the graph is a curve rather than a line – the higher the surface energy the more curved the data.

A plot of the minimum adhesive strength, obtained either from the lowest energy (for low-thickness deposits) or the plateau value (for higher thickness deposits) as a function of thickness is shown in Figure 2.9(c). This is again a good straight line, with a slope of 260 kJ/m^3, which can be extrapolated to an intercept of 480 mJ/m^2 for zero thickness. This can be regarded as an estimate of the work required to overcome adhesion since the thickness effect has been eliminated – it is slightly lower than the intercept found in Figure 2.9(a), suggesting that it may have some physical meaning.

The success of the simple model is encouraging. In Figure 2.9(a) the slopes of the lines for different surface energies are similar, which would be expected as the simple model assumes that ψ_v the work to fracture and disrupt the deposit is independent of the surface energy. The work per unit volume is in the region of 240~260 kJ/m^3. The intercepts appear to be a function of surface energy. At higher surface energies the model breaks down; it might be expected that under these circumstances a different mode of failure might take place and the simple model is no longer appropriate.

The micromanipulation technique, using a specially designed stainless steel T-shaped probe, has been developed to measure the adhesive strength of food fouling deposits. Variation in adhesive strength can be measured, and the effects of sample heating time, sample hydration time, surface roughness, medium temperature and the thickness of sample identified. The

AFM identifies the relationship between deposits and the surfaces. The AFM combined with the micromanipulation technique will be valuable in measuring surface properties. It will be necessary to study a wider variety of more realistic deposits: it would be interesting to look at deposits in which adhesion is stronger than cohesive forces. Measurement of nano- and micron- scale forces might reveal some interesting information.

2.10 Conclusions

Fouling is formed as a result of a variety of processes. It is essential to observe the responses between different food deposits and surfaces. This will help towards improving cleaning. This information can be used to find suitable cleaning in place (CIP) regimes for different surfaces and equipment. Many studies have been carried out to improve CIP processes, such as work done at Birmingham and described by Aziz *et al.* [2006], Christian *et al.* [2003] and Liu *et al.*[2006], using surface modification and antifouling surfaces, but it is not known in practice whether they give optimal conditions. Low surface energies can reduce adhesion, but more work is needed to understand the effect of surface energy onto fouling removal and its possible effects on cleaning in place (CIP).

The AFM provides a method for detecting nanoscale information. Applications of AFM are potentially widespread in food research; it can see molecular interaction, surface topography, and deposit characterization. The AFM analysis could be used to determine physical, chemical and structural mechanisms of fouling and cleaning. However, the limiting factor in applying AFM to food research is the lack of appropriate methodology for different food deposits. Increasing understanding on AFM technology and developing corresponding

methodology for complicated food deposit systems, could lead to a more detailed understanding of cleaning at macromolecular and nanometre levels.

Micromanipulation experiments have measured the adhesive/cohesive strength of deposits in terms of the work required to remove them from the surface. Different food deposits have been studied. Tomato paste, bread dough and egg albumin deposits have a lower adhesive than cohesive strength, whilst others (whey protein) have a lower cohesive than adhesive strength. A range of coated surfaces has been used to study the effect of surface energy on the force required for removal of tomato deposits. Minima are found, as predicted by theory. A simple material model has been developed and used to analyse the results in terms of the work required to remove the deposit per unit surface area and volume.

Chapter 2 Figures and Tables:

	AFM	STM	TEM	SEM	STEM	VASE	RBF, FM AND CLSM
Color						✔	✔
Compositional mapping		✔					
Film thickness	✔	✔					✔
Friction/ electrostatic/ magnetic force mapping	✔						
Grain structure			✔	✔	✔		
Imaging			✔	✔	✔	✔	
Microstructure							✔
Morphology	✔	✔	✔	✔	✔	✔	✔
Opacity						✔	
Optical properties							✔
Profilometry	✔	✔					
Spectroscopy		✔					
Target binding specificity						✔	
Topographic imaging	✔	✔					

Atomic force microscopy (AFM)
Scanning tunnelling microscopy (STM)
Transmission electron microscopy (TEM)
Scanning electron microscopy (SEM)
Scanning transmission electron microscopy (STEM)
Variable angle spectroscopic ellipsometry (VASE)
Light microscopy (RBF, FM and CLSM)

To characterize surfaces a wide range of experimental tools is available. Some equipment can be used in combination with each other to help create a better picture. Imaging, profilometry and/or quantitative measurements of film thickness can be determined by the equipment in the table above.

	AES	EDS	XPS	EELS	FTIR	FT Raman	UV/Vis
Structural order						✓	
Spectroscopy		✓					
Imaging and mapping	✓	✓	✓	✓		✓	
Imaging						✓	
Identification of unknown compounds						✓	
Elemental composition	✓	✓	✓	✓			
(Except H and He)							
Depth profiling	✓		✓	✓			
Chemical state			✓	✓		✓	
Chemical functional group identification					✓		
Bonding state						✓	
Analysis of surface catalysis and redox reactions *in situ*							✓
Phase transitions						✓	

Auger electron spectroscopy (AES)
Energy-dispersive X-ray spectroscopy (EDS)
X-ray photoelectron spectroscopy (XPS)
High-resolution electron energy-loss spectroscopy (EELS)
Fourier transform infrared spectroscopy (FTIR)
Fourier transform Raman spectroscopy (FT Raman)
UV-Visible spectroscopy (UV/Vis)

Elemental composition and chemical state measurement can be determined by the techniques above.

	(HRTEM)	LEED	XRD
Crystallographic structure	✔	✔	
Grain structure	✔		
Defects	✔		✔
Imaging	✔		✔
Morphology	✔		✔
Crystallographic structure/ orientation/ phase			✔
Crystallite size			✔
Concentration depth profile			✔
Film thickness			✔
Crystallographic structure	✔	✔	

High-resolution transmission electron microscopy **(HRTEM)**
Low-energy electron diffraction **(LEED)**
X-ray diffraction **(XRD)**

Table 2.3:

Microstructure, crystallography, and defects measurements can be determined using the above techniques.

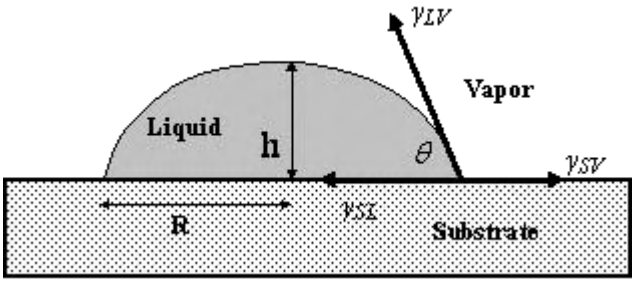

Figure 2.1: Interfacial tensions at the three phase contact line. R is the radius of the drop base and h is the height of droplet. The drop is small enough, thus, the gravity action can be neglected. (Contact angle manual University of Birmingham).

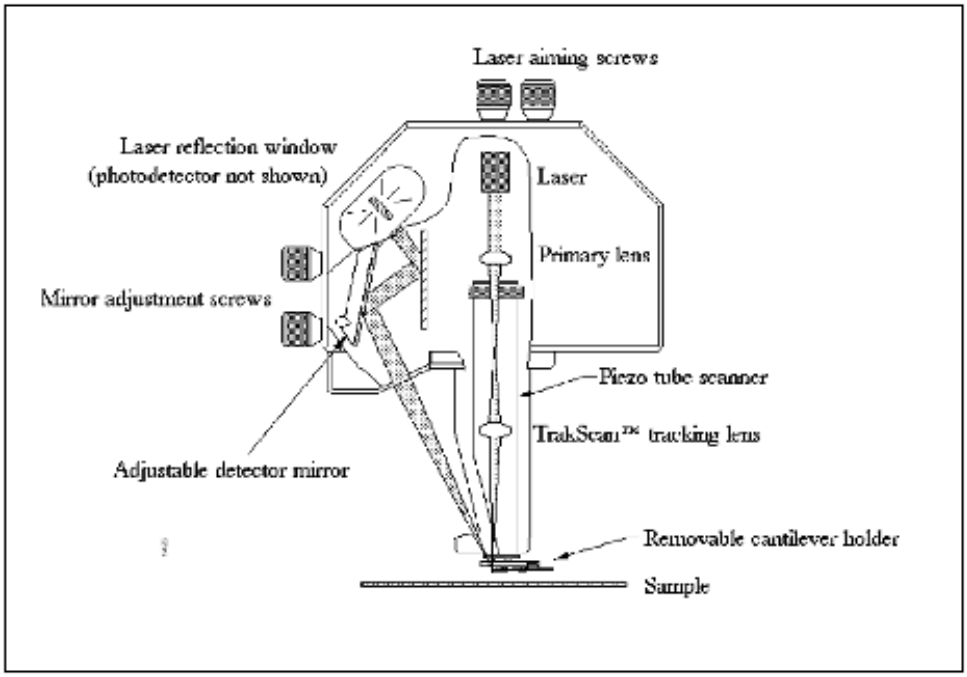

Figure 2.2: Image of AFM Scanner. (Veeco manual Handbook)

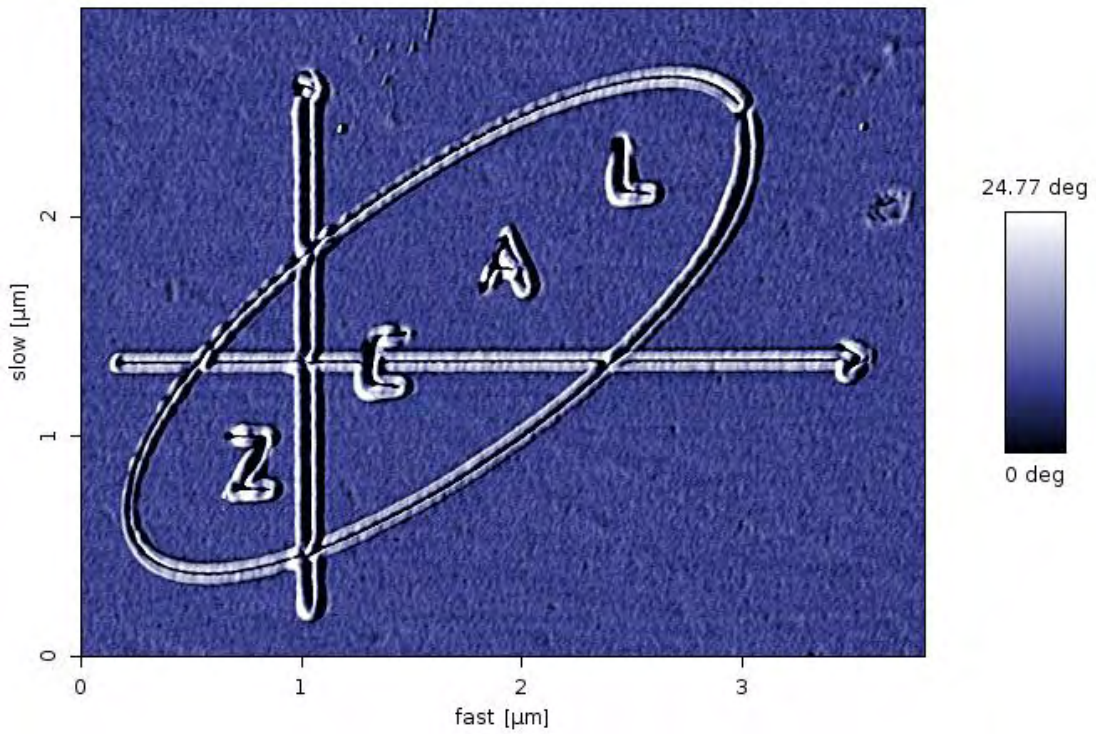

Figure 2.3: Etched logo of project on polycarbonate surface using a diamond probe with the AFM.

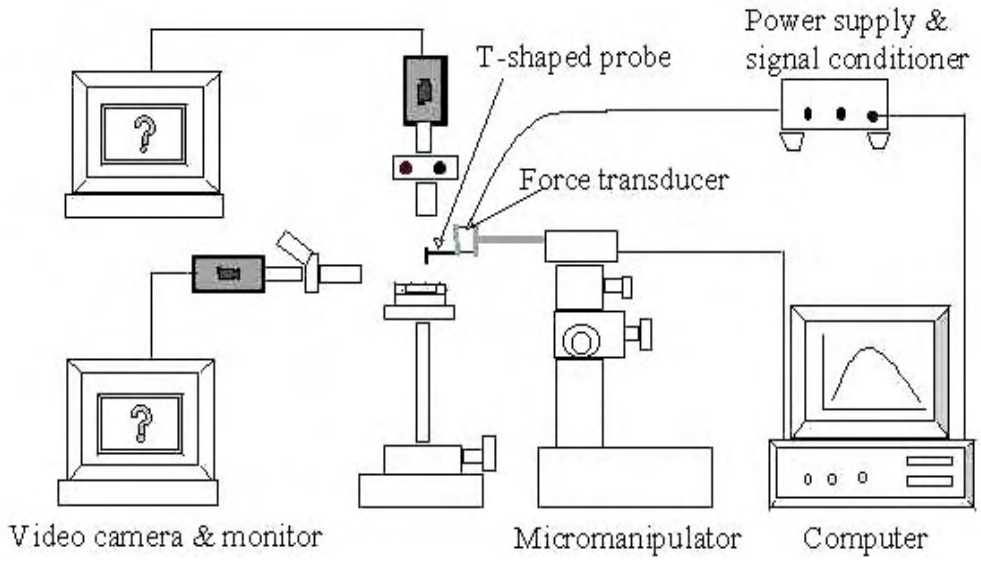

Figure 2.4: Micromanipulation rig at Birmingham University. (Liu *et al*. [2005])

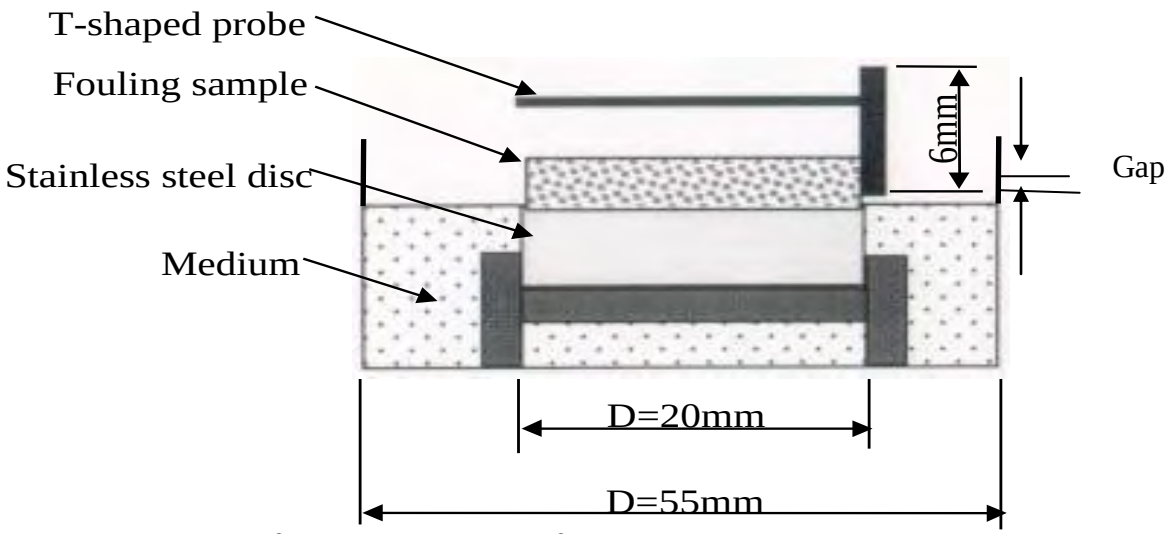

Figure 2.5: Schematic of the T-shaped probe, fouling sample and stainless steel disc. (Liu *et al*. [2005])

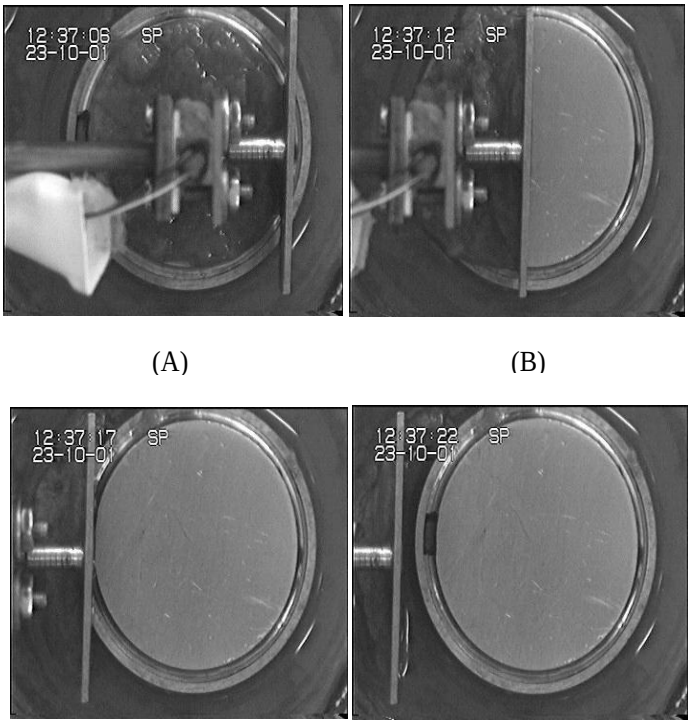

(A) (B)

(C) (D)

Figure 2.6: The sequence of fouling sample pulling processes by the T-shaped probe: (A) → (B) → (C) → (D). (Liu *et al*. [2005])

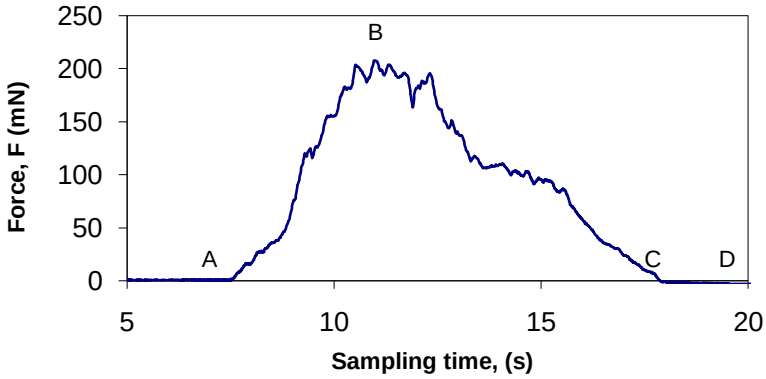

Figure 2.7: Typical curve showing force versus sampling time for pulling a fouling sample. (Liu *et al*. [2005])

(a)

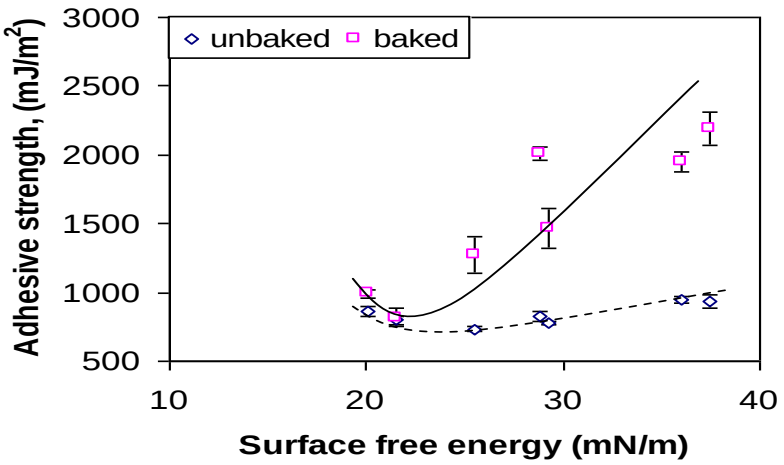

(b)

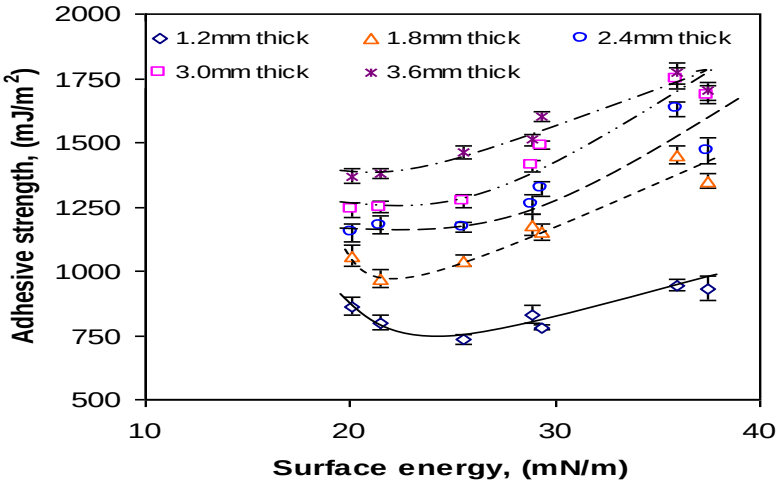

Figure 2.8. Variation of apparent adhesive strength with surface free energy (a) for baked and unbaked tomato pastes; (b) for unbaked tomato paste samples of different thicknesses. (Liu *et al*. [2005])

(a)

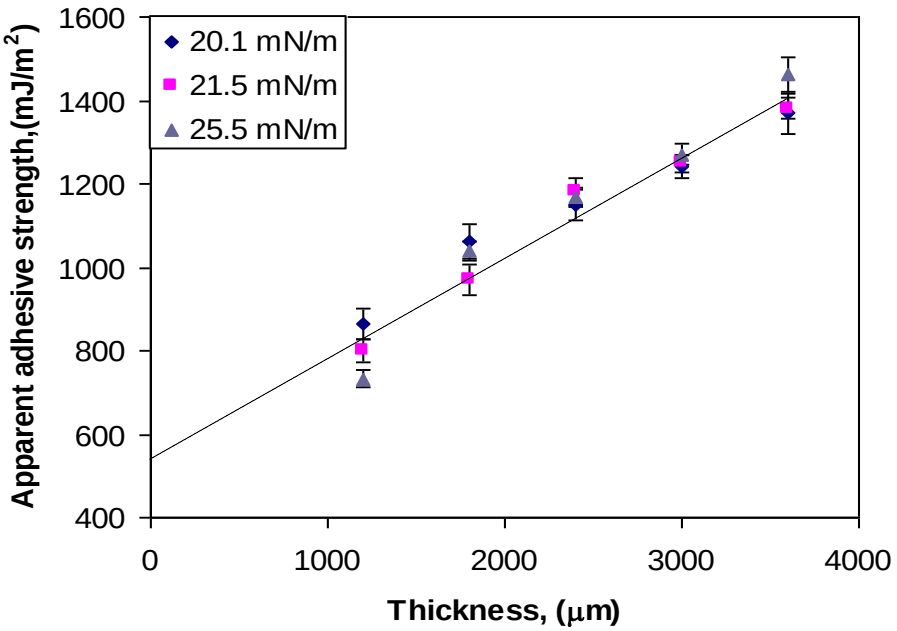
20.1 mN/m
21.5 mN/m
25.5 mN/m
Apparent adhesive strength,(mJ/m2)
Thickness, (μm)
1600
1400
1200
1000
800
600
400
0
1000
2000
3000
4000

(b)

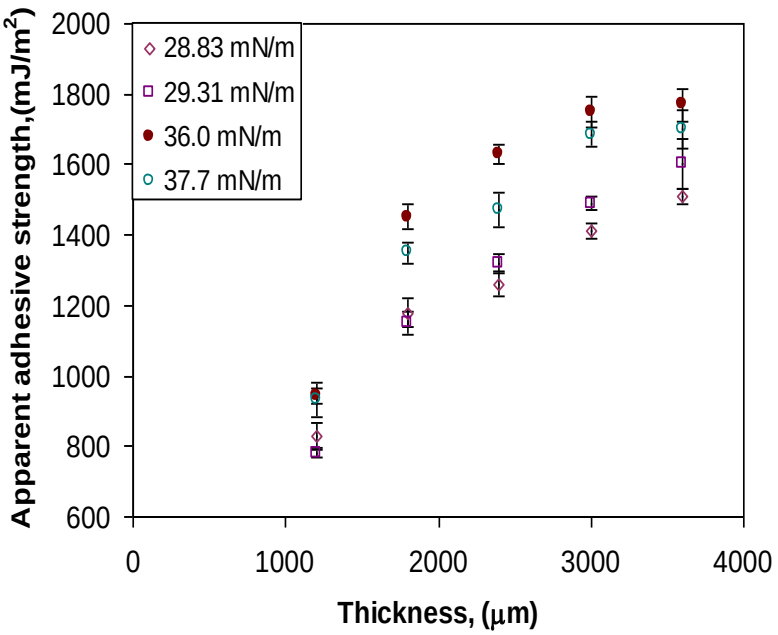
28.83 mN/m
29.31 mN/m
36.0 mN/m
37.7 mN/m
Apparent adhesive strength,(mJ/m2)
Thickness, (μm)
2000
1800
1600
1400
1200
1000
800
600
0
1000
2000
3000
4000

(c)

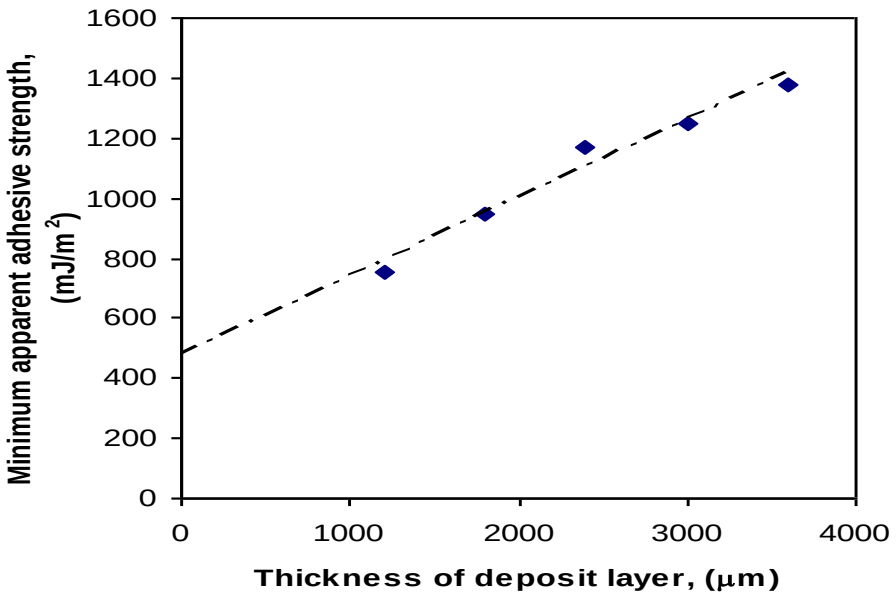

Figure 2.9. Variation of apparent adhesive strength with thickness for unbaked tomato paste deposits (a) onto three surfaces of energy 20-25 mN/m, showing a good fit to a straight line as suggested by equation (2.4), (b) onto four surfaces of energy >25mN/m, showing increasing deviation from linearity with surface energy (c) at the minimum apparent adhesive strength, showing a good straight line (Liu *et al*. [2005]).

CHAPTER 3: MATERIALS AND METHODS.

Introduction and aims.

Chapters 1 and 2 introduced the industrial cleaning problems in the food sector and demonstrated that for both economic and environmental reason it is crucial to optimise protocols. In the two previous chapters, the use of AFM and micromanipulation to investigate cleaning processes has also been reviewed. The aim of this chapter is to a give detailed description of the methods, procedures and materials used to obtain the results that are discussed in Chapters 4, 5 and 6.

In Chapter 2 the use of micromanipulation to study the forces involved in the removal of deposits from surfaces was discussed. Micromanipulation was used to study the removal of four different deposits on different surfaces types: stainless steel, PTFE, glass and ceramic. In Chapter 1 the selection of the deposits to be used in this thesis was defined: Turkish delight, caramel, sweetened condensed milk (SCM) and toothpaste deposits. These are representative of deposits from the food and personal care industries.

Chapter 2 has discussed the deposit failure modes of deposits that take place during cleaning. Three types of removal measurement were possible:

(i) adhesive failure, when deposit is totally removed without deformation by breakage at the surface (such as is seen in Figure 2.6);

(ii) joint mode failure, when the deposit breaks at the surface and the bulk deforms. Both adhesive and cohesive forces are overcome;

(iii) partial removal this mode was sometimes forced upon the deposit by the micromanipulation probe in order to measure cohesive strength of the material, [Liu *et al.* 2005, 2006].

As discussed in Chapter 2 the micromanipulation probe allows the forces involved in removal to be quantified, and it has proven possible to use the method to identify the effects of different surfaces. In a practical cleaning situation, shear forces act on the deposit as a result of fluid flow. Cohesive and adhesive behaviour of deposits will change as cleaning chemical is added or as a result of the hydration by water alone. At some point during cleaning the effects of the flow will predominate and the deposit will be removed.

In this thesis, the usability of the AFM was tested in three different studies:

(i) To find whether different components of a fluid product have significantly effects on the interactions between particles and surfaces, i.e. discovering if it might be possible to change the surface interactions of a material by changing its composition. In Chapter 4 this hypothesis was using the components of toothpaste.

(ii) To study whether nano-scale measurements can predict the behaviour at larger length scales. A series of experiments were carried out using the AFM in which the interaction between deposits and different surfaces was studied and a micromanipulation probe to study the removal of deposits at a micron-mm scale. Chapter 5 reports these results using a series of deposits including SCM, toothpaste, caramel and Turkish delight.

(iii) To study the variation of the adhesion forces with respect to temperature. The initial adhesion of deposits occurs at elevated temperature, so it would be useful to understand how the magnitudes of the forces change with temperature. A Nanowizard (JPK) was used to study the types of adhesion force between surfaces and whey protein at temperatures between 30ºC and 90ºC.

In Chapters 4, 5 and 6, AFM analysis was performed using either a Dimension 3100 Nanoscope AFM (Veeco, UK) or a Multimode (Veeco, UK) at the University of Birmingham or a Nanowizard II AFM (JPK, Berlin) at the JPK offices in Berlin. Each AFM was housed on a vibration isolation table to minimise the effect of ambient noise on imaging and measurement quality. JPK processing software (JPK, Berlin) and Nanoscope V613r1 processing software (Veeco UK) was used. (Figures 3.1, 3.2, 3.5, 3.6)

The aim of this work as whole was to identify whether AFM has a role in fouling and cleaning studies, in terms of being able to relate measured adhesion forces to cleaning parameters. The work consisted of three strands:

(i) Surface characterisation using AFM, which determined the surface parameters of glass, PTFE, stainless steel and ceramic with the aid of imaging in tapping and contact mode. This work revealed adhesion measurement data by doing fluid work between the different surfaces and deposits.

(ii) Adhesion measurements at two length scale to make comparisons between the nano and micron scale.

(iii) Force measurements at low and high temperatures. This work was designed to gain understanding of the aqueous environment and toothpaste ingredient solutions, to see how different components reacted with the surfaces.

AFM and micromanipulation should show similar behaviours at each length scale. In thermal processing thermally labile materials form fouling deposits and adhesion should increase with temperature.

Surface and deposit selection and preparation.

3.2.1 Surfaces

In Chapters 4, 5 and 6 stainless steel 316L, ceramic, glass and PTFE surfaces were used in experiments. The compositions and characteristics of these surfaces have been discussed in detail in Chapter 2. Chapter 2 gave the reason for selecting these materials:

- Stainless steel is widely used in the food processing industry,
- PTFE is used here to see any differences in force interactions or removal behaviours compared to stainless steel. PTFE has been used to identify antifouling or easy- to-clean behaviours in system such as marine fouling, by Callow *et al.* (2002) and in dairy fouling by Rosmaninho *et al.* (2005).
- Ceramic and glass are used in the food industry as hygienic surfaces both to prepare and serve food.

The materials employed were as follows,

(i) Stainless steel 316L round discs 14 mm in diameter and 1-2 mm thick,

(ii) PTFE coated round discs 14 mm in diameter, and 1-2 mm thick,

(iii) Glass (SiO_2) discs 14 mm diameter and 1-2 mm thick,

(iv) Ceramic squares 14 x 14mm and 1-2 mm thick.

All were prepared in-house at the University of Birmingham by the Engineering workshop.

3.2.2 Composition of Deposits.

The cleaning map shown in Figure 1.1 explains the selection of deposits. A wide variety of fouling deposits are formed in industry which require different modes of cleaning. The severity of the fouling deposit differs depending on the material properties. The cleaning map defines three foulant types; low viscosity fluids, high viscosity fluids and cohesive solids. Figure 1.1 was used as the basis of deposit selection for investigations: toothpaste, whey protein, SCM, Turkish delight and caramel were chosen. Biofilms were omitted from the scope of this work owing to the complexity of forming reproducible deposits. The chosen deposits are from Types 1 and 3: those that are removed by water alone (toothpaste) and those that require chemical removal (whey protein, SCM, Turkish delight and caramel). The model foulants have the following compositions (Table 3.1 contains details):

(a) Toothpaste is a suspension of different particles that are approximately 0.5 μm in diameter, titanium dioxide, zinc citrate, sorbitol and silica as well as saccharin, sodium lauryl sulphate and water, (GSK, UK). Each component was mixed with HPLC water, purchased from Sigma Aldrich (UK).

(b) Confectionery deposits:

(i) Caramel contains glucose, sugar, whey powder, palm oil and water, (given by Cadburys, (UK)). Caramel is derived from the caramelisation of sugar by heating it slowly to around 108° C. As the sugar melts and approaches this temperature, the molecules break down to give caramel. The darker colour and the flavour arise due to the Maillard reaction, which occurs between an amino acid and a reducing sugar [Grandhee, *et al.* 1991]. The chemical interaction suggests that high temperature causes the Maillard reaction to occur.

(ii) Turkish delight contains agar, glucose, starch, sugar and water (given by Cadburys, UK). Turkish delight is made from starch, agar and sugar and has a soft, sticky consistency with a gel-like structure. The component are heated up at 100ºC, then dissolved using hot pressurised water at 135ºC.

(iii) Sweetened condensed milk (SCM) contains sugar, butterfat, whey protein and water (given by Cadburys, UK) and is an intermediate in chocolate making. It contains milk from which water has been evaporated and sugar added. This mix is heated to 85-90°C for several seconds. This heating destroys some microorganisms, decreases fat separation and inhibits oxidation. The sugar extends the shelf life, increasing the osmotic pressure, which inhibits microorganism growth. The sweetened evaporated milk is cooled and lactose crystallization induced. The materials are processed in a unit, in which evaporation takes place whilst SCM is sheared and heated. Here fouling deposits forms which are difficult to remove.

(iv) Whey protein (WPC) was prepared by the method defined by Christian [2003]. The WPC solution was prepared from whey powder to have a total β-lactoglobulin concentration of 0.3 wt%. β-lg is the major protein responsible for fouling from whole milk, as discussed by Christian [2003]. The amount of WPC powder used was determined using the following equation:

$$Mass\,of\ \ powder\ added\ (g) = (0.3 \times y) \times \left(\frac{1}{0.0144} \right) \qquad \textbf{(3.1)}$$

Where *y* (l) is the volume of WPC solution to be prepared, and the value 0.0144 arises from the β-lg content of WPC powder. An electronic mixer was used to ensure the WPC solution was homogeneous. The blades of the mixer were completely covered by the water, switched on and the powder added. After approximately 10 minutes the mixer was switched off, removed and wiped clean. The WPC solution was left for a further 20 minutes to de-aerate at 25ºC.

3.2.3 Deposit preparation.

Toothpaste ingredients.

For experiments described in Chapter 4 the following toothpaste ingredients were all dissolved or suspended in HPLC (High Performance Liquid Chromatography) grade water (Sigma-Aldrich, UK), using weight/weight concentrations. These solutions were used to investigate pull off forces using the multimode AFM :

(i) Saccharin [$C_7H_5NO_3S$], 0.3% w/w (Sigma-Aldrich, UK).

(ii) Sorbitol [$C_6H_8(OH)_6$], 65% w/w, (Sigma-Aldrich, UK).

(iii) Sodium lauryl sulphate [$C_{12}H_{25}NaO_4S$], 3% w/w (Sigma-Aldrich, UK).

(iv) Zinc citrate [$Zn_3(C_6H_5O_7)_2$], 3% w/w (Sigma-Aldrich, UK).

(v) Titanium dioxide [TiO_2], 10% w/w (Sigma-Aldrich, UK).

3.2.4 Deposits on surfaces.

The samples in section 3.2.3 were analysed using the Multimode AFM (Veeco, UK) in force mode. The Multimode AFM is designed around a stationary probe. Samples were scanned back and forth beneath the probe. The multimode has an added feature of being able to do fluid work via its fluid cells. With the multimode AFM the systems were studied under liquid conditions in force mode to gain force data, as shown in Chapter 4.

The D3100 AFM works by keeping the samples stationary whilst scanning the probe back and forth above them. Typically, samples were fixed to 1.4 cm metal disks, and then magnetically attached to the top of the scanner tube. The scanner moves back and forth, allowing the probe to extract information such as surface roughness data from the sample surface. With the D3100 AFM, ceramic, glass, stainless steel and PTFE surfaces were studied in contact and tapping mode to obtain surface images and roughness data.

3.2.5 Sample preparation for Micromanipulation.

Chapter 2 has described previous work using the micromanipulation probe of Liu *et al.* [2002]. A series of experiments were carried out where SCM, caramel, toothpaste and Turkish delight were spread onto stainless steel discs and studied using the micromanipulation technique. As detailed in Chapter 2 the technique was developed to measure the adhesive strength of food fouling deposits using a T-shaped probe made of stainless steel chip. The T-shaped probe was connected to the output aperture of a transducer (model BG-1000, Kulite

Semiconductor, Leonia, NJ, USA), which was itself mounted on a three dimensional micromanipulator (MicroInstruments, Oxon, UK).

Micromanipulation experiments in chapter 5 required 0.2 g of Turkish delight, caramel, SCM and toothpaste to be uniformly spread over the whole surface. It was possible to do this with stainless steel, PTFE and glass discs, but not with the ceramic surface as it was too rough and caused very inconsistent results. In all cases the initial thickness of the deposit layer was approximately 0.7 mm. To simulate cooking, SCM deposit layers were baked in a pre-heated laboratory fan oven at 80ºC for 1 hour, the other deposits were used unbaked. The T-shaped probe was then passed at different cut heights over the surface and the force required for removing the food deposits measured. All runs used a probe speed of 1.1 mm/s. A minimum of five measurements were performed per cut height.

3.2.6 Nanowizard II AFM (JPK, Berlin): force measurements preparation.

The Nanowizard II AFM (JPK) (Figure 3.1) has a lateral scan range of 100µm by 100µm and a vertical range of 15µm, which enabled force data for sticky deposits. In Chapter 5 the caramel, Turkish delight, SCM and toothpaste deposits were spread thinly over a glass slide (Agar Scientific). The thickness of the deposits was 50-60µm determined using the AFM optics. The force measurements were taken on the deposits with the Nanowizard II (JPK) AFM. The modified tip was immersed in the deposit and retracted to get force data.

In Chapters 5 and 6 tip modification of the AFM tipless cantilevers was required to enable surface deposit interactions to be studied. Commercially available AFM tips were pre-made

with different attached materials such as silica of different sizes proving very expensive. Here the interest was in forces between deposits and stainless steel, glass and PTFE. Ceramic was omitted as it was too rough and heavy for the tipless cantilever. To obtain a force curve the requirement was a tip with an attached particle of stainless steel or PTFE or glass. As this was not commercially available tip modification was required.

Both components of epoxy glue were mixed together on a glass slide. Another glass slide was taken, a drop of epoxy was spread using a spatula. Using the AFM built-in video system of the Dimension 3100 AFM, the tip was put in contact with 0.2 ml droplet of epoxy glue, then spread over a tipless Si cantilever of nominal length 225 μm. The nominal spring/force constant was 48 Nm^{-1} from Hooke's law and nominal resonance frequency was 190 kHz were used. [This is when maximum cantilever oscillation amplitude occurs (Windsor Scientific, UK)]. After putting epoxy glue on the tip, the glue was allowed to semi-cure, this prevented the glue from spreading all over the surface of interest. The microparticle was attached onto the tip and left for 5 minutes

This allowed an unquantifiable amount of epoxy at the tip apex. Comparing the size of the droplet on the slide before and after touching with the AFM tip, one can estimate the amount of epoxy deposited onto the tip by trial and error. The amount of deposited epoxy should not be more than a few cubic microns. Using the motorised stage on the Dimension 3100 AFM, a 30μm nominal diameter microparticle of stainless steel, PTFE and glass, was first isolated from the powders; the epoxy covered tip was put in contact with the stainless steel (Reade, USA) or glass (Polysciences, UK) microparticles.

Glass and Stainless steel modification tip. Using the AFM built-in video system, the tip was put in contact with 0.2ml droplet of epoxy. A 30μm nominal diameter microparticle of

stainless steel/ glass, was put into contact with epoxy covered tip. After keeping the tip on the stainless steel microparticle for 5-10 minutes, the tip was disengaged and stored for further processing. (Figures 3.3 and 3.4).

PTFE modification tip. For the PTFE tip, a coating of 200 nm of trichloro(3,3,3-trifluoropropyl)silane (Aldrich, UK) was applied to the glass microparticle by vapour deposition. A Petri dish with 5ml of trichloro(3,3,3-trifluoropropyl)silane was put in a glass container. The attached glass microparticle tips were placed on a silica wafer next to the Petri dish. The glass container was sealed air tight, then covered with foil, and placed in a vacuum cupboard. The glass microparticle tips were left for 24 hours before the thickness of deposition was measured using the Dimension 3100 AFM. Using the AFM built-in video system of the Dimension 3100 AFM, the tip was put in contact with a 0.2 ml droplet of epoxy. A 30μm nominal diameter microparticle of PTFE, was put into contact with the epoxy covered tip. After keeping the tip on the microparticle for 5-10 minutes, the tip was disengaged and stored for further processing.

For experiments contained in Chapter 6 the same sample preparation methods were used as in Chapter 5 for preparing stainless steel and PTFE tips for the caramel, whey protein and SCM. The Nanowizard II AFM was attached to a heating stage (JPK, Germany), which heated and controlled the temperature. This was done to obtain force measurements at different temperatures.

3.3 AFM analysis.

3.3.1 Dimension 3100.

Chapter 2 introduced the concept of the Dimension 3100 (Figure 3.2) Scanning Probe Microscope (SPM) which produces high-resolution, three-dimensional images by scanning a sharp tip over the sample's surface. A stepper motor was coupled to a lead screw which translates to the slide with the sample attached. A separate motor drive controlled the height of the microscope and tip relative to the sample's surface. All images were acquired using either a Dimension 3100 AFM (Veeco) or Nanowizard II (JPK). The Nanowizard II AFM operated an 'E' scanner, with a maximum lateral range of 100 µm x100 µm and a maximum vertical range of 15 µm. The Dimension 3100 AFM had a maximum lateral range of 106 µm x 106 µm and a maximum vertical range of 5.5 µm in contact mode, but 2.75 µm in tapping mode.

Contact Mode AFM imaging was performed using triangular 200 µm length thick- legged Au-coated pyramidal-tipped Si3N4 cantilevers (Veeco) with nominal spring constants of 0.12 Nm^{-1}.

Tapping Mode AFM imaging was performed using rectangular 180 µm length pyramidal-tipped Si cantilevers (Veeco) with nominal spring constants of 40 Nm^{-1} and resonant frequencies in the range 250-350 kHz.

The feedback control loop was optimised by increasing the integral and proportional gains in a sequential manner. The values of the integral and proportional gains employed were a function of the tip velocity and the surface chemistry of the sample. For each image acquired, either the deflection signal (Contact Mode AFM) or the amplitude signal (Tapping Mode AFM) was monitored during this process. The optimum values were those which immediately

preceded uncontrolled oscillation of the cantilever, which occurred when the integral and proportional gains were set too high. All images were acquired at scan rates between 0.2-2.0 Hz; each image being composed of 512 x 512 pixels. Height data was acquired for each image, usually accompanied by deflection data for Contact Mode AFM. Amplitude and phase data were also usually acquired in addition to height data for Tapping Mode AFM.

3.3.2 Roughness Analysis.

The roughness of the surfaces was measured at the nanoscale using the AFM. Data was expressed as:

- **RMS (R_q):** The Root Mean Square (RMS) roughness i.e. the standard deviation of the Z values within a given area.

$$\text{RMS} = \frac{\sqrt{\sum_{t=l}^{N} (Z_l - Z_{ave})^2}}{N} \qquad \textbf{(3.2)}$$

- **Z_{ave}** is the average Z value within the given area Z_l is the current Z value, and N is the number of points within a given area.
- **R_a:** is the mean roughness representing the arithmetic average of the deviations from the centre plane.

$$R_a = \frac{\sum_{l=1}^{N} \left| Z_l - Z_{cp} \right|}{N} \qquad \textbf{(3.3)}$$

- $\mathbf{Z_{cp}}$ is the Z value of the centre plane, and Z_i is the current Z value, and N is the number of points within a given area.
- **R max:** The difference in height between the highest and lowest points on the surface relative to the mean plane.

3.3.4 Cantilever spring constants.

The spring constant is a measure of the flexibility of a cantilever and will determine the resolution with which forces can be measured. A number of researchers have investigated the calibration of spring constants, in particular Sader *et al.* [2005], who also studied the frequency response, torsional frequency response, and effect of fluid viscosity on AFM cantilevers. Other publications include that of Senden, *et al.* [2001] and Cleveland, *et al.* [1995], who studied the effect of adding mass to the free end of a cantilever, and Torii, *et al.* [1996] and Gibson, *et al.* [2005], who studied the deflection of an AFM cantilever when pressed onto another cantilever. In each case, the research was done to make sure that the parameters in Hookes law were still appropriate, i.e that force and displacement are linearly related. The calibration of the spring constants of cantilevers was performed before the force measurements were undertaken. This was done by pressing on a calibrated cantilever with a non calibrated cantilever and determining the spring constant. The spring constants calibrations of the cantilevers were performed before the adhesion measurements. This is an important step in ensuring the complete validity of results obtained, and this was done before every experiment.

3.3.5 AFM adhesion measurements

All force measurements were performed using a MultiMode AFM (Veeco) for experiments in Chapter 4 or a Nanowizard II AFM (JPK) for experiments in Chapter 5 and 6.

Multimode AFM (Veeco) experiments were operated in Contact Mode in a liquid environment. This was because experiments all toothpaste ingredients were made up as suspensions or solutions in HPLC water. A glass fluid cell (Veeco) with a silicone O-ring (Veeco) was employed for all force measurements. For each tip/sample combination, the sample was housed in a 5 mL capacity Luer-Lok plastic syringe (Fisher Scientific) prior to introducing the liquid to the fluid cell through clean silicone tubing (Veeco). Prior to performing each measurement, the fluid cell was rinsed thoroughly with HPLC water (Fisher scientific) and dried through absorption of H_2O using a small piece of paper towel (Kimberly Clark).

When filled with sample solution, the fluid cell was sealed off using tubing clips and the system allowed to thermally equilibrate at room temperature (21°C). Equilibration was considered to have occurred once the vertical and horizontal deflection of the cantilever had stopped fluctuating. This generally took between 20-60 minutes and was dependent on the starting temperature of the fluid cell system, sample condition and cantilever. Force measurements were performed using triangular thick-legged Au-coated cantilevers, each with a silica microparticle (6000nm tip diameter) attached at its apex (BioForce Nanosciences, USA), with nominal spring constants of 0.58 N m^{-1}. A range of approach and retract velocities (2,000 nm s^{-1}, 14,000 nm s^{-1}, 20,000 nm s^{-1}) were employed to assess the effect of measurement speed on the measured forces. The real-time data was exported using

Nanoscope v6.12r1 software (Veeco, USA) to provide cantilever deflections, the measured forces were calculated from the monitored deflection relative to the baseline deflection using Hooke's law. The experiments were repeated a least five times to gain accuracy and consistency. An example of a force curve is shown in Figure 3.7. On the curve:

- Point 1: The tip approaches the surface, but is not in contact with it. Non-contact repulsive forces will be observed during the approach phase as an upwards deflection of the cantilever.
- Point 2: Jump-to point. The tip is pulled down onto the surface by attractive forces near the surface.
- Point 3: As the tip is pressed into the surface, the cantilever bends upwards.
- Point 4: As the cantilever retracts from the surface, it relaxes. The tip is still in contact with the surface.
- Point 5: As the cantilever continues to retract from the surface, the cantilever continues to bend downwards as surface attraction holds onto the tip.
- Point 6: Pull-off point. The tip breaks free of surface attraction and the cantilever snaps upwards.
- Point 7: The tip continues to retract from the surface. No further contact with the surface is made.

Real-time 'Deflection-Separation' data was initially acquired for all measurements, displaying the motion of the cantilever relative to the separation distance between the cantilever tip and the surface. Upon completing the measurements, the data was processed off-line in Microsoft Excel to provide mean “pull-off” force values for all tip/sample combinations, as well as

mean values for any electrostatic forces observed during measurements. Forces were obtained by multiplying the distance of cantilever motion by the cantilever spring constant, as described by Hooke's law.

Nanowizard II (JPK) AFM force measurements detailed in Chapter 5 and 6 were performed whilst operating in Contact Mode. Force measurements were performed using modified tipless Si cantilevers of nominal length 225 µm, nominal force constant 48 Nm^{-1} and a nominal resonance frequency of 190 kHz (Windsor Scientific, UK) throughout. Deposits measuring 50µm to 60µm were spread on glass slides using a small spatula. The tip was engaged to the sample and force measurements taken. The tip was cleaned after each experiment in a HPLC water bath. Force over radius normalises the forces so that results from different tips can be compared. Different tip radiuses have a different contact/interaction area with a sample, meaning different forces, (Drucker, *et al.* [1992], Israelachvili, *et al.* [1987]). A minimum of five measurements were performed per deposit surface. The standard errors where calculated by (standard deviation/√n).

JPK processing software (JPK, Berlin) was used throughout for real-time analysis and post-capture image processing. Samples were immobilised onto glass slides (Agar Scientific, UK) using a small syringe needle (Fisher Scientific, UK) prior to AFM analysis. All sample handling was carried out using Dumostar tweezers (Agar Scientific, UK) to minimise the risk of sample contamination.

3.3.6 Thermal Heating Adhesion Measurements.

For experiments and detailed in Chapter 6 the Nanowizard II (JPK) AFM was adapted to include a heating stage. The temperature control limits of the heating stages were between 0ºC and 100ºC. The temperatures used in the thermal heating studies were 30ºC, 50ºC, 70ºC and 90ºC. This was done to see how holding the deposits at different temperatures affected the adhesion strength to the microparticles. JPK processing software (JPK) was used throughout for both real-time analysis and post-capture image processing. Sample preparation the same as in section 3.3.4. The cantilevers were cleaned in between experiments with HPLC water.

3.4 Experimental errors

A number of factors could contribute to experimental errors:

1. *Deposit production*: The natural behaviour of food deposits to lose moisture to the atmosphere can cause change in the deposit structure on the surface before removal. So retaining original moisture is essential as results can vary and cause inconsistency. Error was minimised by doing experiments one at time: deposits were used quickly to minimise any moisture change.
2. *Experimental procedures*: Switching the cantilevers and cleaning the tips during experimental work might have created errors. Generally each deposit was studied with its own cantilever to eliminate contamination between different deposits. In all cases the spring constants of the cantilever were measured.
3. *Cantilever:* The cantilever can become contaminated, and damaged very easily. Accidental breakage of a tip before the end of a set of experiments could cause

inconsistency in results: any breakages would be seen optically using the microscope and the cantilever replaced.

4. *Inaccuracy of equipment:*

- Imaging: There can be errors associated with tip shape; as the tip sharpness can degrade over time. The tip shape needs to be monitored over time to see any wear. [Veeco Instrument Manual]: this was done using the optical microscope as noted above.
- Noise/vibrations levels in the room can cause fluctuation in image resolution.
- Force measurements: Some deviation from the baseline (i.e points 1,7 on Figure 3.7) can occur. This will affect the measured values as there will be uncertainty in the "no deflection" value taken from the data. It is important to know the contact area and penetration depth of the particle into the deposit because the presence of deposit on the cantilever will change its behaviour. Things such as the cantilever tilt and the spring constant of the cantilever are also very important.
- Fluid measurements: These tend to have noisier baselines than air measurements, due to both thermal noise and diffraction of the laser light in the liquid medium. Similarly it is difficult to pick the "zero deflection" point of the data. The presence of contaminants, especially if they adsorb to surfaces, will affect the results so it is important that the cantilevers are clean.

Repeated experiments were done to maintain consistency (the numbers of repeats are noted in the experimental sections) and regular cleaning was undertaken to reduce contamination from deposits. Cantilevers were used consistently for one experiment type. Wear and tear on the cantilever was analysed regularly.

3.5 Conclusions

This chapter has introduced the techniques and procedures followed to obtain the results given in Chapters 4, 5 and 6. These experiments will provide an opportunity to see if the AFM is a viable tool for adhesion measurements of food deposits. Experimental control and systematic results will help to determine utilisation of the AFM and make relevant comparisons with micromanipulation. The AFM tip modification was a novel technique developed to make force measurement in very sticky deposits.

As discussed in Chapter 2 AFM has been used to study modified surfaces. The method established here for tip modification will help to quantify the PTFE surface and make comparisons possible between PTFE type surfaces and fouling deposits.

In Chapter 4, experiments were done to study the different effects of components of fluids that might affect adhesion. This might be useful in defining ways to vary the composition of formulations to minimise fouling or aid of cleaning. This information will help better understanding of the aqueous environment in which AFM adhesion force measurements can be performed and to understand the interactions which may occur between the aqueous environment and toothpaste ingredient solutions.

Chapter 5 introduced AFM experiments that can be related to micromanipulation data, to see if nano and micro-scale measurement can be related. To study the interactions between interfacial measurements at two length scales would be valuable in developing ways to test surfaces for their fouling potential and cleanability.

The experiments in Chapter 6 are to further develop the studies and experiments done in Chapter 5. The effects of temperature on fouling and cleaning from a range of materials which are known to be thermally labile as cleaning rates are known to be temperature-dependent.

Chapter 3 Figures and Tables:

Figure 3.1: Nanowizard II AFM (JPK Berlin).

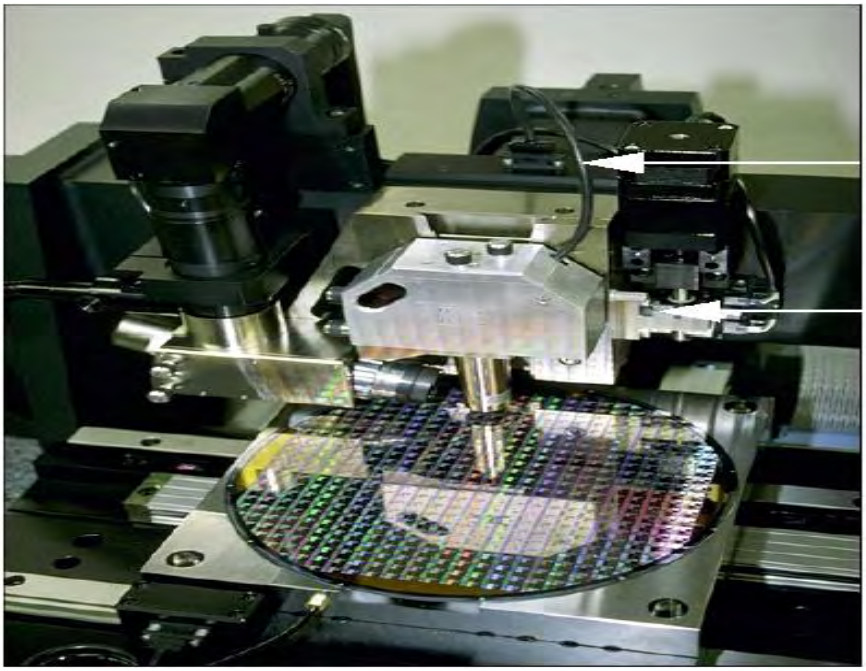

Figure 3.2: Dimension 3100 AFM (Veeco, UK).

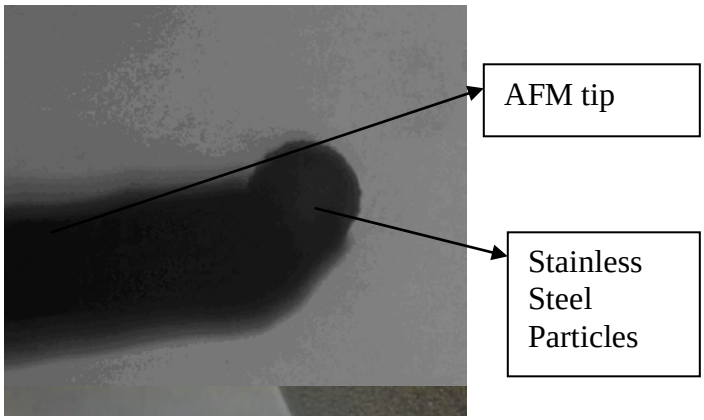

Figure 3.3: Stainless steel particle attached to AFM Tipless cantilever, from the AFM optical viewer.

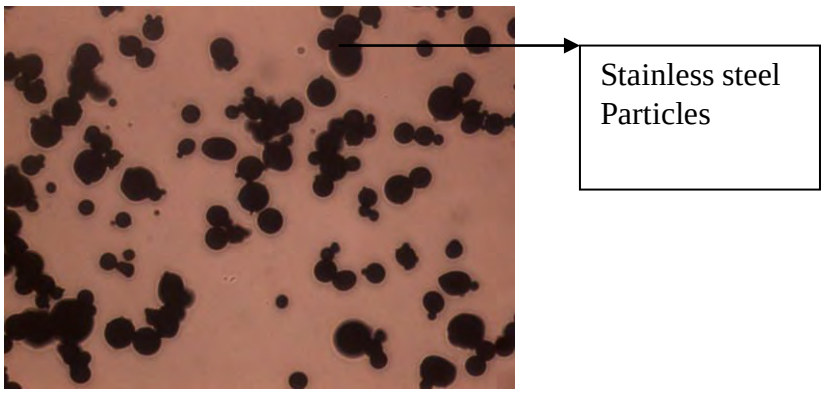

Figure 3.4: Stainless steel particles snapshot on the glass slide from the AFM optical viewer.

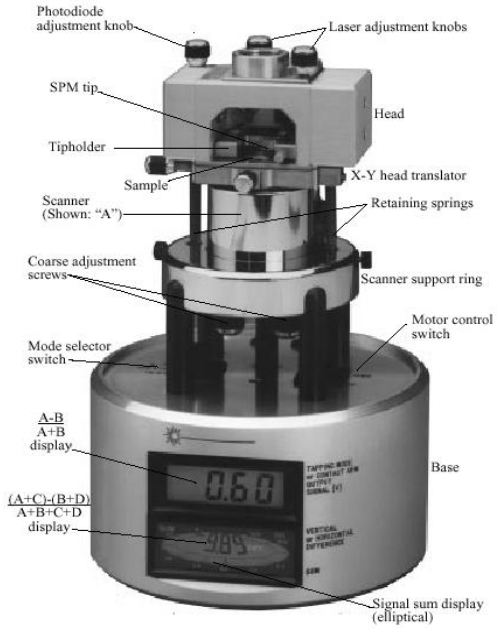

Figure 3.5: Multimode Mode AFM (Veeco, UK).

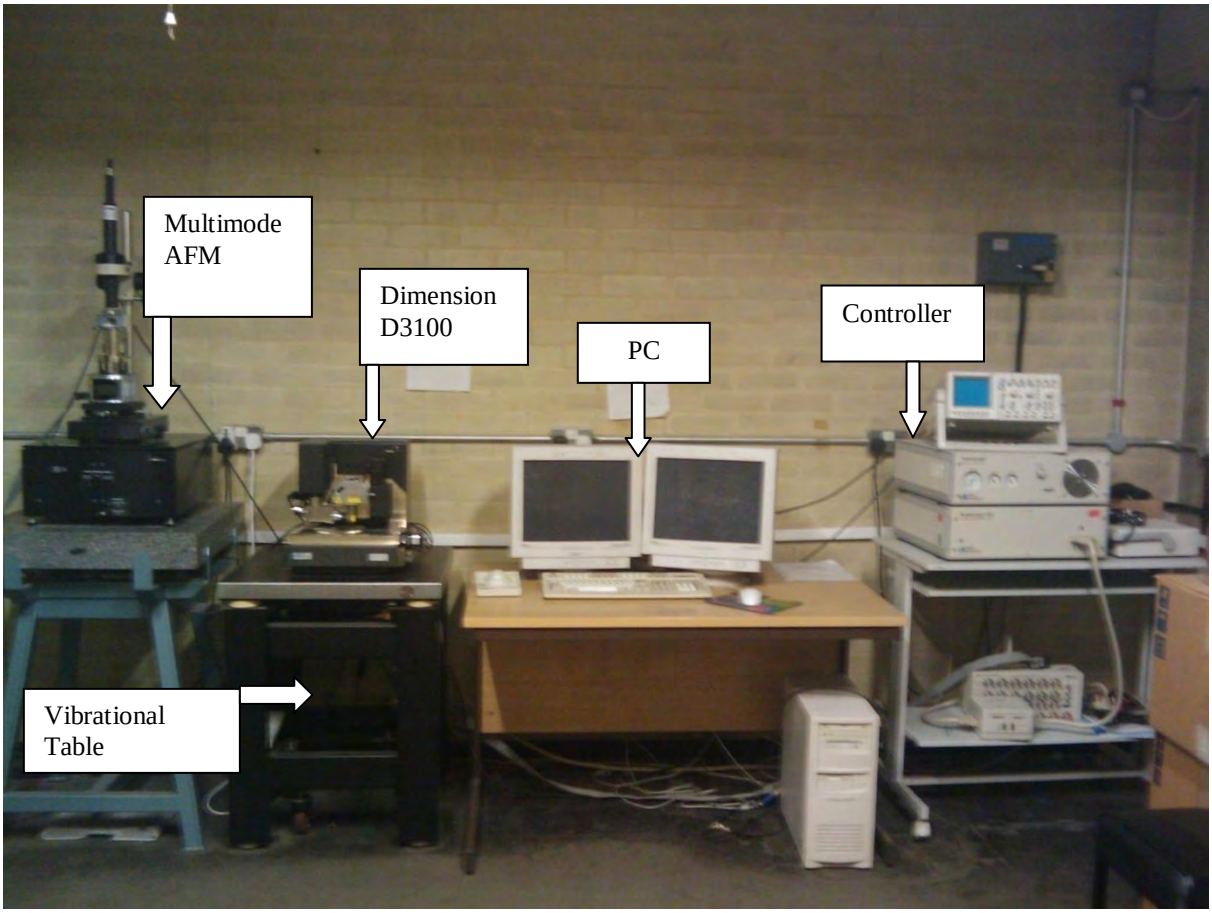

Figure 3.6: The AFM set up at the University of Birmingham.

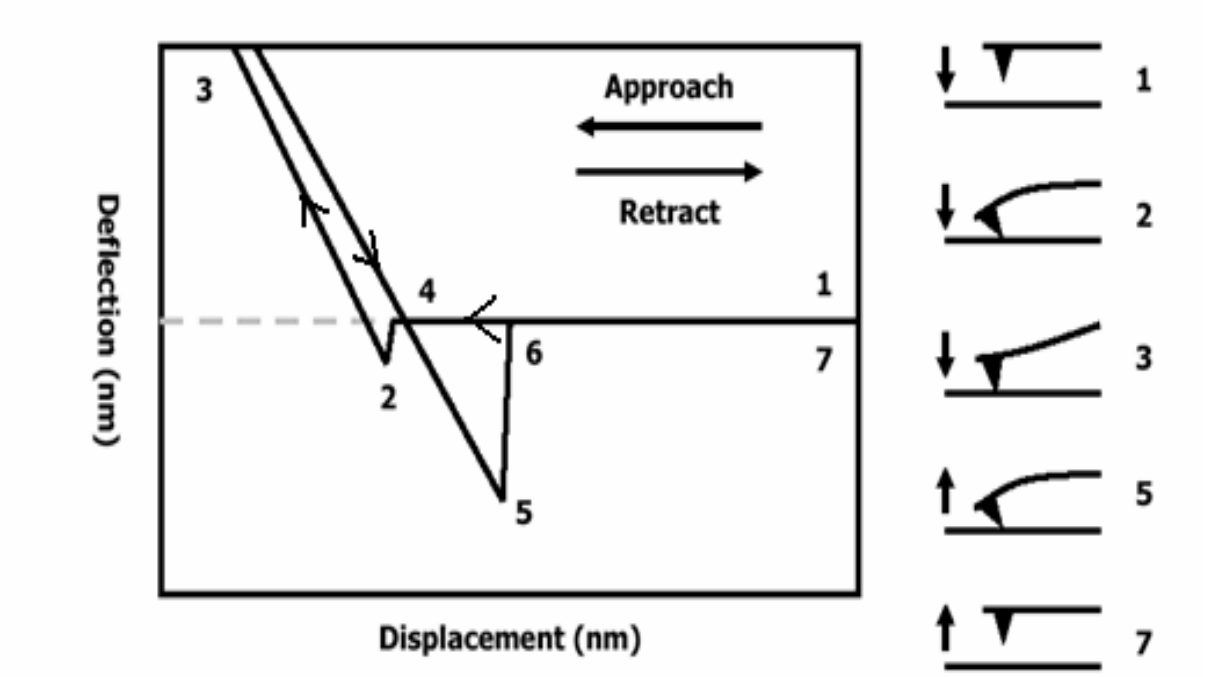

Figure 3.7: Hypothetical AFM deflection-displacement force curve. It is based on a diagram from the Veeco, MultiMode™ AFM Instruction Manual.

CARAMEL	Weight %	TURKISH DELIGHT	Weight %	SCM	Weight %	TOOTHPASTE	Weight %
Water	8.4	Water	19	Sugar	50	Saccharin	0.3
Glucose D 42	26.7	Glucose 63DE	55.3	Butterfat	7	Sorbitol	65
Sodium chloride	0.3	Agar	0.6	MSNF (milk solid not fat)	17	Sodium lauryl sulfate	3
GMS 30%	0.3	Starch	0.7	Water	26	zinc citrate	3
Sodium carbonate	0.1	Sugar	24.3		0	Titanium dioxide	10
Whey powder	5.1		0		0	Water	18.7
Palm Oil	11.3		0		0		0
Glucose D II 42	32.2		0		0		0
Granulated Sugar	5.1		0		0		0
ISO Glucose	10.3		0		0		0

Table 3.1: Ingredients and composition of SCM, caramel, Turkish delight and toothpaste.

CHAPTER 4: Surface and deposit characterisation and toothpaste ingredients force measurements.

The objective of the work presented in this chapter is to obtain better understanding of the aqueous environment in which AFM adhesion force measurements can be performed and to understand the interactions which may occur between the aqueous environment and toothpaste ingredient in solution. Chapters 1 and 2 gave a brief background to this issue.

It is important to have an understanding of the aqueous medium in which adhesion interactions occur. The properties of the medium will affect adhesion as they affect the properties of surfaces that come into contact in any medium [Burgess, 1999]. Force measurements using AFM between two surfaces in different solvents or solvent mixtures such as seen in Kanda, *et al.* [1999] and in aqueous media of different ionic strengths [Drucker, *et al.* 1992 and Carambassis, *et al.* 1999] exhibit different adhesion forces [Clear, *et al.* 1999]. The nature of the surfaces between which measurements are made is also an important consideration; as this can alter or cause different interactions. For example, the preferential orientation and arrangement of ions and solvent molecules at surfaces, as well as moieties present in the terminal region of the surfaces affecting the properties of a system. Surface

roughness and surface charge will also affect the adhesion between two surfaces. Surface charge occurs through the ionisation or dissociation of surface groups, such as the deprotonation of carboxylic acid groups, or through the adsorption of ions from solution onto a previously uncharged surface.

Chapter 3 has discussed methods that have been developed to quantify surface interactions between stainless steel 316L, ceramic, glass and poly(tetrafluoroethylene)-coated stainless steel with a series of components using the atomic force microscope (AFM). The interactions between surfaces of stainless steel 316L, ceramic, glass and poly(tetrafluoroethylene)-coated stainless steel materials were tested in different suspensions of toothpaste ingredients. Both soluble compounds and insoluble colloidal particles were introduced to the aqueous medium using a fluid cell. The surface roughness was determined using the AFM. Surface free energies were estimated from contact angle experiments using drops of water and sorbitol. Scanning electron microscopy (SEM) and AFM images were taken to identify the microstructures of surfaces and deposits. Visualising the microstructure help characterise the surfaces and give a broader understanding of what is happening on the surface layer. Differences in surface interaction should help in characterising the system and reveal how different ingredients affect fouling and cleaning.

4. Surface characterisation.

4.1. Surface topography and roughness.

Roughness analysis of the four surfaces was undertaken using the Dimension 3100 (Veeco) AFM, to investigate if there is any correlation between surface roughness and adhesion

interaction. As discussed in Chapter 2 the roughness of a surface is critical when choosing surfaces for cleaning equipment. Table 4.1 shows roughness measurements of ceramic, stainless steel 316L, glass and PTFE measured using AFM. AFM topographic images of the four materials investigated here are presented in Figure 4.1.

- Figure 4.1(a) shows the surface layer of PTFE in a 100µm by 100µm scan, showing very little surface imperfections. The surface roughness was measured as 75.6 nm. The image shows the surface height and that the structure is flat and uniform.
- Figure 4.1(b), shows that the stainless steel surface had an uneven surface layer, with a significant amount of surface imperfections in a 100µm by 100µm scan. The roughness of stainless steel was measured as 230 nm. The surface height shows the grain structure to be randomly distributed.
- Figure 4.1(c) shows the surface height of ceramic. This is the roughest of the four surfaces (RMS value of 485 nm compared with that of the stainless steel of 230 nm) and has a very uneven surface, shown by the colour range in a 100µm by 100µm scan.
- Figure 4.1(d) shows the surface height of glass, with little imperfections, in a 100µm by 100µm scan and surface roughness of 5.36 nm.

The roughness scans were taken at ten different points on the surfaces to give reproducible and accurate data. The Nanowizard software package (Veeco) was used to obtain the surface roughness information.

4.2 Scanning electron microscopy (SEM)

Scanning electron microscopy (SEM) involves the bombardment of a sample with high-energy electrons, whereby the low energy secondary electrons and high energy backscattered electrons emitted from the sample reaching the detector will vary as a result of sample geometry. This allows an image of the sample to be produced. If the surface is not electrically conductive it must be coated with a thin metallic layer (for example, Au deposited by sputtering). SEM can also be used to image patterns and chemically different domains on surfaces.

SEM images of ceramic, stainless steel, PTFE and glass discs were acquired using a XL30 ESEM FEG (University of Birmingham), operating at pressures of 10^{-4} mbar using a 20 kV electron source gun. The samples were prepared for SEM imaging by sputter coating them with Au in an Agar automatic sputter coater (Agar Scientific).

SEM images of the ceramic, stainless steel, PTFE and glass surfaces were taken using the procedures described. The SEM images in Figures 4.2 show the characteristic depth of the four surfaces of interest at 50 μm scan size. Figure 4.2(c) shows the ceramic surface which is porous with rough surface imperfections at length scale of 50 μm. Figure 4.2(d) shows glass to be smooth with little imperfections, as silica is bound together tightly. Figure 4.2(a) shows the PTFE polymer chain is tightly bound which results in a smooth surface with no or little imperfection on the surface layer and Figure 4.2(b) shows the grain structure of stainless steel with surface imperfections making it rougher than glass and PTFE appears crystalline.

4.3 Measurements of contact angles.

A Goniometer (of University of Birmingham) (Figure 4.3) was used to measure the contact angles of different surfaces. Contact angle measurements allow the wetting behaviour of a surface to be assessed in a relatively short time under ambient conditions. The wetting behaviour of the liquid droplet on a solid surface can be measured by taking a drop of water (or liquid of interest) from a syringe, and passing it through the plastic tubing the surface of interest. The surface is placed on the staging deck of the goniometer and the dynamic contact angle is measured. As the droplet volume increases the advancing contact angle of the surface is measured. As the surface droplet volume decreases the receding contact angle of the surface is measured. [Chen *et al.* 1991]

The equilibrium contact angles of water (HPLC, Sigma) and 65% w/w sorbitol solution were measured on glass, PTFE, ceramic and stainless steel. This procedure was repeated five times. The surfaces were pre-soaked in hot water with ammonia solution to keep them clean. The surface tension of water (HPLC grade) is known to be 0.072 Nm^{-1} [Sigma]. Glass is hydrophilic with an affinity to water, and has low surface energy with a drop of water. However, with a drop of sorbitol solution the surface energy is larger. Figure 4.4(a) plots the contact angles for the two systems and the four surfaces. In two cases (PTFE and glass) the contact angle is greater than 90º. The image of a typical drop can be seen in Figure 4.5. It is possible to extract surface energy data from contact angle measurements. Equation 4.1 relates the solid-vapour interfacial surface energy, γ_{SV}, the solid-liquid interfacial energy and γ_{SL} the liquid-vapour energy (i.e. the surface tension), γ by $\theta_{C,}$ is the equilibrium contact angle.

$$0 = \gamma_{SV} - \gamma_{SL} - \gamma\cos\theta_c \qquad \textbf{(4.1)}$$

This assumes a perfectly flat surface. In many cases surface roughness and impurities cause a deviation in the equilibrium contact angle from that predicted by Young's equation. The equation defines contact angles in terms of surface energies. If water is very strongly attracted to the solid surface the droplet will completely spread over the solid surface and the contact angle will be close to *0*°. In other situations:

- Less strongly hydrophilic solids will have a contact angle up to 90°.
- On highly hydrophilic surfaces, water droplets will exhibit contact angles of 0° to 30°.
- If the solid surface is hydrophobic, the contact angle will be larger than 90^{o}.
- On highly hydrophobic surfaces the surfaces have contact angles as high as 150° or even nearly 180°.

Images of contact angle drops on the surfaces are shown in Figure 4.5. The drop is immersed on each surface and the angle is measured.

Even on a perfectly smooth surface a drop will assume a wide spectrum of contact angles between the highest (advancing) contact angle, θ_A, and the lowest (receding) contact angle, θ_R. The equilibrium contact angle (θ_C) can be calculated from θ_A and θ_R as was shown by Tadmor [2004]:

$$\theta_C = \arccos\left(\frac{r_A \cos\theta_A + r_R \cos\theta_R}{r_A + r_R} \right) \qquad \textbf{(4.2)}$$

where, $$\gamma_{sv\text{-}} - \gamma_{sv} = \gamma\cos\theta_c$$

$$\gamma_{sv—}\gamma_{sv} + \gamma = \gamma(1+\cos\theta_c)$$

$$r_{\mathrm{A}} = \sqrt[3]{\frac{\sin^3\theta_{\mathrm{A}}}{2 - 3\cos\theta_{\mathrm{A}} + \cos^3\theta_{\mathrm{A}}}} \qquad \textbf{(4.3)}$$

and,

$$r_{\mathrm{R}} = \sqrt[3]{\frac{\sin^3\theta_{\mathrm{R}}}{2 - 3\cos\theta_{\mathrm{R}} + \cos^3\theta_{\mathrm{R}}}} \qquad \textbf{(4.4)}$$

The contact angle can also be used to determine an interfacial energy (if other interfacial energies are known). Equation (4.1) can be rewritten as the Young-Dupre equation:

$$\gamma(1 + \cos\theta_{\mathrm{C}}) = \Delta W_{\mathrm{SLV}} \qquad \textbf{(4.5)}$$

where ΔW_{SLV} is the adhesion energy per unit area of the solid and liquid surfaces when in the medium V.

Figure 4.4(b) shows the surface energies calculated from equation (4.5). The surface energies of the species whose contact angles are > 90º are low, as here $\cos\theta_c$ is negative. The data for water and sorbitol are in all cases similar apart from on glass, were the water has a very low surface energy of water is very low, but for sorbitol is much larger. [Chen *et al.* 1991]

4.4 Characterisation of surface interactions for toothpaste ingredients.

Toothpaste is a multi-component particulate material which contains titanium dioxide, zinc citrate, saccharin, sorbitol and sodium lauryl sulphate materials. Each component has a different role. Each component of toothpaste will affect the environment of the surface in different ways. Silica particles are used in toothpaste as an abrasive material. Hence silica was chosen as one of the particles of interest. The role of saccharin in toothpaste is to act as a sweetener. Sorbitol retains moisture, sodium lauryl sulfate causes the foaming action upon cleaning, zinc citrate is the antibacterial agent and titanium dioxide gives the colour. AFM was employed to provide information on the interaction forces between a colloidal silica microparticle and the four surfaces of interest, in presence of the toothpaste ingredients listed above. These experiments were performed to help understand the forces in cleaning behaviour of toothpaste on different surfaces, and to help make comparisons between micro and nano meter scale forces. This study will help to identify critical components and may even help change the formulation of toothpaste. It was not possible to use the D3100 AFM as the z-range was too small. Thus the Multimode AFM was used to perform fluid force measurements. Chapter 3 gave the detailed procedure and methods.

4.4.1 AFM Force measurements in fluid environments.

Force measurements were performed using a Multimode AFM (Veeco). The materials and methods employed are discussed in Chapter 3. Pull-off forces were measured for the interaction between the silica microparticle and the four surfaces: stainless steel, PTFE-coated stainless steel, glass and ceramic material surfaces in the presence of the different aqueous media.

Force curves obtained are shown in Figures 4.6 (a,b,c,d,e). The results are presented in Table 4.2, which shows the pull-off forces between silica microparticles and the toothpaste components in the presence of aqueous media. There was negligible variation in the measured pull-off force with velocity for all systems. Hence the data presented in Table 4.2 are for the force measurements performed at 14,000 nm s^{-1}. Figures 4.7(a,b,c) demonstrate that there was negligible variation of the force curves at different velocities: 200 nm s^{-1}, 2000 nm s^{-1} and 14,000 nm s^{-1}, which suggest the rate of change of position does not affect adhesion.

The product of an AFM adhesion force measurement is a plot of cantilever deflection versus cantilever displacement (deflection-displacement). The deflection-displacement plot shows the movement of the AFM cantilever relative to its distance from the surface with which it is intended to interact. The pull off forces between the silica microparticle and the surface materials will be determined by the surface chemistry of both the silica and the material, as well as the interaction of the surfaces with the aqueous media. All experiments were repeated a least five times.

In the presence of saccharin solution, sodium lauryl sulphate solution, zinc citrate solution and titanium dioxide suspension, no pull-off forces were measured for the four surfaces. In fact a repulsive interaction was generally observed. Figure 4.6(a) shows an example of such a repulsive interaction plot. It shows the cantilever deflection versus cantilever displacement in zinc citrate solution when no pull off force is was seen. The data suggested that the polyanionic charge on the silica surface (which will be deprotonated in aqueous solutions such as zinc citrate and the other solutions mentioned above) dominates the interaction. Stainless steel, glass and ceramic surfaces all present oxygen-rich surface chemistries in the form of chromium oxide, silicon dioxide and aluminium oxide.

Figure 4.6(b) shows an example of a ‘‘hydrophobic effect’’ deflection-displacement curve, in which a ±0.09 mNm^{-1} adhesion force was seen to result from the interaction between the silica attached tip and stainless steel surface in presence of HPLC water. This interaction also occurred with the ceramic surface, as shown in Table 4.2, with an adhesion force of ±0.01 mNm^{-1}. It has previously been established that for hydrophobic surfaces immersed in water, an attractive force exists that cannot be accounted for by dispersion forces alone [Mantel, *et al*. 1995]. The origin of the hydrophobic effect shown in Figure 4.6(b) is often believed to be changes in water structure adjacent to hydrophobic surfaces, which are entropically unfavourable and impose a new, more ordered structure on the water molecules. This gives rise to an attractive force between the silica and the surfaces. In water, both the ceramic and stainless steel surfaces exhibit a long-range attractive interaction with the silica microparticle and this interaction is indicative of a hydrophobic force. The oxide-terminated stainless steel and ceramic surface could give rise to such a force. The glass surface would not be expected to and indeed does not as the glass surface is terminated with silicon hydroxide moieties.

One component of the toothpaste sorbitol solution. shows strong adhesive interactions of 1.70mNm^{-1} between stainless steel surface discs using the silica microparticle, as shown in Figure 4.6 (c) here the tip is pulled towards the surface in an attractive regime. Sorbitol is used as humectant in many types of products for protection against loss of moisture such as in toothpaste, mouthwash, chewing gum, cookies and cakes. It is also used in glues and sticky tapes to help retain adhesive properties [Britten 1998]. Of the four surfaces only stainless steel exhibited an adhesive interaction with the silica microparticle in sorbitol solution. This is surprising (Table 4.2) as PTFE might not have been expected to display an adhesive interaction given its hydrophobic surface chemistry. The oxygen-rich surfaces of the stainless steel, glass and ceramic, (see Chapter 2) might have been expected to demonstrate similar

adhesive interactions. However the hydrophobicity, surface energy, and roughness of the surface can all alter the behaviour of an individual surface interaction.

Figure 4.6 (c and d) shows the different AFM force plots for the interaction of stainless steel and PTFE with sorbitol. The behaviour of the curves relates to the surface interactions between the sorbitol drop and the PTFE and stainless steel respectively. The interaction between sorbitol and stainless steel is significant, and would not have been predicted by the macro-scale contact angle measurement. The data suggests that effects may manifest at the nanoscale, which are not predicted by the macro-scale measurements of conventional contact angle. The contact angles suggest that stainless steel has a higher surface energy compared to PTFE, with sorbitol and water. Force curves of PTFE shows no attraction with water or sorbitol as PTFE has lower surface energy compared to stainless steel. Further work on the adhesion of toothpaste was carried out and is discussed in the next chapter.

4.5 Conclusion

AFM can be used to measure attractive or repulsive forces over micron-scale separations with sub-nanometre sensitivity between a probe tip or colloidal particle and a sample surface, elucidating local chemical and mechanical properties like adhesion, and even thickness of adsorbed molecular layers or bond rupture lengths.

Atomic force microscopy has been employed to measure the adhesive interactions between a colloidal silica microparticle and stainless steel, PTFE-coated stainless steel, glass and ceramic surfaces, in the presence of a number of solutions and suspensions of ingredients found in commercially available toothpaste. In the presence of most ingredients a repulsive behaviour was observed, indicative of ionic double layer effects, as the silica microparticle will be charged in aqueous solution. A hydrophobic effect-type attraction was observed for the interaction between the silica microparticle and the stainless steel and ceramic surfaces.

The four different types of materials chosen for study were stainless steel, ceramic, glass and PTFE. Results showed:

- Ceramic and stainless steel surfaces were substantially rougher than the PTFE and glass surfaces.
- Contact angle measurements showed that the different surfaces behave differently with a drop of water and sorbitol.
- AFM found different types of behaviour in the presence of saccharin solution, sodium lauryl sulphate solution, sorbitol, zinc citrate solution and titanium dioxide suspension.

Chapter 4 Figures and Tables:

Figure 4.1 (a): PTFE

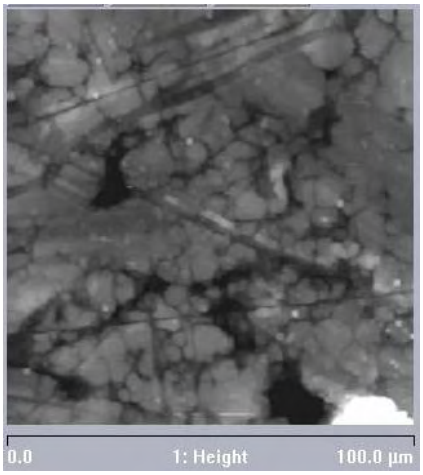

Figure 4.1 (b): Stainless steel

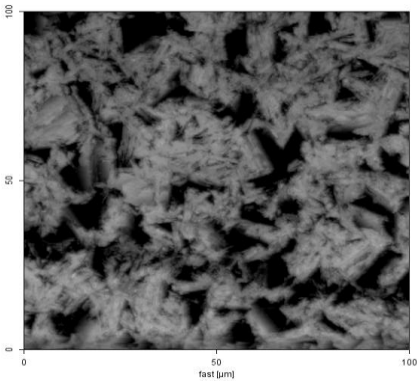

Figure 4.1 (c): Ceramic

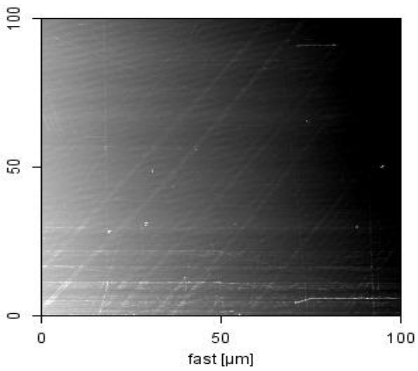

Figure 4.1 (d): Glass

Figure 4.1: AFM topographic scans of the four surfaces (100µm by 100µm Scan). The ceramic and stainless steel are rougher than PTFE and glass. This is seen by the imperfections in the images. The darker colour represents uniformation of the surface, the lighter colour represents surface composition or defects.

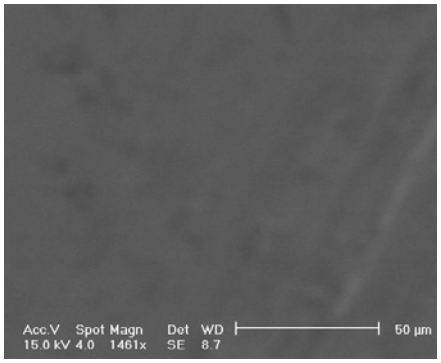

Figure 4.2 (a): PTFE

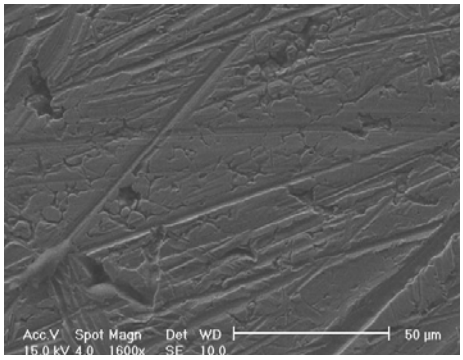

Figure 4.2 (b): Stainless steel

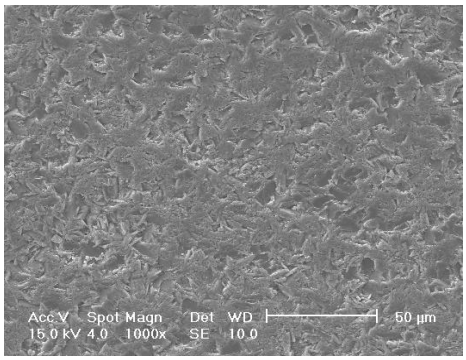

Figure 4.2 (c): Ceramic

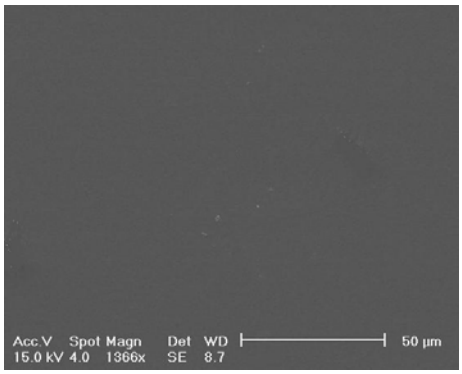

Figure 4.2 (d): Glass

Figure 4.2: SEM images of the microstructure of the four surfaces of interest at 50µm scan size. Ceramic and stainless steel show increased roughness compared to PTFE and glass.

Figure 4.3: Goniometer used for contact angle experiments. (Kruss website).

Figure 4.4: Contact angles

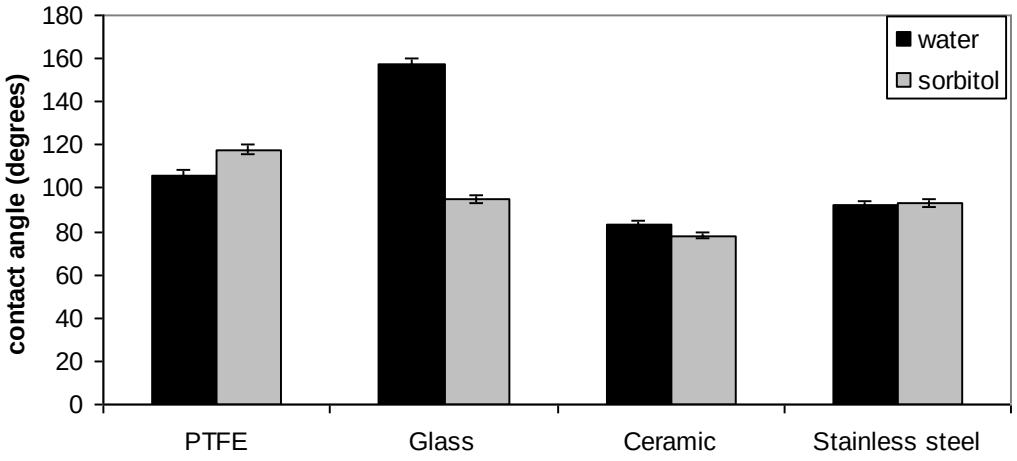

Figure 4.4 (a): Contact angles on the four surfaces with water and sorbitol, repeated least five times.

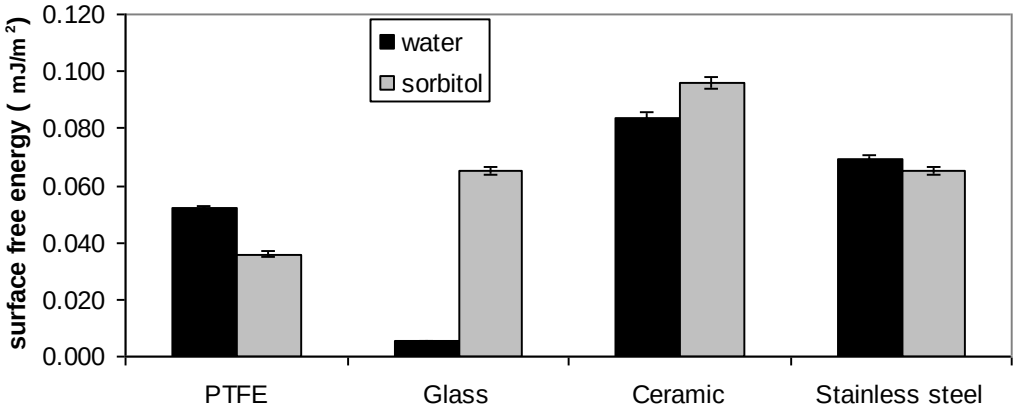

Figure 4.4 (b): Surface energies of sorbitol and water on the four surfaces, calculated from Young's equation.

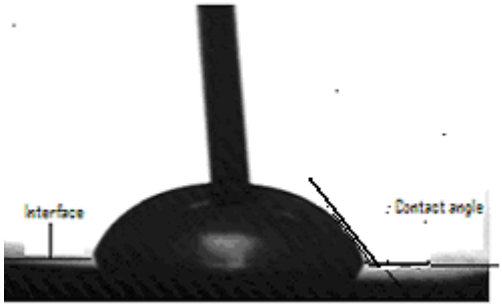

Figure 4.5 (a): Water drop on ceramic (83º)

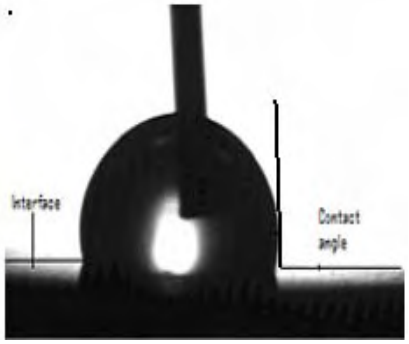

Figure 4.5 (b): Water drop on glass (92º)

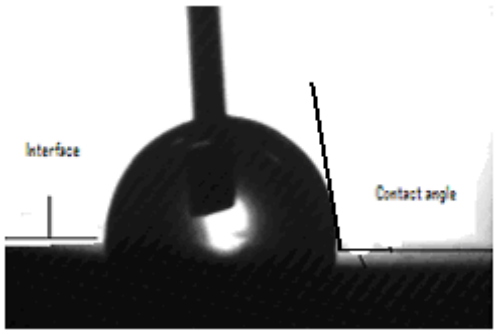

Figure 4.5 (c): Water drop on PTFE (106º)

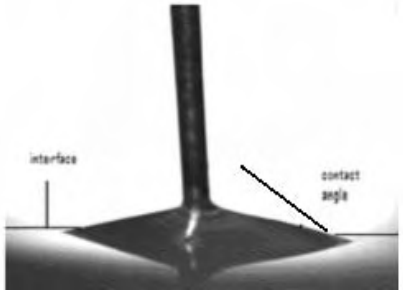

Figure 4.5 (d): Water drop on stainless steel (157º)

Figure 4.5: Images of water drops on the four surfaces, showing typical contact angles.

Figure 4.6: AFM force plots.

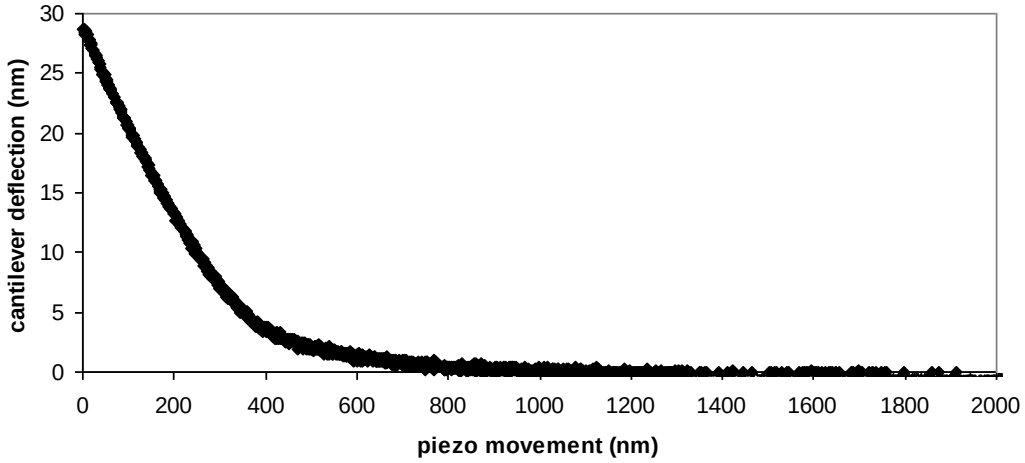

Figure 4.6 (a): Example of a retract plot recorded in Zinc citrate solution in the presence of a glass surface using an AFM cantilever modified with a SiO_2 microparticle. Zero is no deflection.

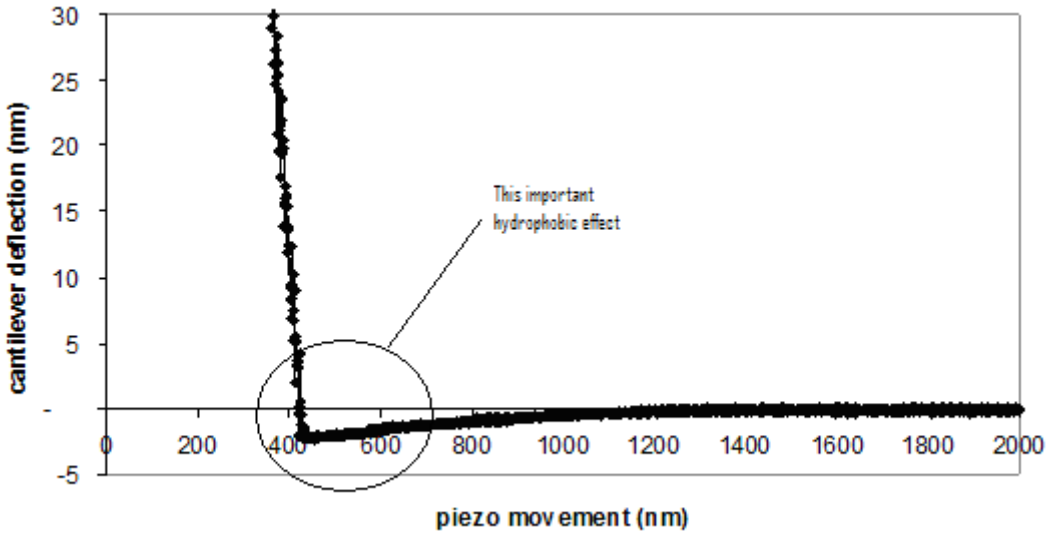

Figure 4.6 (b): Example of retract plot recorded during water in the presence of a stainless steel surface using an AFM cantilever modified with a SiO_2 microparticle. This is a typical ‘‘hydrophobic effect’’ curve.

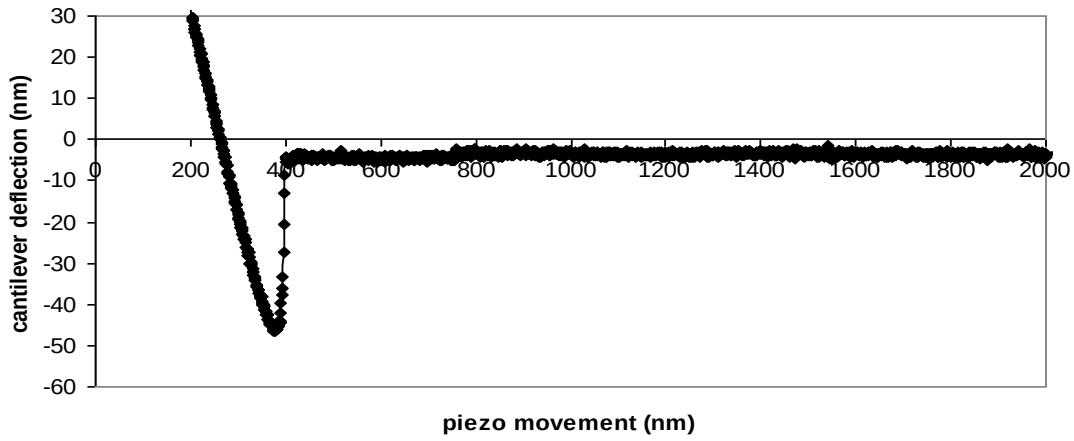

Figure 4.6(c): Example of retract plot recorded in sorbitol solution in the presence of a stainless steel surface using an AFM cantilever modified with a SiO_2 microparticle.

es 4.6: Examples of negligible variation saccharin with velocity

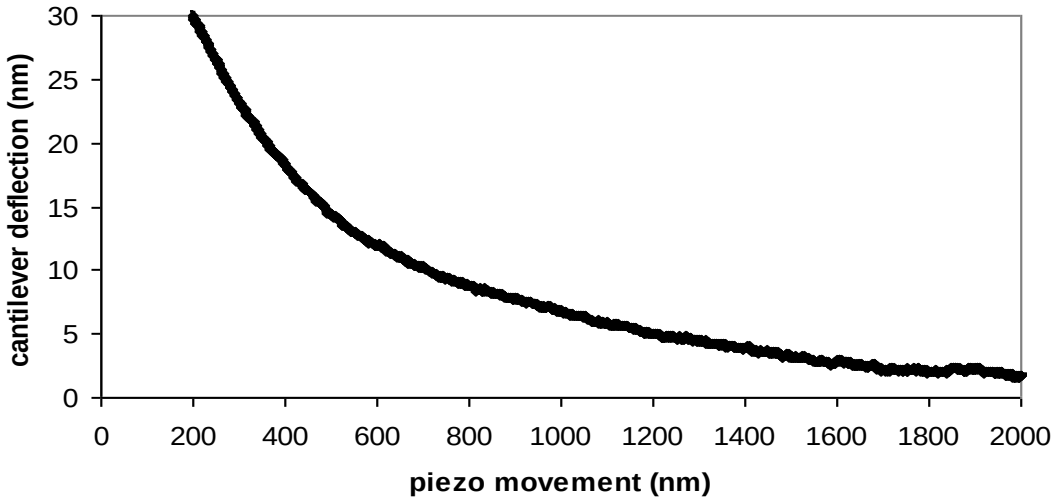

Figure 4.6 (d): Example of retract plot recorded in sorbitol solution in the presence of PTFE surface using an AFM cantilever modified with a SiO_2 microparticle.

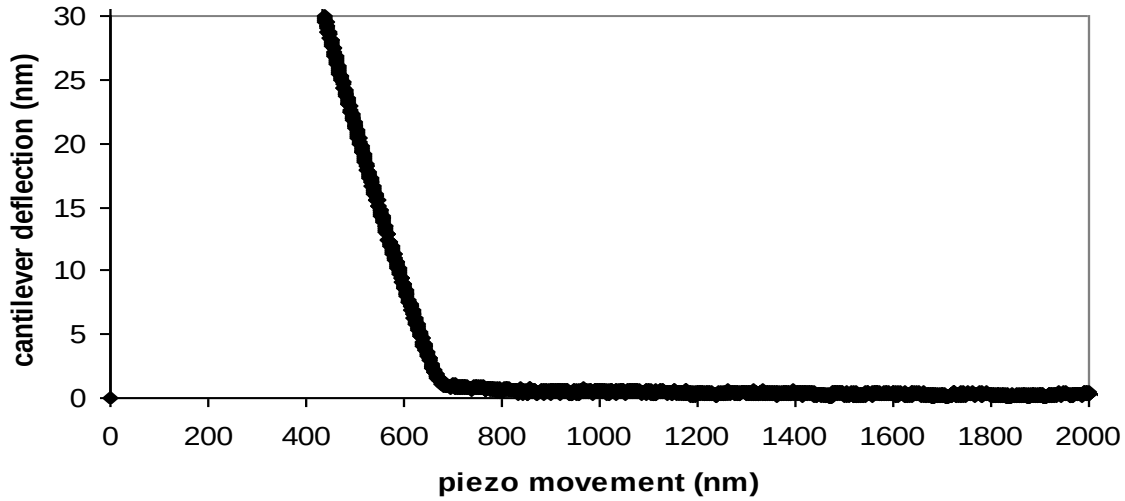

Figure 4.6 (e): Example of retract plot recorded in water in the presence of PTFE surface using an AFM cantilever modified with a SiO_2 microparticle.

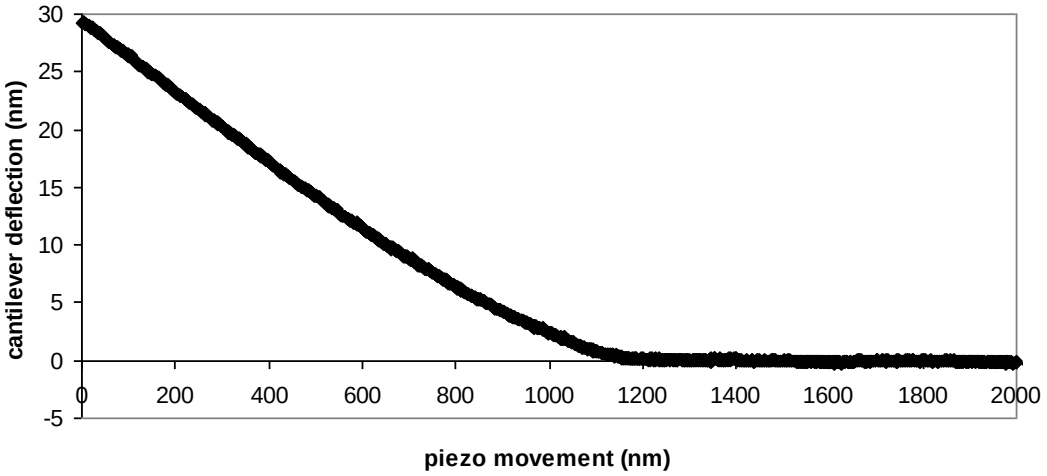

Figure 4.7 (a): Example of retract plot recorded in saccharin solution in the presence of a ceramic surface using an AFM cantilever modified with a SiO_2 microparticle. (Velocity of 2000 nm s^{-1}).

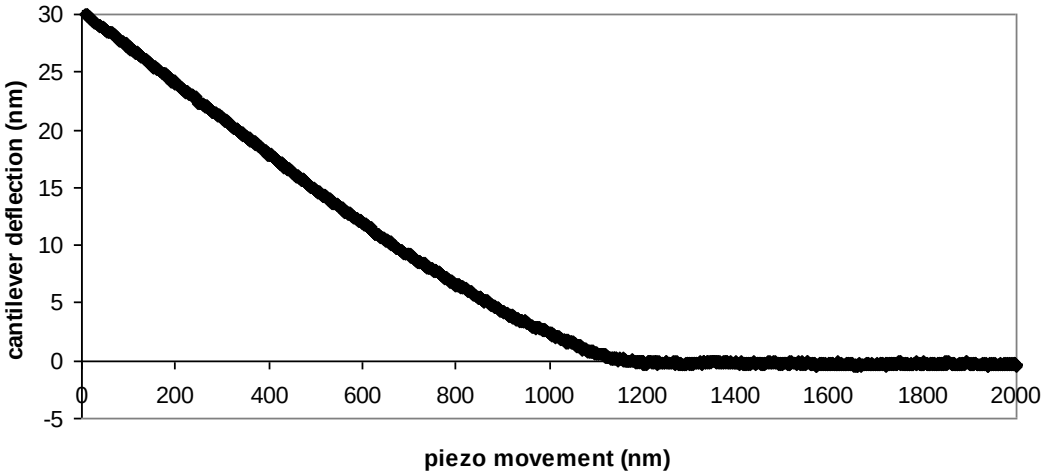

Figure 4.7 (b): Example of retract plot recorded during saccharin solution in the presence of a ceramic surface using an AFM cantilever modified with a SiO_2 microparticle. (Velocity of 200 nm s^{-1}).

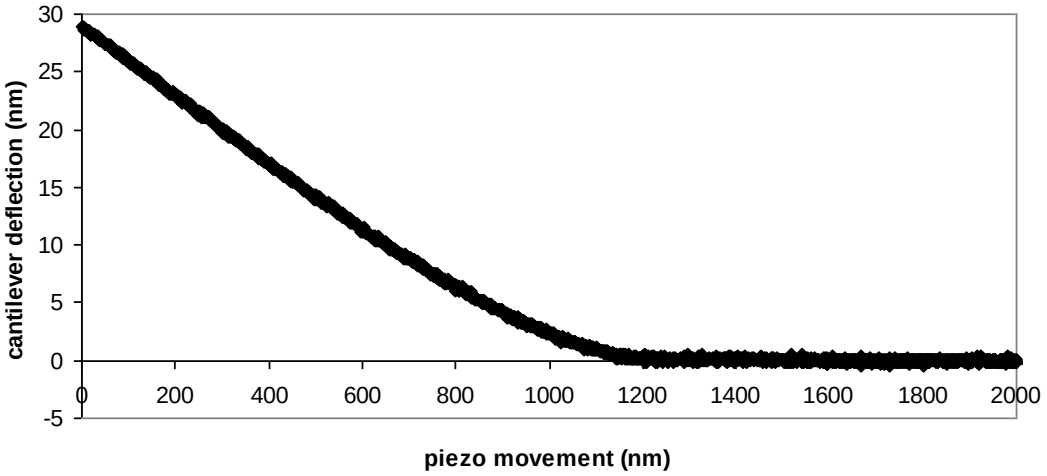

Figure 4.7 (c): Example of retract plot recorded during saccharin solution in the presence of a ceramic surface using an AFM cantilever modified with a SiO_2 microparticle. (Velocity of 14000 nm s^{-1}).

Quantity (nm)	Ceramic	Stainless steel	PTFE-coated stainless steel	Glass
Z-range	+/- 3473	+/- 1564	+/- 564	+/- 207
R_{rms}	+/- 485	+/- 230	+/- 75.6	+/- 5.36
R_a	+/- 369	+/- 92.2	+/- 59.6	+/- 2.37

Table 4.1: Roughness analyses of the stainless steel, PTFE, ceramic and glass surfaces, using the D3100 AFM. Data is an average of a least 5 points. Units are nm.

F/R (mN/m)				
Aqueous medium	Stainless steel	PTFE-coated stainless steel	Glass	Ceramic
Water	+/- 0.09 ± 0.01	No attraction	No attraction	0.01 ± 0.00
Sorbitol solution	+/- 1.70 ± 0.08	No attraction	No attraction	No attraction

Table 4.2: Pull-off forces between silica microparticle and materials in the presence of aqueous media. Force/ radius = (F/R) The experiments were repeated at least five times.

CHAPTER 5: Comparison between measurements using Atomic Force Microscopy and those of Micromanipulation.

Previous chapters have identified surface interactions as being critical in fouling and cleaning, and have described work to characterise surface interactions using methods such as AFM and micromanipulation. The last chapter outlined that interactions at a nano-scale can be quantified between systems that are known to cause fouling/cleaning problems, and that different surfaces and deposits have different responses. No previous work has been attempted to study measurements at two length scales. It would be valuable to do this for a range of reasons: (i) to develop ways of testing surfaces for their fouling potential and cleanability, (ii) to identify what are the smallest scale results obtainable, (iii) it may be that AFM measurements can give data relevant to lab or plant scale relating the two.

Here, microparticles of each of the tested surface materials were attached to tipless AFM cantilevers with epoxy resin. The microparticles were next immersed into different food deposits and then pulled away using the AFM and the interactions were quantified with the different soils of interest: toothpaste, caramel, Turkish delight and sweetened condensed milk (SCM). At the higher scale the interactions were studied using micromanipulation at different gap widths (the height above the surface that the micromanipulation probe passes) of 20µm,

100µm, 200µm, 300µm and 400µm between the probe and the different deposits. The method is described in Chapter 2, and experimental details are given in Chapter 3.

Figure 5.1 shows video stills of the removal process of toothpaste at a gap width of 20µm using the micromanipulation probe. The aim here is to compare the measurements from AFM and micromanipulation to see differences and similarities. The two measurement methods are capable of giving numerical results for the strength of the forces involved in adhesion; it is not clear, however, whether the nano (AFM) - and micro (micromanipulation) scale can be compared and whether this approach might be used to quantify cleanability or identify low-fouling or easy to clean surfaces. Therefore in this chapter both AFM and micromanipulation have been used to measure the force required to remove the four chosen deposits from the three surfaces of interest. Ceramic was not used in these experiments, as the microparticles were found to be too large and heavy to attach to the tip, which caused the tip to break.

5.1 AFM studies.

The spherical 30µm glass, stainless steel and PTFE particles were first attached to the AFM tip using epoxy; Chapter 3 discusses the materials and methods used to obtain the following results. Typical sets of results are shown in Figure 5.2.1, which displays data for the interaction between stainless steel microparticles and caramel. The approach speed of the cantilever for all experiments was 3µm/s, followed by a 5 second pause on the deposit surface and then removal at the speed of 0.25µm/s. Figure 5.2.1 shows the data for five different at five different places on the surface (within 10µm distance from each other measurements) . The data shows

- that force variation are very little amongst neighbouring points.

- whilst at a wider scale, the variation is more substantial, with mean values varying from 0.05 to 0.35N/m.

The pull-off forces between the particles and the food materials reflect the surface chemistry of both the particles and the food materials. The result is dependant on the contact made with the sphere and where on the surface the sphere touches. The principal factors responsible for adhesion between surface and deposits include: (i) van der Waals forces, (ii) electrostatic forces, (iii) and contact area effects; the greater the area the greater the total attractive force. The forces between elements of the deposit depend on the nature of the material; deposits may be covalently bonded or held together physically. [Liu, *et al.* 2006]. This chapter will study the pull off forces using the AFM of different deposits with different surfaces and then a comparison will be made with micromanipulation forces.

5.1.2. Caramel.

As discussed in chapter 3, caramel is derived from the caramelisation of sugar; it is made from sugar by heating it slowly to around 108° C. Figure 5.2.2 shows the AFM pull off forces between glass, PTFE and stainless steel microparticles attached to AFM tips immersed in caramel deposits of thickness between 50-60 μm. Figure 5.2.2 shows the variation between the three surfaces, for averages of 5 measurements taken at 5 different regions of the surface.

There is a clear difference between the forces measured for the three surfaces. A strong adhesive force of mean 0.4(±0.02)N/m was seen between glass and caramel, whereas stainless steel and the PTFE surface show a lower adhesive forces of 0.18(±0.02)N/m, whilst the results showing PTFE surface exhibiting the lowest force of 0.04(±0.02)N/m.

The results obtained for PTFE were as expected given the hydrophobic nature of the fluorinated surface. Water and water-containing substances like most foods do not wet PTFE; therefore adhesion to PTFE surfaces is inhibited is low as discussed in chapter 2.

5.1.3 SCM

The composition of SCM is discussed in Chapter 3. The results shown in Figure 5.3 show the forces between glass, PTFE and stainless steel microparticle and SCM.

- The results generally are lower in magnitude than those for caramel. SCM exhibited the strongest attraction to glass of 0.22(±0.02)N/m, approximately twice the magnitude of the force of contact with the stainless steel, and significantly less than the forces of 0.35(±0.03)N/m seen for the combination of glass and caramel.
- The results for stainless steel had a greater variation of 0.1(±0.03)N/m between the forces measured at different points than it was found for the glass and PTFE surfaces: the mean force measured is significantly less than that for caramel.
- The forces between SCM and the PTFE microparticle show near zero adhesion forces of 0.01(±0.001)N/m.

SCM structurally is different from caramel. SCM contains milk and sugar from which water has been evaporated, compared to caramel which is a cooked sugar with lower water content, and polymerises as no or little water remains in the product. Therefore it adheres to surface more.

5.1.4 Turkish delight

Figure 5.4 shows data for the forces between the three microparticle surfaces with Turkish delight. The results show that the forces are lower than those measured for SCM and caramel.

- Both glass and stainless steel microparticle immersions showed adhesion forces one order of magnitude lower than with SCM showing adhesion of 0.096(±0.0001)N/m and caramel showing adhesion of 0.183(±0.01)N/m.
- The most significant difference is that PTFE showed the highest of the three surfaces, the adhesion force with Turkish delight showing 0.04(±0.001)N/m adhesion than with SCM 0.002(±0.0002)N/m and caramel 0.01(±0.002)N/m. The forces for PTFE are however more similar for the three systems than for those of the other two surfaces.

Turkish delight has a gel like structure, which pulls off the surface more easily compared to SCM and caramel. However with PTFE the Turkish delight adhered to the surface. This could be due to cross linking of the agar to PTFE of some possibility of charging on the surface. Agar is a polymer made up of the sugar galactose. Agar polysaccharides serve as the primary structural support for Turkish delight. Also the low water content of Turkish delight could also suggest the adhesion to PTFE.

5.1.5 Toothpaste

Toothpaste is made up of different particles, which is discussed in Chapter 3. Figure 5.5 highlights that toothpaste has the lowest adhesion forces from all four deposits;

- Toothpaste shows a force of 0.01(±0.003N/m) with glass.

- The force seen with stainless steel is 0.005(±0.0001)N/m and PTFE is 0.004(±0.0001)N/m.

The interactions with the glass microparticle and toothpaste provided the greatest adhesion force at all locations. The PTFE and stainless steel showed low adhesion in line with the caramel and SCM deposits. Toothpaste adhesion forces were lower than Turkish delight.

5.1.6. Summary.

Figure 5.6 summarises the adhesion behaviour of the combination of each microparticle and deposit. The relative strengths of the interactions between each type of deposit and surface can be seen.

- Overall it can be seen that the measured forces for the different surfaces vary by more than a factor of 10, from caramel at the highest value to toothpaste at the lowest;
- The forces between the deposits and the glass microparticle show the largest adhesive behaviour with caramel, SCM, and toothpaste;
- Turkish delight exhibits the greatest adhesion on PTFE microparticle, although for Turkish delight and toothpaste the forces are very low in general.

The soils investigated here generally adhere most strongly to the glass surface with the exception of Turkish delight. The results suggest that the general behaviour of deposit and substrate (microparticle) is that glass gives the largest adhesion compared to stainless steel and PTFE.

The data suggests that PTFE surfaces would in general be better than stainless steel in terms of reducing fouling or cleaning. The use of PTFE-based surfaces in fouling reduction has been discussed in Chapter two, and it has been shown to work in some cases; however there is a difficulty in producing PTFE coated equipment, which is cheap and robust in operation. It is clear that this sort of surface can give either reduced fouling or more effective cleaning. Further investigation is required to help explain why Turkish delight is so different. One possible explanation could be that Turkish delight slides off the surface.

5.2 Micromanipulation measurements.

5.2.1 Caramel behaviour on stainless steel, glass and PTFE surfaces.

In Chapters 2 and 3 the background to these experiments and the procedure followed are described. Experiments were carried out using 0.7mm thickness of material, by passing the blade of the micromanipulation probe over the surface at different cut heights above the surface.

Figure 5.7 shows pulling energy (measured force per unit area from where deposit is removed) for measurements taken using the micromanipulation system for different gap widths (of 20µm, 100µm, 200µm, 300µm and 400µm) between the probe and the caramel deposit. The data shows that, for removal in all cases, the pulling energy increases with increasing height above the surface and the slopes of the lines of pulling energy versus thickness are similar. Stainless steel shows the highest pulling energy with slightly higher energies than glass and PTFE, whilst PTFE shows the lowest interaction. For the AFM data, shown in Figure 5.2.2, PTFE again gives much lower adhesion forces. This is due to the

different molecular interactions between different surfaces and caramel. There is thus partial agreement between the two methods. The micromanipulation method will measure a range of parameters – such as the deformation and flow of the fluids deposits, and so it might not be expected that there would be complete agreement. Here stainless steel and glass show very similar behaviour, as opposed to the differences seen using AFM; the different surface roughness of the two substrate might also be expected to have an effect.

5.2.2 SCM behaviour on stainless steel, glass and PTFE surfaces.

Figure 5.8 shows the behaviour seen with SCM on stainless steel, glass and PTFE at different cut heights. The results show with increasing thickness the pulling energy decreases for the three systems. Stainless steel shows the greatest pulling force with SCM compared to glass and PTFE, whilst PTFE shows the smallest. The micromanipulation data does not show the very large differences seen by the AFM.

Liu *et al.* [2005] gives a simplistic model for the behaviour of a system of thickness L cut at height x; assuming that the work to remove unit volume of materials is constant, then the energy should decrease with x, with an equation of the form

$$\sigma = A + (L-x)B$$

where A is the energy required to cut the surface, and B that to deform the deposits. The model suggests that the slope of all the lines should be similar, but that intercepts at x=0 might be different and surface dependent. It can be seen in Figure 5.8 that the slopes of the

lines are not dissimilar, whilst the intercepts again show that the least pulling energy is found for PTFE, whilst the largest forces are for stainless steel. The model is clearly simple – but there are clearly both surface and bulk effects involved in the micromanipulation measurements, this is representative of what we see when cleaning surfaces.

5.2.3 Turkish delight behaviour on stainless steel, glass and PTFE surfaces.

Micromanipulation experiments for Turkish delight are illustrated in Figure 5.9. The results show that with increasing thickness the pulling energy decreases for stainless steel, glass and PTFE. The data for stainless steel and glass are very similar, with that for PTFE being significantly greater at low cut heights – this is a very interesting result which is essentially the same as is seen for the AFM in Figure 5.4. That PTFE shows the greatest interaction with Turkish delight is supported by both AFM and micromanipulation, and is surprising given the results from previous work discussed in Chapter 2. This could suggest some crosslinking with the agar and PTFE surface or Turkish delight could be pulling off the coating of PTFE in removal. It was seen that Turkish delight slides off the surfaces at different cut heights and thicknesses. The values of pulling energy are less than for SCM and caramel deposits, but the difference is not as large as for AFM. This again indicates that the micromanipulation method measures both surface and bulk effects; the rheology of the material will control how it deforms and flows under the effects of the moving blade.

Toothpaste, SCM, caramel and Turkish delight deposits are non- Newtonian fluids investigations carried out by Konstantia Asteriadou and group at the University of Birmingham using a rheometer. All deposits process viscoelastic behaviours. Toothpaste

behaves to the Herschel-Bulkley model. SCM, caramel and Turkish delight are all shear thinning fluids this is a result of:

- Orientation of non-spherical particles in the direction of flow.
- Orientation of polymer chains in the direction of flow and breaking of polymer chains during flow.
- Deformation of spherical droplets to elliptical droplets in an emulsion.
- Breaking of particle aggregates in suspensions.

5.2.4 Toothpaste behaviour on stainless steel, glass and PTFE surfaces.

Figure 5.10 shows the behaviour seen with toothpaste on stainless steel, glass and PTFE at different cut heights. The results show that with increasing thickness the forces decrease. Stainless steel requires the largest pulling energy, glass follows quite closely and PTFE demands the least. It was seen that at larger thickness there was no complete removal was achieved. This is similarly seen with Turkish delight and SCM, but the reverse is seen with the caramel deposit. AFM showed that toothpaste showed the strongest adhesion to glass whilst with the micromanipulation it demonstrated the strongest interaction with stainless steel.

5.3 Discussion.

Figure 5.11 shows a comparison of the data for the micromanipulation experiments, plotting the results to remove the deposit for a cut height of 20 microns. This can be compared with Figure 5.6 – the first difference is obviously that a log scale is needed in Figure 5.6 in order to visualise the very low values seen for the toothpaste and PTFE data, whilst the results of Figure 5.11 do not show the same magnitude of variation because the micromanipulation measures both bulk and interfacial properties.

The data for the two systems is well-matched, especially given the fact that – seemingly anomalous – result for Turkish delight, on PTFE shows the greatest adhesion and the same trend in both cases. The data for stainless steel and glass are more closely matched, but both are greater than PTFE for caramel, SCM and toothpaste. AFM shows similar trends to micromanipulation.

The work of Chapters 1 and 2 has suggested a possible classification of deposits, which could be useful if it allows decisions to be made about selection of cleaning protocols. Deposits which fail adhesively – by failure of bonds at the interface between the deposit and the surface - may well need to be treated differently from those which fail due to breakdown of cohesive forces. [Liu, *et al.* 2005, 2006]; see Chapter 2. The data seen here suggest that the cohesive energies between elements of the toothpaste deposits are smaller than those of the adhesion between the stainless steel, glass and PTFE surfaces and toothpaste. The energy required for removal decreases as the gap between probe and substrate increases. This is the opposite to the behaviour of caramel, as shown in Figure 5.7, which shows that it is easier to remove the whole of the deposit than it is to remove a surface layer.

Figure 5.2.2 highlights that for caramel; glass has the highest surface interactions and PTFE the lowest. The micromanipulation shows that the pulling energy is high for both glass and stainless steel and low for PTFE. Micromanipulation and AFM agree; the high values for stainless steel many reflect the roughness of the surface. The force required to remove deposits increases with cut height, suggesting that the deposit- deposit bonds are stronger than deposit-surface bonds.

For SCM, the AFM shows that glass has again the highest energy and PTFE the least. The micromanipulation data shows that stainless steel has the highest removal energy, PTFE the lowest. Here the force decreases with height above the surface, suggesting that the adhesion forces are stronger than the cohesive ones.

For Turkish delight, however, the PTFE shows the largest removal force, which is surprising, given that micromanipulation gives the lowest force with PTFE. Glass and stainless steel show similar AFM force behaviour, and similar pulling energies. Again the pulling energy decreases with increasing cut height.

For toothpaste, low force measurements are seen with AFM for all cases, with PTFE slightly lower than the rest. Micromanipulation records lower pulling energies for PTFE. The data of Figure 5.6 shows that surface interaction can vary by more than a factor of 10 for the three confectionary deposits, reflecting the different chemistries of the material. The caramel and SCM have the highest force, which is also shown by the micromanipulation pulling energies.

The work here has used AFM and micromanipulation equipment to identify adhesive and cohesive effects in the cleaning of food deposit. The caramel deposits are essentially highly cohesive. (physical properties of deposits cause intermolecular attraction between like-

molecules). On the other hand, SCM, Turkish delight and toothpaste are adhesive. The results suggest that for SCM, toothpaste and Turkish delight, the cohesive forces between elements of the deposits are weaker (loosely bound) than those of adhesion between surface and deposits, which is opposite to the behaviour of caramel. Thus it is easier to remove the whole of the deposit than to remove a surface layer.

This indicates that AFM and micromanipulation technique can identify the different mechanical properties of fouling deposits. In both measurement methods the results show caramel to display adhesive failure and toothpaste, Turkish delight and SCM to show cohesive failure. The PTFE surface generally shows lower adhesion with both AFM and micromanipulation. Both measurement methods measure adhesion force, however the size of force is larger with micromanipulation due to the sample size and amount.

The AFM measures the force at smaller scale areas than micromanipulation. AFM is a more sensitive measurement method, and more parameters are required to set up experiments, such as the need for the right size particle and the right cantilever stiffness. Also it is not known until the experiment is performed how much z-range is required. In comparison, micromanipulation is relatively simple to use and set up. Most deposits are easily compatible, compared to the AFM. The AFM requires more preparation to set up an experiment. Both methods are acceptable as the overall data sets show similar behaviour with each deposit. Micromanipulation and AFM show similarities in adhesion forces. However, the range of adhesion is on two length scales, making it very difficult to compare. It is clear that, as found by other researchers, the surface energy affects the force required for removal. The advantage of AFM is that it is an instrument commonly used in the development and characterisation of new materials, which may initially only be available in very small quantities. Measurements

using such small samples have been shown to be a good prediction of macroscale behaviour – this may help material designers identify potentially new antifouling surfaces without having to do experiments at higher scale.

5.4. Conclusions.

Force measurements were performed using modified tipless Si cantilevers attached with a microparticle of different surfaces; the tip was engaged to the sample and force measurements taken. Micromanipulation experiments required 0.2 g of Turkish delight, caramel, SCM and toothpaste to be uniformly spread over the whole surfaces for removal.

PTFE surfaces would in general be better than stainless steel in terms of reducing fouling or cleaning. The use of PTFE-based surfaces in fouling reduction is well known and it has been shown to work in some cases; however there is a difficulty in producing PTFE coated equipment which is cheap and robust in operation.

AFM and micromanipulation are both beneficial tools for the measure of adhesion. AFM works at the nm-scale whilst micromanipulation measures at the μm-mm scale. The aim of this work was to see to what extent the two methods give comparable results. The removal technique for the deposits in AFM and micromanipulation is different. AFM measures the vertical force of removal of the particle from a surface, whilst the micromanipulation pulls horizontally to get the adhesion force.

A range of results were obtained exhibiting that in some cases AFM and micromanipulation data agree well, for example PTFE shows lowest forces with all deposits with both

techniques, however, some effects seen with the AFM differ to those of micromanipulation. For example the forces size is greater with the latter.

Chapter 5 Figures:

Figure 5.1: Removal of toothpaste from stainless steel using the micromanipulation rig, at a cut height of 20 μm. On the left is a stainless steel disc fully covered with toothpaste. The middle is partially removed toothpaste. On the right is the surface after passage of the probe. The probe was moved at 1.1 mm/s over a displacement of 1.5 mm.

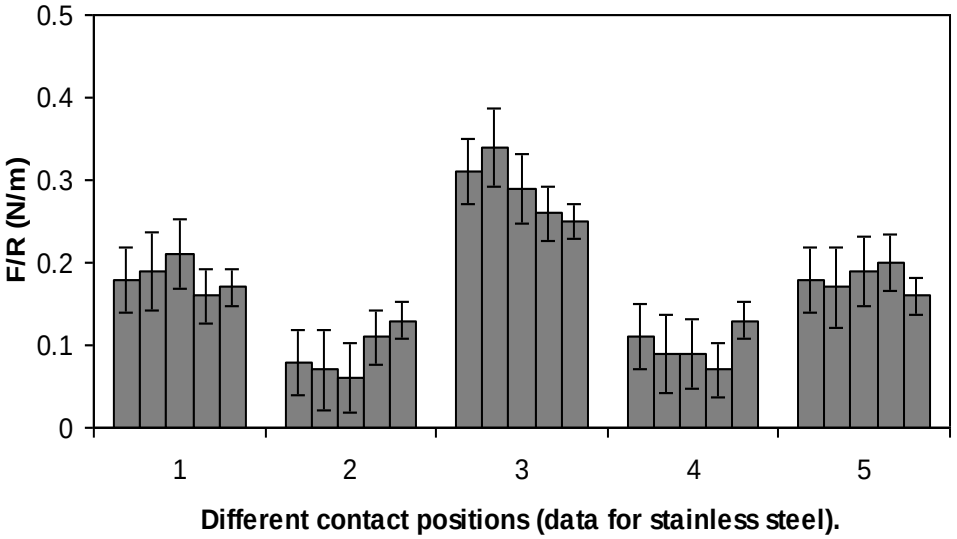

Figure 5.2.1: Interaction between stainless steel microparticles and caramel, measured using the AFM. Data shows local variation of 5 points at each of the 5 regions on the caramel deposit; error bars shows the equipment error per measurement.

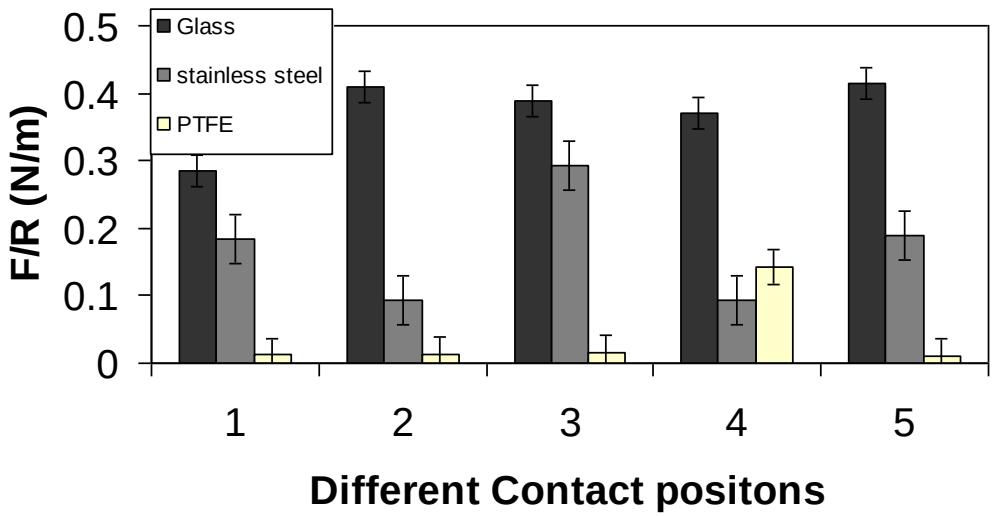

Figure 5.2.2: AFM force measurements of Stainless steel, glass and PTFE microparticles immersed in caramel (spread out between 50µm to 60µm thickness on a glass slide) and then retracted. Data shows results from five different contact positions on the caramel deposit. Error bars represent the global variation of the mean of five experiments. The approach speed for all experiments was 3µm/s, and then a 5 second pause on deposit and 0.25µm/s retraction speed.

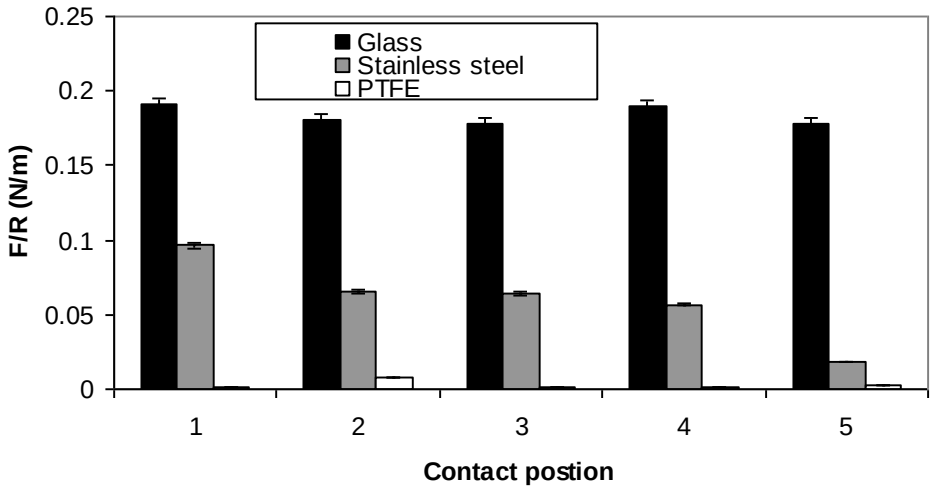

Figure 5.3: AFM force measurements of Stainless steel, glass and PTFE microparticles were immersed in SCM and then retracted off the deposit. SCM was spread out between 50µm to 60µm thick on a glass slide. The approach speed for all experiments was 3µm/s, and then a 5 second pause on deposit and 0.25µm/s retract. Data shows the mean of five experiments at each of five different contact positions on the SCM deposit.

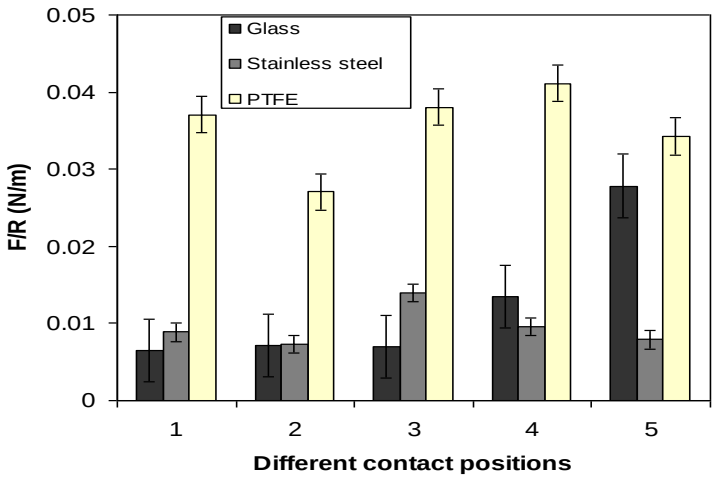

Figure 5.4: AFM force measurements of Stainless steel, glass and PTFE microparticles were immersed in Turkish delight and then retracted off the deposit. Turkish delight was spread out between 50µm to 60µm thick on a glass slide. The approach speed for all experiments was 3µm/s, and then a 5 second pause on deposit and 0.25µm/s retract. Data shows the mean of five experiments at each of five different contact positions on the Turkish delight deposit.

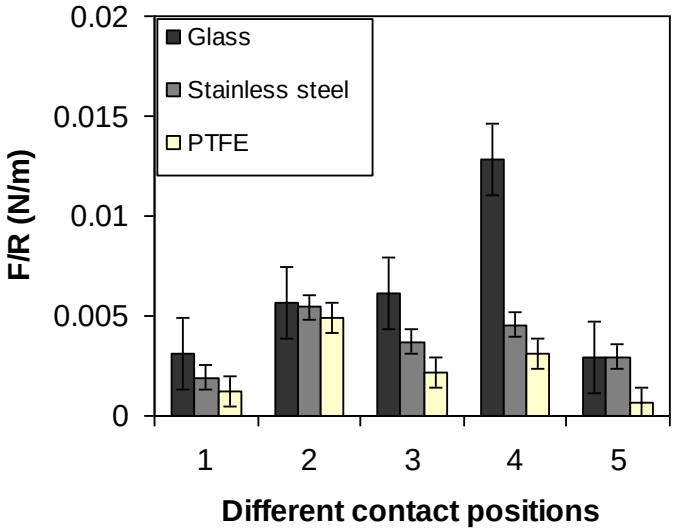

Figure 5.5: AFM force measurements of Stainless steel, glass and PTFE microparticles were immersed in Toothpaste and then retracted off the deposit. Toothpaste was spread out between 50µm to 60µm thick on a glass slide. The approach speed for all experiments was 3µm/s, and then a 5 second pause on deposit and 0.25µm/s retract. Data shows the mean of five experiments at each of five different contact positions on the Toothpaste deposit.

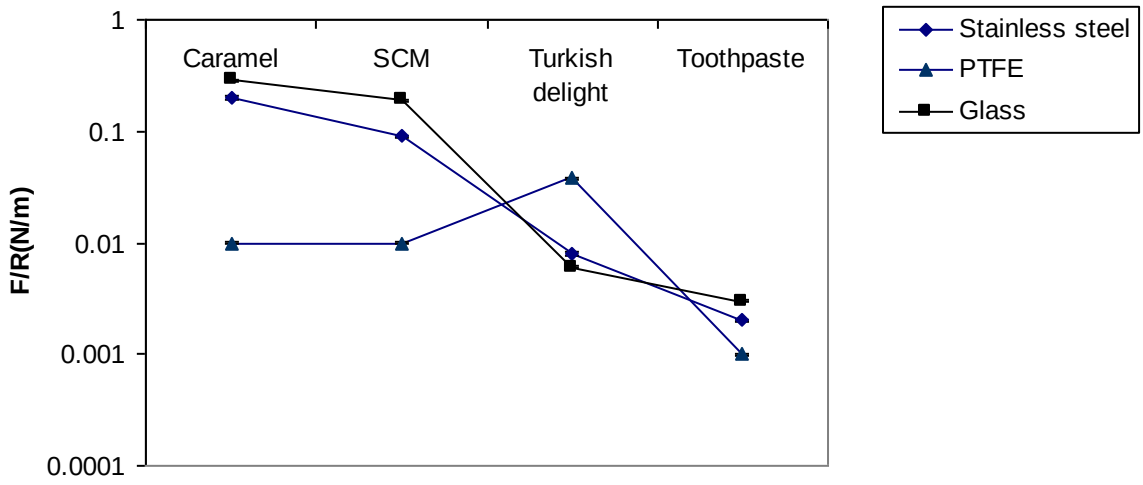

Figure 5.6: Summary of the forces measured by AFM for the different microparticles and all four deposits. (Log Scale).

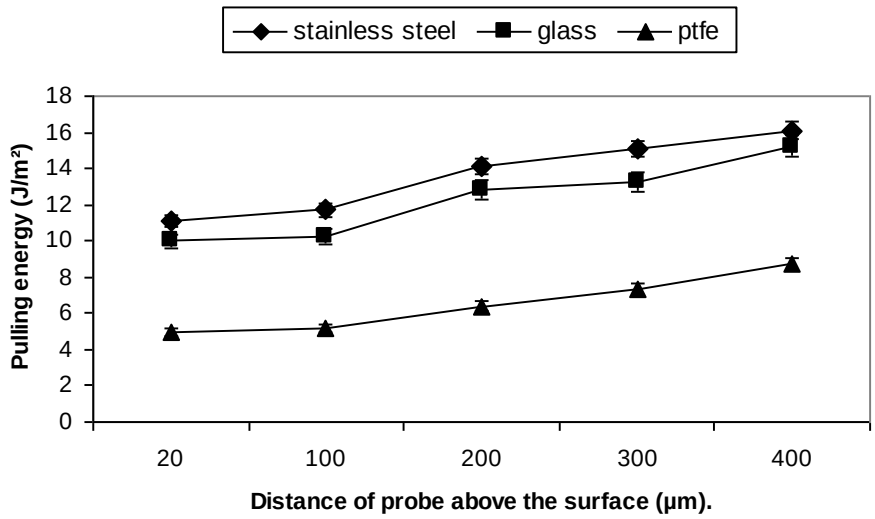

Figure 5.7: Pulling energy for removal of caramel deposit using the micromanipulation probe. The gap between probe and substrate was kept at 20, 100, 200, 300 and 400µm, the surfaces used were stainless steel, glass and PTFE.

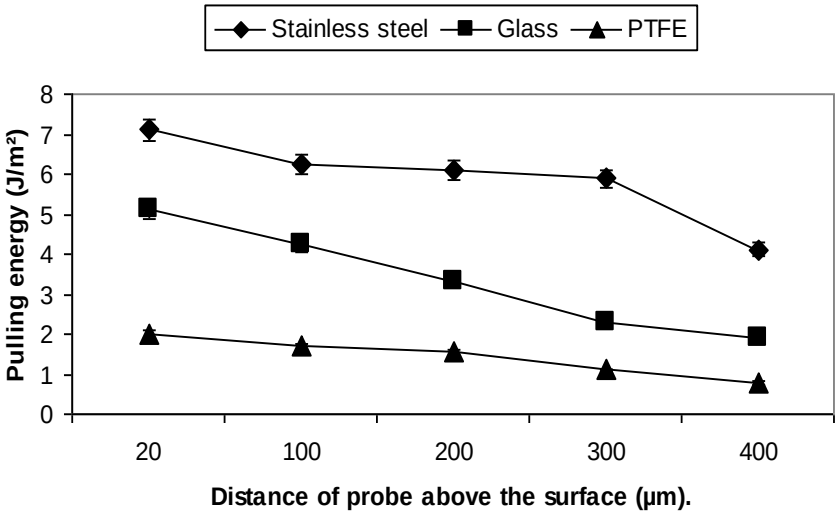

Figure 5.8: Pulling energy for removal of SCM deposit using the micromanipulation probe. The gap between probe and substrate was kept at 20, 100, 200, 300 and 400µm, the surfaces used were stainless steel, glass and PTFE.

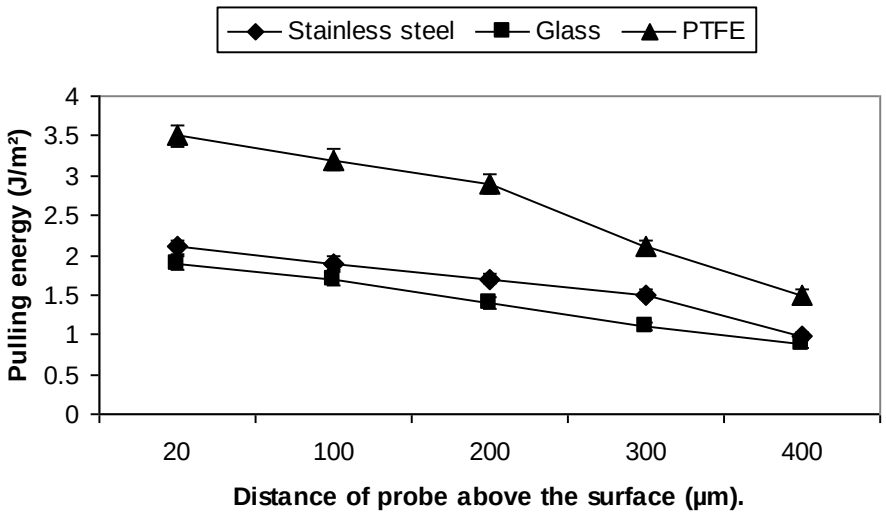

Figure 5.9: Pulling energy for removal of Turkish delight deposit using the micromanipulation probe. The gap between probe and substrate was kept at 20, 100, 200, 300 and 400µm, the surfaces used were stainless steel, glass and PTFE.

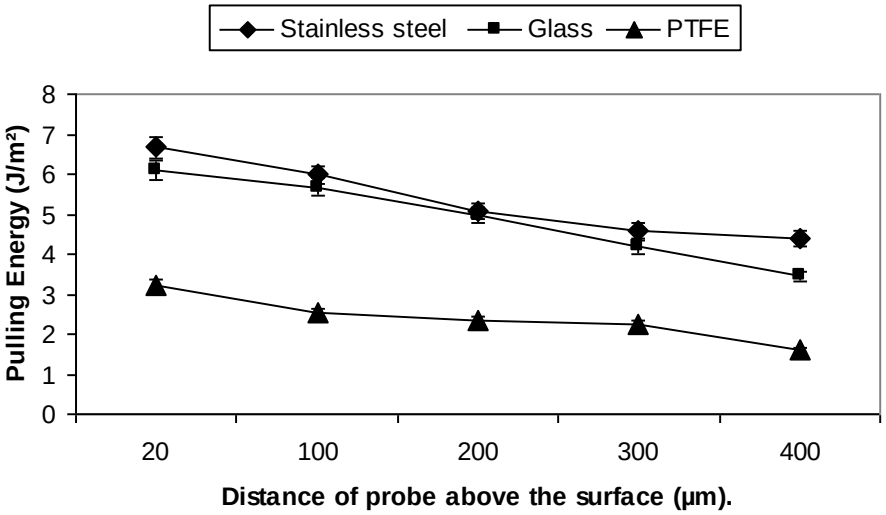

Figure 5.10: Pulling energy for removal of Toothpaste deposit using the micromanipulation probe. The gap between probe and substrate was kept at 20, 100, 200, 300 and 400 µm, the surfaces used were stainless steel, glass and PTFE.

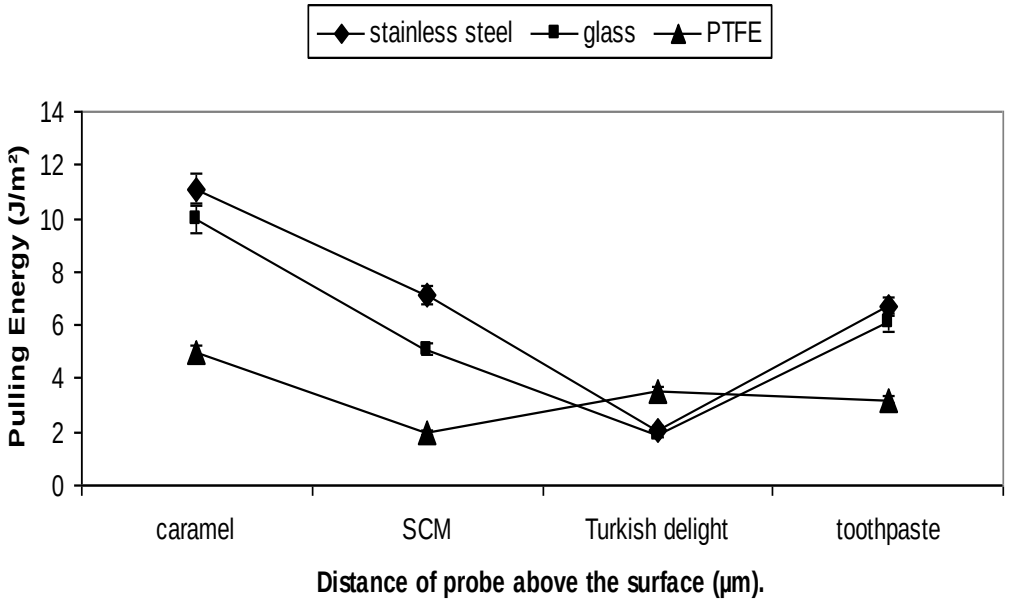

Figure 5.11: Summary of Micromanipulation experiments at 20µm thickness of caramel, SCM, Turkish delight and toothpaste on glass, stainless steel and PTFE.

Chapter 6: Atomic Force Microscopy (AFM) experiments of caramel, whey protein, and SCM deposits at different temperatures.

Most food production processes require heating, the efficiency of which depends on the cleanliness of the heat transfer equipment explained in Chapter 2. In the food sector the thermal instability of food products causes very rapid build up of deposits onto heat transfer surfaces. Most food processing equipment needs to be cleaned regularly to maintain thermal efficiency. Fouling in the food industry is considered to be severe; daily cleaning is needed. Furthermore many food processing plants rely on heat treatment to kill dangerous bacteria, so cleaning is required for food safety reasons.

In Chapter 5, AFM adhesion measurements have been carried out using different microparticles and different deposits. A range of results is obtained that can in some cases be related to the micro-meso-scale of removal measured by micromanipulation. This chapter will further investigate AFM adhesion measurements, when caramel, whey protein and SCM are studied at 30ºC, 50ºC, 70ºC, and 90ºC using an AFM heating stage (seen in Figure 6.1).

Fouling occurs at different temperatures, depending on the deposit, as described in Chapter 2. In thermal processing the most thermally labile materials form fouling deposits, such as β-lactoglobulin, a milk whey protein, which forms the majority of milk pasteuriser deposit, despite being only a small fraction of the protein in milk [Changani *et al.* 1997]. Heating

caramel and SCM involves the loss of water the breaking of carbon-carbon linkages of the sugar molecule at high temperatures (above 130ºC). Adhesion occurs at high temperatures: for example, in milk pasteurisation deposition of proteins occurs onto surfaces held at 75ºC. Most of the measurements of forces are such as those of Chapters 4 and 5, carried out at room temperature. The measurements of adhesion at process temperature would obviously be of value, both to investigate the forces required to cause adhesion at these temperatures as well as to study the ways in which forces change with temperature.

In all cases here the deposits were first heated for 5 minutes and the temperatures maintained and monitored during experiments before pull off forces were measured. Experiments were carried out using a Nanowizard II AFM adapted using a JPK (U.K) heating stage. While experiments were carried out at 30ºC, 50ºC, 70ºC and 90ºC only limited access to the equipment was possible, so only two microparticles were used; stainless steel and PTFE. The variable parameters used in the heating experiments were:

(i) **Different Contact positions**: The same methodology was used in Chapter 5. Different force curves were taken at different positions (at least five) on the deposits to investigate the spatial variation of adhesion.

(ii) **Different Rate:** The speed at which the tip approaches and retracts on and off the deposit was varied, at 0.25, 0.75, 1, 3 and 5µm/s. These rates were chosen to be within the size (40-50µm) of sample used and the Z-range limits of the AFM. The rate was controlled and monitored on screen by the Nanowizard II software; this could be changed as desired.

(iii) **Different Contact Times**: The force curves were taken for different contact times between the tip attached with microparticle and the deposits. The time is varied

between zero seconds, where the tip touches the sample, and then is retracted instantly, the contact times are 0.5, 1, 5 and 10 and 60 seconds. The tip and deposit contact could be seen using the AFM optical camera and the software allows the input of different values and control of the Z-range scanner to move up or down. In some experiments no force curve was obtained for 60 seconds holding times as the deposits engulfed the microparticle and the cantilever would not retract.

These experiments were designed to test the balance between two factors (i) the increase in deposit cohesion which would be expected to occur at high temperature, as a result of thermally-induced reactions, and (ii) any possible decrease in the cohesion as a result of the decrease in the effectiveness of intermolecular forces which occurs at high temperature.

6.1 AFM analysis of interactions between test surfaces and heated caramel.

6.1.1 Different contact positions.

Figure 6.2.1 shows the force of adhesion at different contact positions, when caramel is heated at different temperatures using the stainless steel tip. The results show:

(i) At 30°C the largest adhesion of 0.5 (±0.1)N/m is found between the stainless steel microparticle and caramel at different contact positions; there is however considerable variation between the values measured at this temperature.

(ii) At 50°C some adhesion of 0.3(±0.05)N/m is shown, as the temperature increases the adhesion decreases.

(iii) At 70°C and 90°C the force decreases further, to 0.25(±0.002)N/m. There is some loss of moisture as the sample is heated, and some reactions might take place as the deposit starts to turn into a darker brown colour.

The force decreases with temperature increases Figure 6.3.1 shows the interactions between the PTFE tip and caramel at different contact positions and allows comparison of the two surfaces. There is a decrease in adhesion from 30°C to 90°C but the change between 50ºC and 90ºC is very small. The force at 30ºC is 0.18(±0.02)N/m, at 50ºC is 0.16(±0.02)N/m, at 70ºC is 0.09(±0.02)N/m and at 90ºC is 0.08(±0.02)N/m. The data shows that the magnitude of the adhesive forces between caramel and stainless steel is significantly greater than with PTFE, an effect also seen with unheated caramel in Chapter 5. For both PTFE and stainless steel, the force of adhesion decreases as the temperature increases. It has been noted in the introduction that different effects are possible with an increase in temperature; the caramel deposit will have a lower viscosity with increasing temperature but may also undergo reactions to enhance adhesion. The data suggests that any effect of increased adhesion is minimal, and that the effects of the surface are significant.

6.1.2 Different rates of retraction.

Figure 6.2.2 shows the results on interaction between caramel and stainless steel at varying points. The highest adhesion is seen at 30°C where for all the forces shows the highest adhesion for all the different temperatures is seen under all speeds and points. There is no measurable trend at 30°C when changing the rate of removal of stainless steel from the surface, this could be due to experimental error. Figure 6.2.2 shows at 30°C the mean force is 0.5N/m at 0.25µm/s, 0.55N/m at 0.75µm/s, 0.45N/m at 1.00µm/s, 0.45N/m at 1.5µm/s, 0.58N/m at 3µm/s and 0.45N/m at 5µm/s. Lower values are seen at the other temperatures,

with the same lack of trends at 50ºC; (where values were between 0.43(±-0.02)N/m and 0.33(±0.02)N/m). The data at high temperature does suggest that the faster the rates the lower the force. At 0.25µm/s the F/R values are 0.3(±0.02)N/m, whilst at 5µm/s the values have dropped to 0.23(±0.02)N/m. For PTFE, the values are significantly smaller, as shown in Figure 6.3.2. The trend is that force decreases as speed increases (which shows that there is some effect of increasing rate, which is again to decrease the force): from 0.13(±0.02)N/m at 30ºC, to 0.09(±0.02)N/m, at 50ºC, to 0.07(± 0.02) at 70ºC and to 0.06(±0.02) at 90ºC.

6.1.3 Different waiting times on caramel.

Figure 6.2.3 shows the force of adhesion of the stainless steel microparticle for variable contact times with caramel. It might be expected that as the holding time increases the force between particle and surfaces increases, because more time is available to form bonding interactions with the surface. Very little change in the force is seen between 0.5 and 10 seconds at all temperatures. Figure 6.3.3 shows the force of adhesion for the PTFE microparticle at variable times on caramel. Here as the waiting time increased the adhesion decreased. At 30°C, the adhesion changes from 0.18N/m to 0.08N/m, whilst there is a small effect (0.11 to 0.08N/m) at 90°C. The reason for this decrease is not clear, as an increase would be expected.

6.2 AFM analysis of interactions between test surfaces and SCM.

6.2.1 Different contact positions.

The experiments were repeated using sweetened condensed milk (SCM). Figure 6.4.1 shows the force of adhesion at different contact positions, when SCM is heated at different temperatures using the stainless steel tip. The results show that

(i) at 30°C the largest adhesion force of 0.1(±0.04)N/m is felt between the stainless steel microparticle and SCM deposit at different contact position. This is the same as the caramel, however the values are much smaller.

(ii) At 50°C degrees adhesion of 0.08(±0.02)N/m is felt; with caramel, as the temperature increases the adhesion decreases.

(iii) At 70°C the adhesion forces are 0.07(±0.02)N/m whilst caramel were 0.29(± 0.02)N/m.

(iv) At 90°C the force is 0.05(±0.02)N/m. The data is all lower than for caramel, but similar trends can be identified.

Figure 6.5.1 shows the interactions between the PTFE tip and SCM at different contact positions. The forces are much smaller by more than an order of magnitude compared to caramel at 30ºC where values are 0.006(±0.001)N/m, at 50ºC is 0.0055(±0.001)N/m, at 70ºC is 0.005(±-0.001)N/m and at 90ºC is 0.0045(±0.001)N/m. The decrease with temperature is marked but is proportionally less than that seen for the stainless steel. Overall stainless steel and PTFE both display much weaker forces for SCM than for caramel.

6.2.2 Different rates of retraction.

Figure 6.4.2 shows the results for adhesion forces at different rates of withdrawal from the surface over the four temperatures. Adhesion is seen to be very inconsistent, and few trends can be identified. At 30ºC the adhesion is 0.08(±0.02)N/m at 0.25µm/s, 0.09(±0.02)N/m at 0.75µm/s, 0.09(±0.02) at 1µm/s, 0.08(±0.02)N/m at 1.5µm/s, 0.1(±0.02) at 3µm/s and 0.1(±0.02)µm/s at 5µm/s. No possible trends are seen. The highest adhesion forces are found

for the fastest rate. Figure 6.5.2 shows the results at different rates, for the PTFE, here again no trends are seen, although the force may decrease slightly with the higher rate.

6.2.3 Different waiting times on SCM.

Figure 6.4.3 shows the force of adhesion for stainless steel microparticle at variable times on SCM. The results show:

(i) At 30°C the largest adhesion of 0.09(±0.02)N/m was seen between the stainless steel microparticle and SCM deposit this does not change significantly with hold time on the surface.

(ii) At 50°C degrees some adhesion of 0.08(±0.02)N/m is seen. As the temperature increases the adhesion decreases and no change is seen with time.

(iii) At 70ºC the force is 0.07(±0.02)N/m and at 90ºC the force is 0.06(±0.02)N/m at all times. Figure 6.5.3 shows the force of adhesion for the PTFE microparticle at variable times on SCM. Similar trends can be seen with the PTFE as in Figure 6.4.3 of stainless steel, the smallest adhesion forces are seen at intermediate contact times of 1 to 5 seconds. The stainless steel shows adhesion forces one order of magnitude greater than for PTFE, but the effect of contact time is similar. This suggests that it may be due to deposit properties, such as viscosity/ viscoelasticity that will not be surface-dependent.

6.3.1 AFM analysis of interactions between test surfaces and Whey protein

Whey protein was studied because it is known to be critical in milk fouling, and thus would be useful to compare the magnitude of the forces seen in the whey protein alone and in SCM.

6.3.1 Interactions at different contact positions.

Figure 6.6.1 illustrates the adhesion force at different contact positions, using the stainless steel microparticle when whey protein is heated at different temperatures. The results show

(i) At 30°C the largest adhesion of 0.005(±0.001)N/m was seen between stainless steel and whey protein,

(ii) At 50°C adhesion of 0.004(±0.001)N/m was seen. As observed in all other measurements. When temperature increases the adhesion decreases.

(iii) At 70°C adhesion of 0.0035(±0.001)N/m occurs and at 90°C the force is 0.0025(±0.001)N/m.

SCM showed values between 0.08 and 0.05N/m suggesting that the major contribution to fouling from SCM and stainless steel is not the whey proteins, as the force is an order of magnitude greater for SCM than for the protein alone. In Figure 6.7.1 results show the interactions between the PTFE tip and whey protein at different contact positions. There is a decrease in adhesion from 30°C to 90°C. The force at 30ºC is 0.004(±0.001)N/m, at 50ºC is 0.0038(±0.001)N/m, at 70ºC it is 0.0035(±0.001)N/m and at 90ºC it is 0.0028(±0.001)N/m. The magnitude of adhesion on stainless steel is greater than with PTFE. Data for PTFE is only about 20% less than for stainless steel. It is interesting to compare PTFE, SCM and whey protein, where the force values are quite similar. Figure 6.5.1 and 6.7.1, can be compared as they show values of the order of 0.004-0.006N/m for SCM and 0.004-0.003N/m for whey

protein. This is significantly different to the behaviour of whey protein and stainless steel; it suggests that for PTFE the major contribution to the adhesion in SCM is the whey proteins.

6.3.2 Different rates of retraction.

Figure 6.6.2 shows the results for different rates, changing the speed it takes for the stainless steel microparticle to go into the whey protein deposit and back off. At all temperatures the adhesion is seen to be very inconsistent, with no trend seen between the different rates. Figure 6.7.2 shows the results at different rates, for the PTFE microparticle on the whey protein. There are some effects from the rate of retraction; the minimum adhesion force appears to be at intermediate rates, at 1-1.5μm/s. Data for PTFE and stainless steel surfaces are similar.

6.3.3 Different waiting times on whey protein.

Figure 6.6.3 shows the force of adhesion on stainless steel microparticle at variable times on whey protein. The results show

(i) At 30°C the largest adhesion of 0.004(±0.001)N/m is between the stainless steel microparticle and whey protein deposit at different contact positions. There is little effect of contact time.

(ii) At 50°C degrees some adhesion of 0.003(±0.002)N/m is felt, as for all cases as the temperature increases adhesion decreases. No effect of time is seen.

(iv) At 70ºC force is 0.003(±0.002)N/m and

(v) At 90ºC force is 0.0025(±0.002)N/m at all times.

Figure 6.7.3 shows the force of adhesion between the PTFE microparticle and the whey protein at different times. A similar lack of trend is seen as in Figure 6.6.3. Slightly greater adhesion of 0.0045(±0.001)N/m is seen with stainless steel compared to the force of 0.004(±0.001)N/m with PTFE. In both cases, adhesion seems to be independent of waiting time on the deposits.

This similar behaviour was seen with stainless steel and PTFE in chapter 5 in Figures 5.2.2 and 5.3. Again adhesion decreases as temperature increases. This is due to a slight loss of moisture in SCM when heated; the sample weight decreases with heating by 5%. This trend was also evident with the caramel. However the different order of magnitude on the forces depending on temperature the two particles was not seen.

To summarise the results Figure 6.7.4 compares the force measurements for stainless steel and PTFE microparticle immersed in caramel, SCM and whey protein. At 30ºC and 90ºC data shows results from different contact positions on the deposits; the approach speed of 3µm/s, then a 5 second pause on the deposit and then the rate of retraction is 0.25µm/s. Significant (more than an order of magnitude) differences are seen between forces for the same and different deposits, and between different surfaces for the same deposits. Lower forces are seen at 90ºC in all cases. The higher the temperature, the less the force between surface and deposit. To design systems to resist fouling, these results suggest that measurements at process temperatures are needed.

6.4. Conclusions and implications for fouling studies.

To identify whether the data would be of value in fouling, AFM force measurement experiments have been conducted over a range of temperatures, rates, contact positions, surfaces and contact times. The following conclusions can be made:

- Temperature changes the food deposit structure as well as increasing the rate of some reactions, such as protein denaturation and aggregation. By comparison to the forces found at room temperature in previous chapters, the increase in temperature causes adhesion forces to decrease at different contact points.
- The time the tip sits on each food deposit does not affect adhesion behaviour. The adhesion is similar or consistent at all times, but varies with temperature. This is similar to micromanipulation.
- The rate of retraction on the deposit causes some variability in the adhesion behaviour. The effect on adhesion with retraction rate is not predictable.

The two surfaces used; PTFE and stainless steel show that adhesion occurs with both but is less with PTFE than stainless steel. The results of Chapters 5 and 6 show similar effects – micromanipulation and AFM data appears to be comparable, suggesting that it is possible to use AFM to study cleanability.

The experimental data shows that the forces of adhesion are much less at high temperature than at low temperatures. This is especially interesting as fouling deposits form at high temperatures; such as the 60-100ºC at which caramel is processed, and the 70-90ºC for milk pasteurisation, which causes deposition of Type A protein-rich deposit. Deposit must form at these high process temperatures, but the adhesive forces are very small – much

smaller than would be predicted by doing experiments with AFM and micromanipulation at room temperature. It is interesting that the trends of the measurements at room temperature are the same as those at high temperatures. Any effective models for fouling must account for adhesion of deposits onto surfaces with the low adhesion forces seen here, such as for whey protein and stainless steel. The effect of these forces must be greater than the effect of surface shear in creating a deposit. The results suggest that equipment or flow regimes to resist fouling will be overdesigned if only data for adhesion at room temperature is considered. This potentially is an important result: data at room temperature for cleaning is much easier to obtain than that at high temperature.

The experiments suggest that only by doing experiments on measuring adhesion at real process temperatures will an accurate measurement be obtained. This is especially important if we are to use computational models for fouling and cleaning, in which the shear stress on the surfaces of plant or deposit can be predicted. The forces measured at room temperature are a significant overestimate of those, which are found at temperature. Of course it is well known that cleaning becomes easier at high temperatures [as discussed in Chapter 2] but these results allow quantification of it.

It was expected that the adhesion force between particle and surface would increase with time as – for example, whey protein denaturation and aggregation proceeds and bonds form. The data suggests that these reactions have little effect on the adhesion forces, at least as measured by AFM; more work needs to be done to determine what effects, if any, reaction processes have on adhesion at these temperatures.

Chapter 6 Figures:

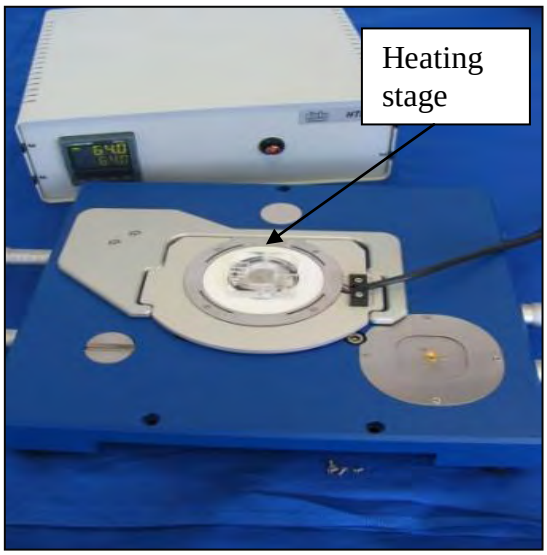

Figure 6.1: The Nanowizard II (JPK) adapted with a heating stage (JPK).

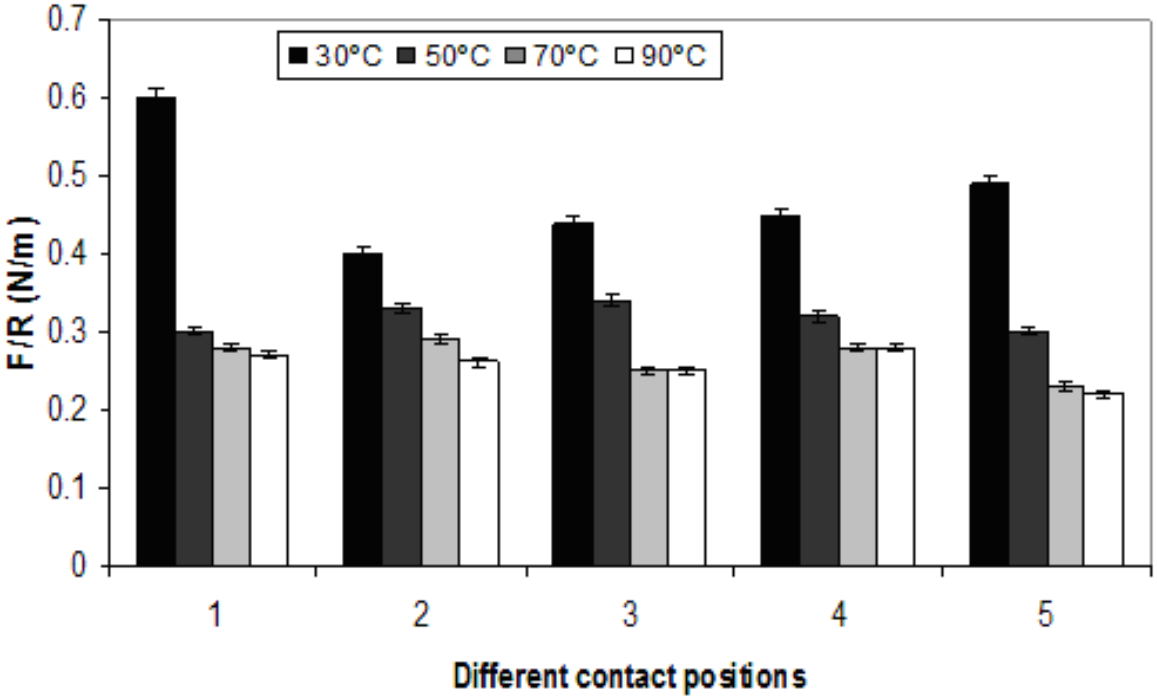

Figures 6.2.1: Force measurements of a Stainless steel microparticle immersed in caramel and then retracted off the deposit. Caramel was spread out between 50µm to 60µm thick on a glass slide, then the caramel was heated for 5 minutes at each temperature and the temperature was monitored and controlled at required temperature. Data shows results from five different contact positions on the caramel deposit. The approach speed for all experiments was 3µm/s, then a 5 second pause on deposit and rate of retract was 0.25µm/s. The data shows variation of the mean of the five experiments. F/R at different contact positions. (The error bars show the average of five experiments)

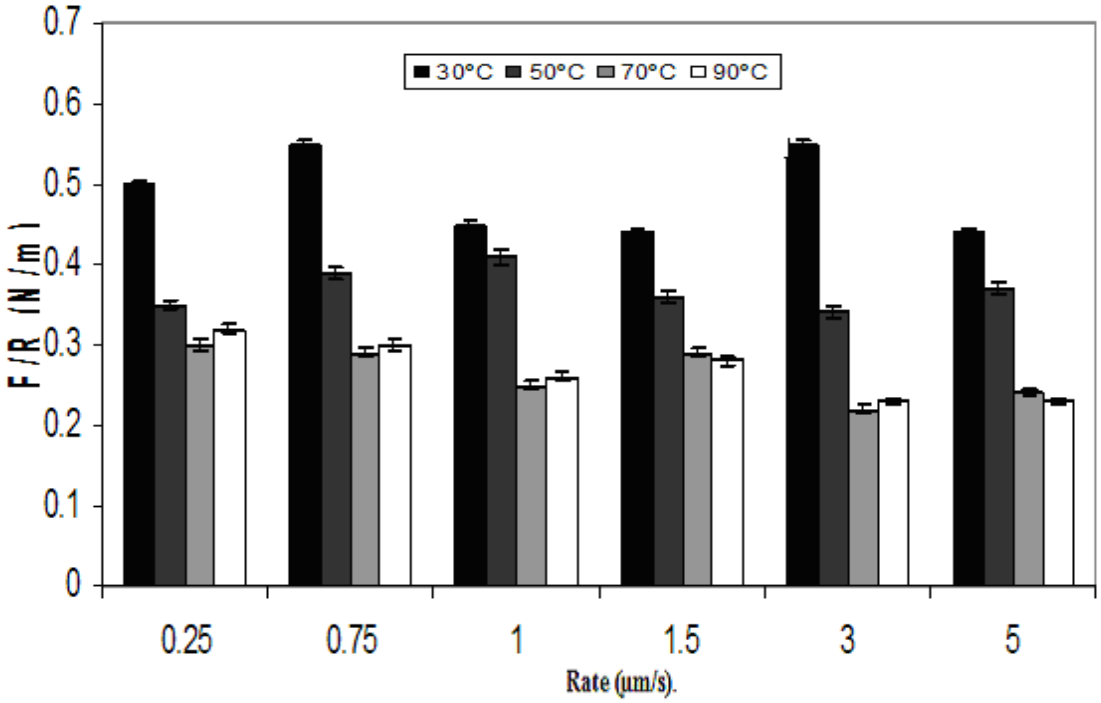

Figure 6.2.2: Force measurements of a Stainless steel microparticle immersed in caramel and then retracted off the deposit, at variable rates. The deposit was spread out between 50µm to 60µm thick on a glass slide, then the caramel was heated for 5 minutes at each temperature and the temperature was monitored and controlled at the required temperature. The retract speed for all experiments was 0.25, 0.75, 1.00, 1.5, 3 and 5µm/s. The tip was held on the deposit for 5 seconds before retraction.

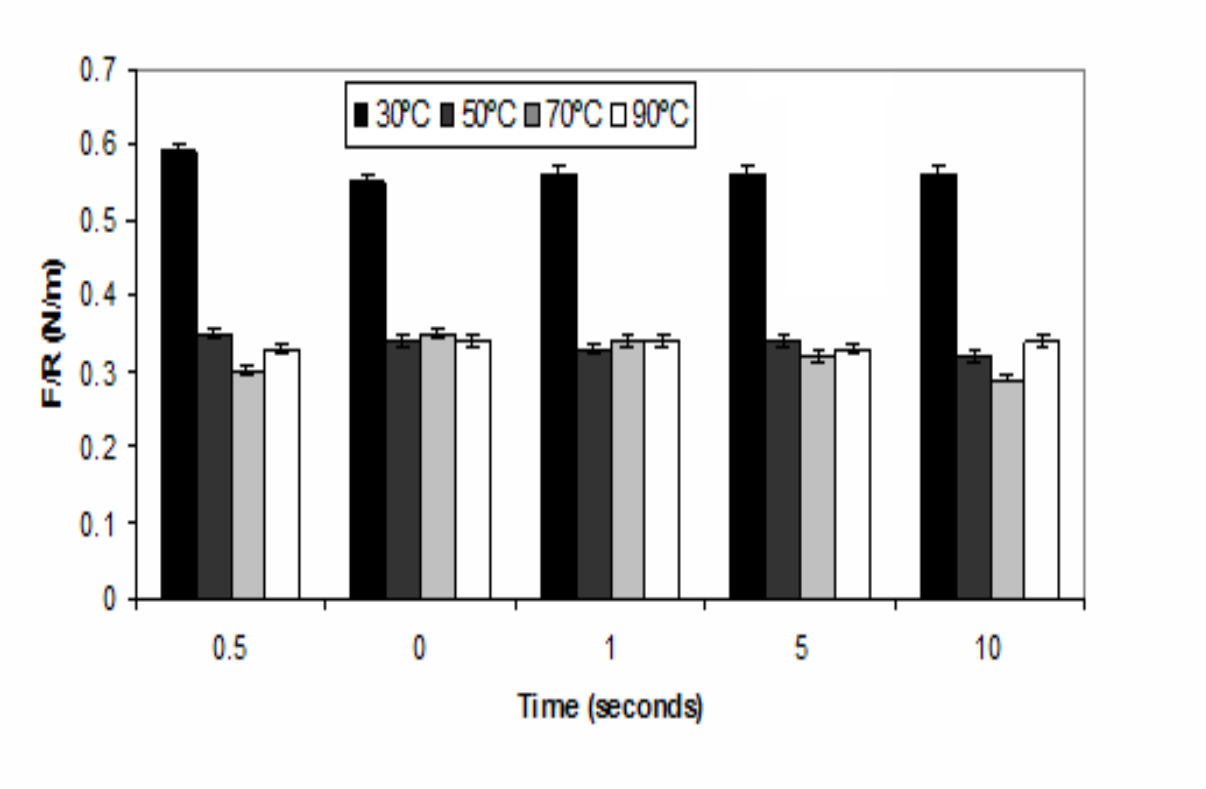

Figure 6.2.3: Force measurements of a Stainless steel microparticle immersed in caramel and then retracted off the deposit, at variable times. The deposit was spread out between 50µm to 60µm thick on a glass slide, then the caramel was heated for 5 minutes at each temperature and the temperature was monitored and controlled at the required temperature. The waiting times on the deposits for the experiments were 0, 0.5, 1.0, 5.0 and 10 seconds. The approach speed for all experiments was 3µm/s and a rate of retraction was 0.25µm/s.

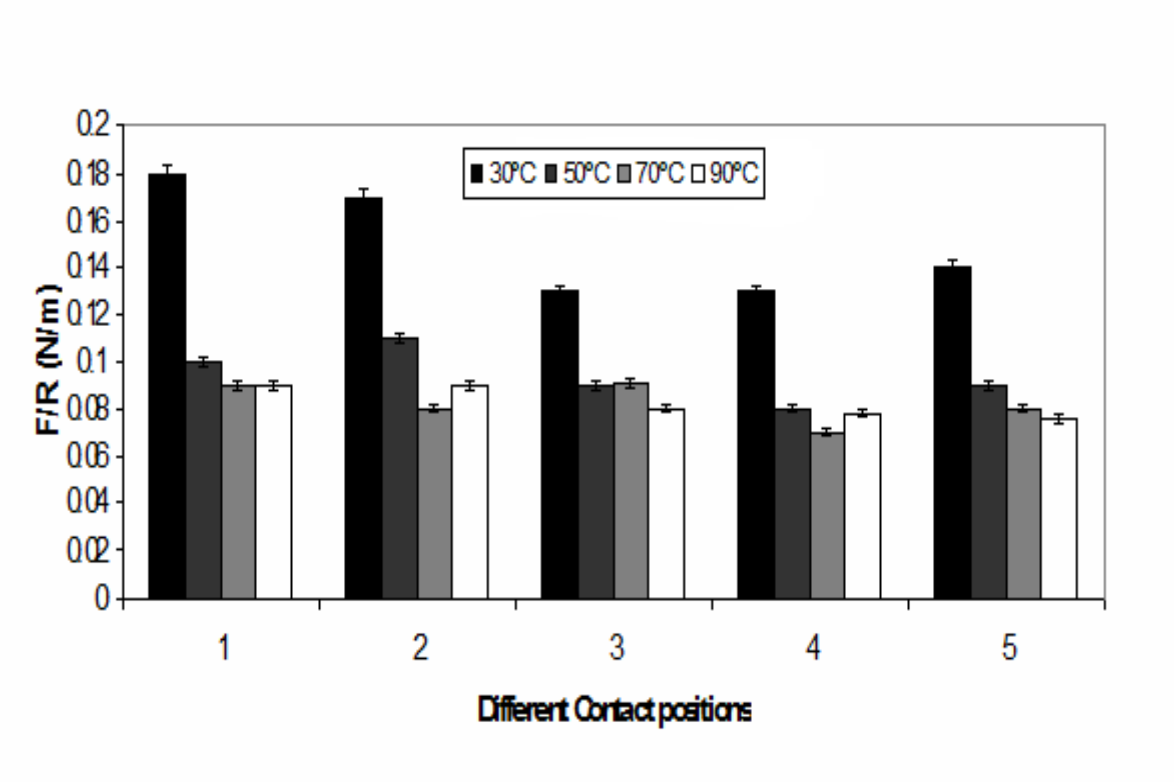

6.3.1: Force measurements of a PTFE microparticle immersed in caramel and then retracted off the deposit. Caramel was spread out between 50µm to 60µm thick on a glass slide, then the caramel was heated for 5 minutes at each temperature and the temperature was monitored and controlled at required temperature. Data shows results from five different contact positions on the caramel deposit. The approach speed for all experiments was 3µm/s, then a 5 second pause on deposit and rate of retraction was 0.25µm/s. The data shows a global variation of the mean of the five experiments.

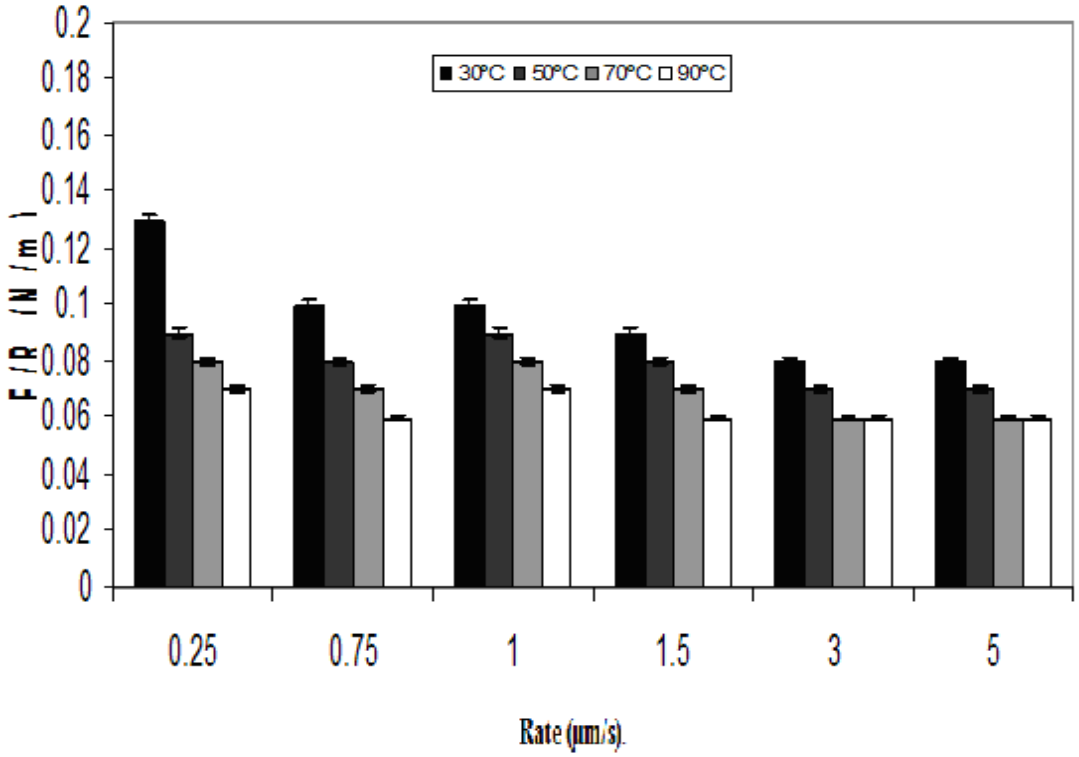

6.3.2: Force measurements of a PTFE microparticle immersed in caramel and then retracted off the deposit, at variable rates on caramel. The deposit was spread out between 50µm to 60µm thick on a glass slide, then the caramel was heated for 5 minutes at each temperature and the temperature was monitored and controlled at the required temperature. The retraction speed for all experiments was 0.25, 0.75, 1.00, 1.5, 3 and 5µm/s. The tip was held on deposit for 5 seconds.

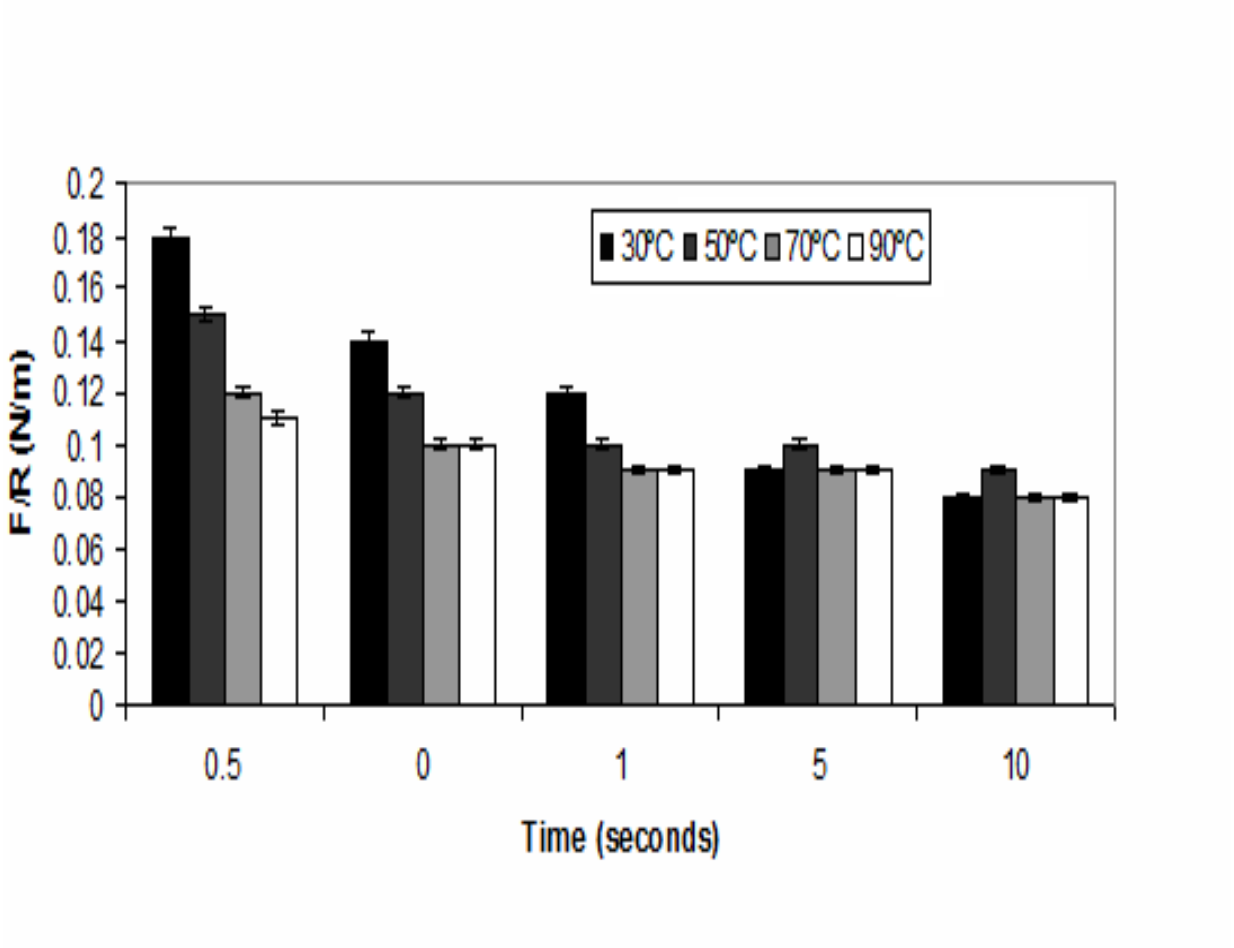

6.3.3: Force measurements of a PTFE microparticle immersed in caramel and then retracted off the deposit, at variable times on caramel. The deposit was spread out between 50µm to 60µm thick on a glass slide, then the caramel was heated for 5 minutes at each temperature and the temperature was monitored and controlled at the required temperature. The waiting times on the deposits for the experiments were 0, 0.5, 1.0, 5.0 and 10 seconds. The approach speed for all experiments was 3µm/s and a rate of retract was 0.25µm/s.

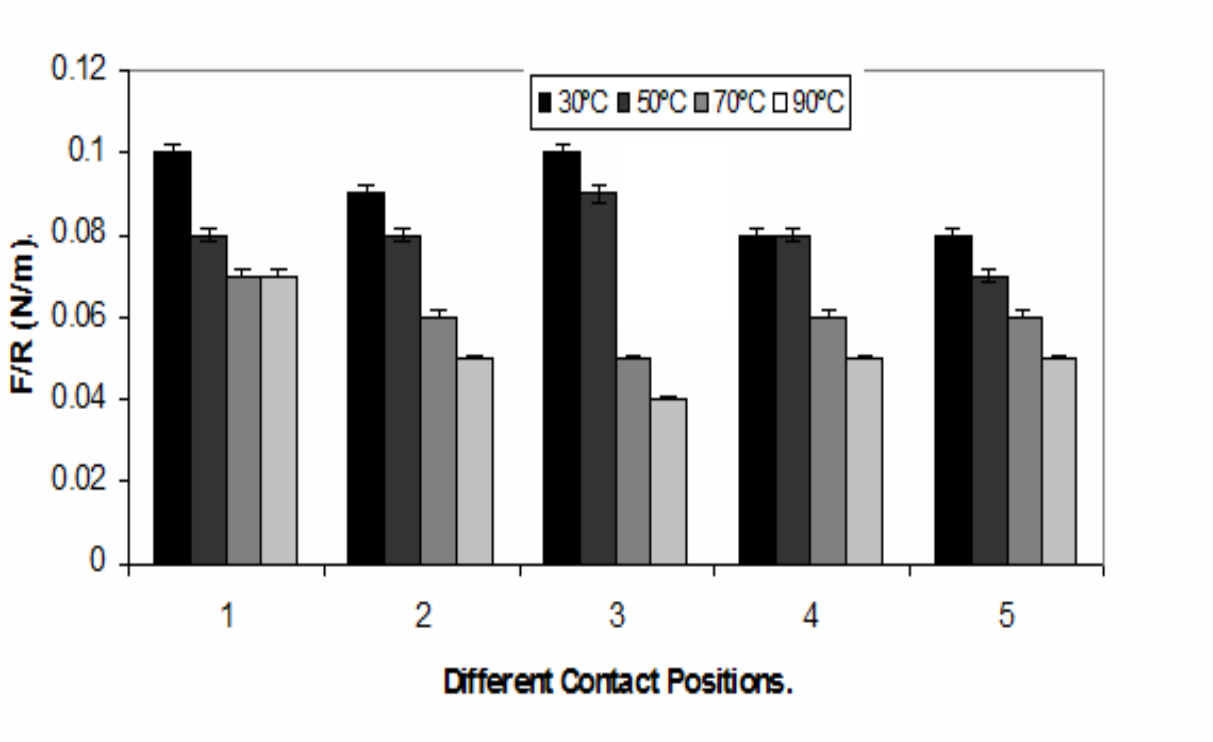

6.4.1: Force measurements of a stainless steel microparticle immersed in SCM and then retracted off the deposit. SCM was spread out between 50µm to 60µm thick on a glass slide, then the SCM was heated for 5 minutes at each temperature and the temperature was monitored and controlled at required temperature. Data shows results from five different contact positions on the SCM deposit. The approach speed for all experiments was 3µm/s, then a 5 second pause on deposit and rate of retract was 0.25µm/s. The data shows a global variation of the mean of the five experiments.

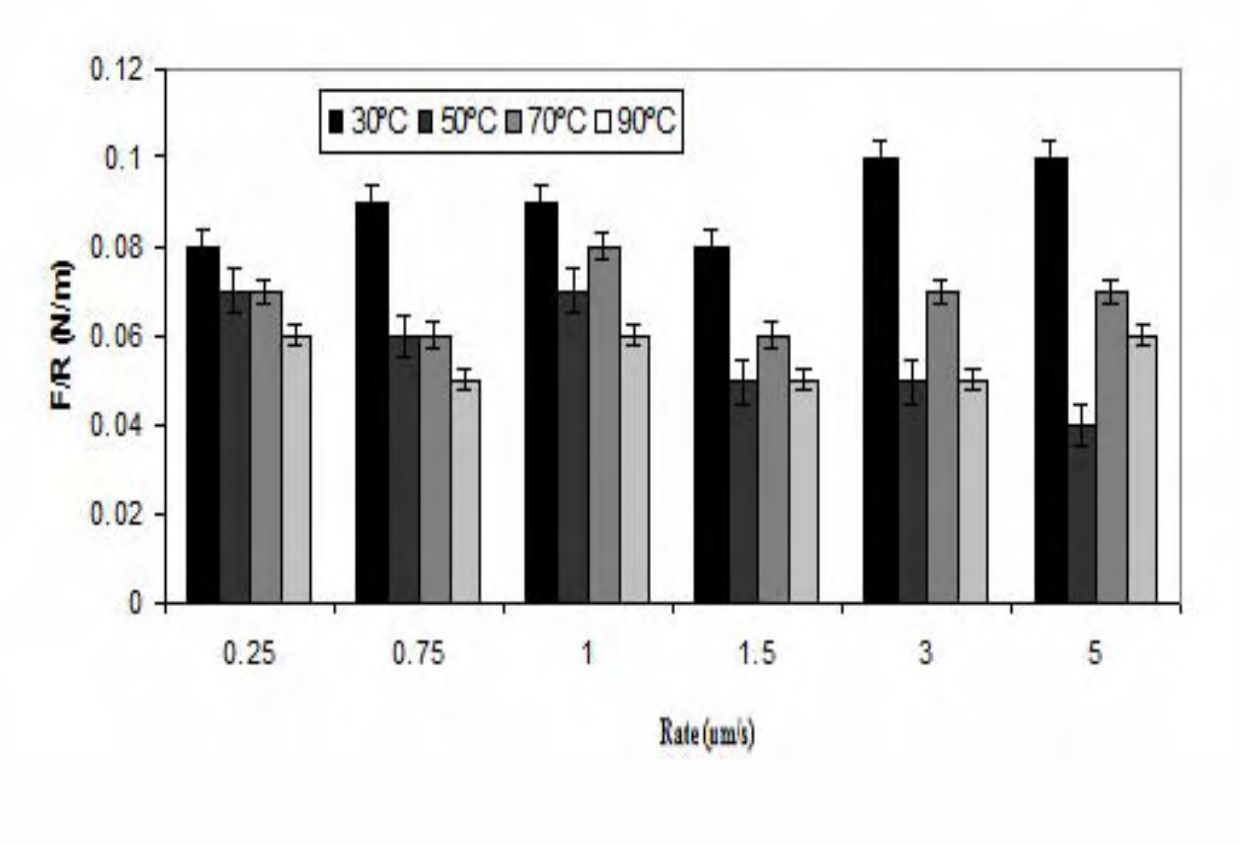

6.4.2: Force measurements of a stainless steel microparticle immersed in SCM and then retracted off the deposit, at variable rates on SCM. The deposit was spread out between 50µm to 60µm thick on a glass slide, then the SCM was heated for 5 minutes at each temperature and the temperature was monitored and controlled at the required temperature. The retract speed for all experiments was 0.25, 0.75, 1.00, 1.5, 3 and 5µm/s. The tip was held on deposit for 5 seconds.

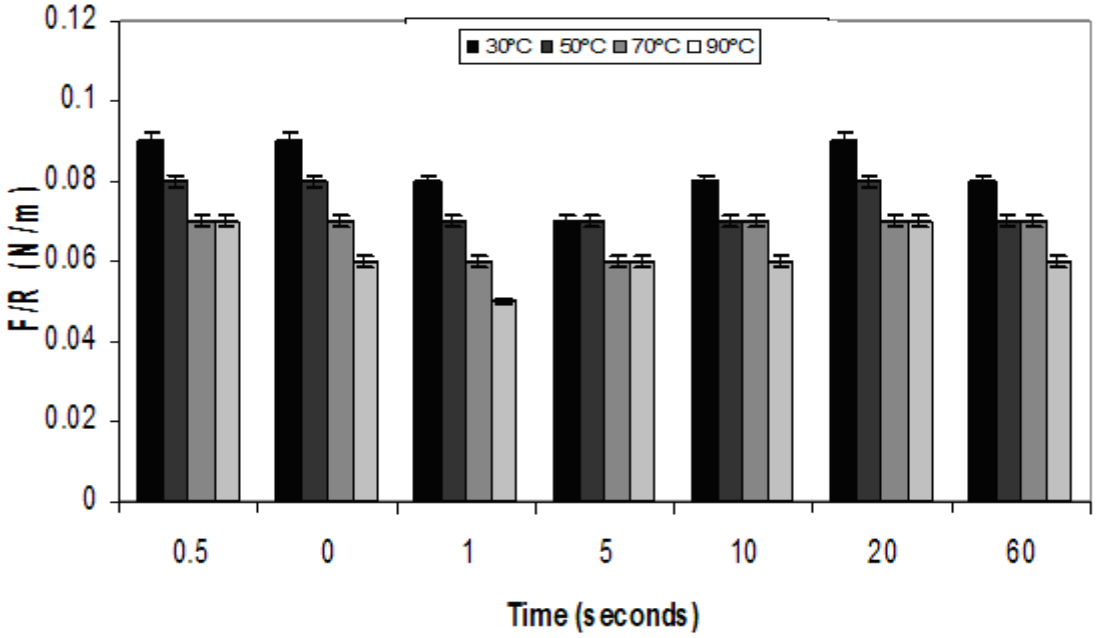

6.4.3: Force measurements of a stainless steel microparticle immersed in SCM and then retracted off the deposit, at variable times on SCM. The deposit was spread out between 50µm to 60µm thick on a glass slide, then the SCM was heated for 5 minutes at each temperature and the temperature was monitored and controlled at the required temperature. The waiting times on the deposits for the experiments were 0, 0.5, 1.0, 5.0, 10, 20 and 60 seconds. The approach speed for all experiments was 3µm/s and a rate of retract was 0.25µm/s.

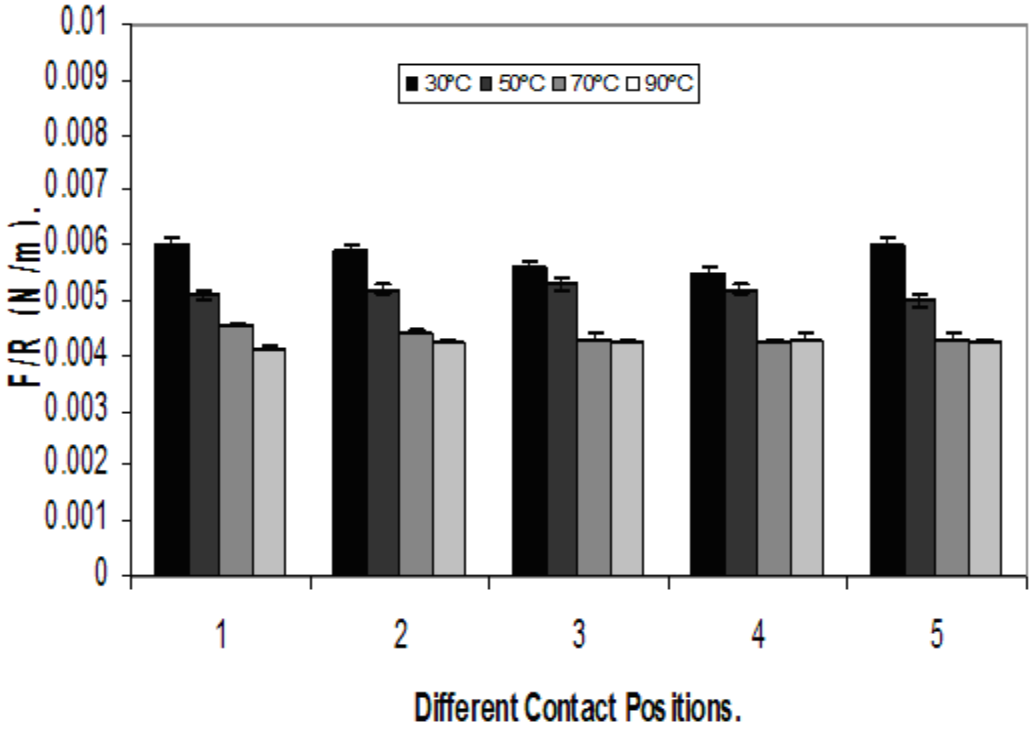

6.5.1: Force measurements of a PTFE microparticle immersed in SCM and then retracted off the deposit. SCM was spread out between 50µm to 60µm thick on a glass slide, then the SCM was heated for 5 minutes at each temperature and the temperature was monitored and controlled at required temperature. Data shows results from five different contact positions on the SCM deposit. The approach speed for all experiments was 3µm/s, then a 5 second pause on deposit and rate of retract was 0.25µm/s. The data shows a global variation of the mean of the five experiments.

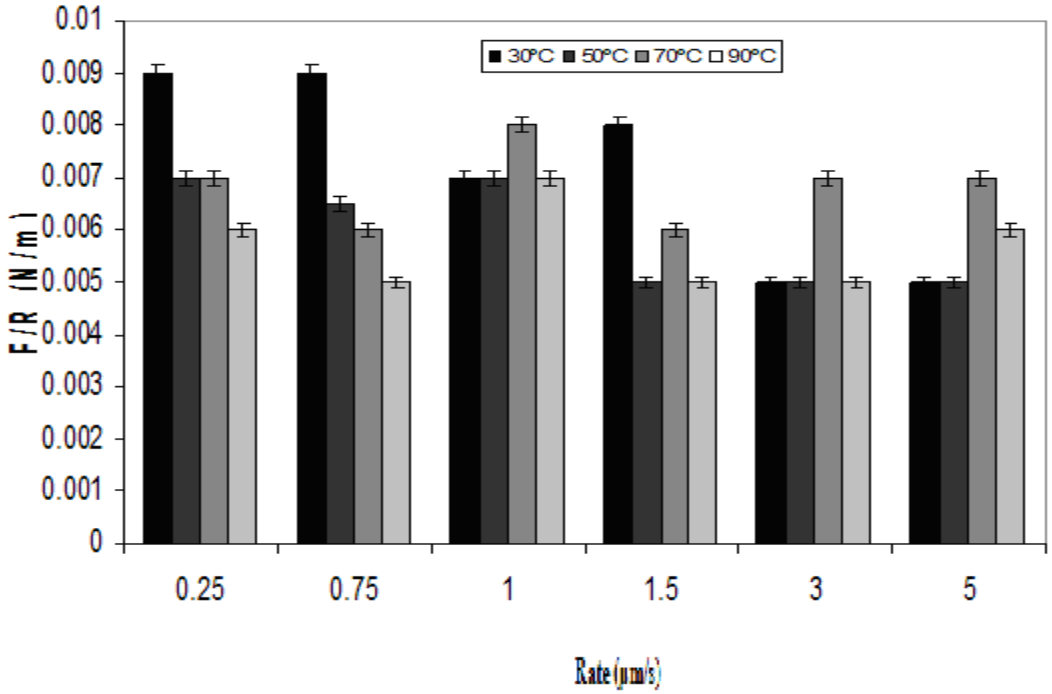

6.5.2: Force measurements of a PTFE microparticle immersed in SCM and then retracted off the deposit, at variable rates on SCM. The deposit was spread out between 50µm to 60µm thick on a glass slide, then the SCM was heated for 5 minutes at each temperature and the temperature was monitored and controlled at the required temperature. The retract speed for all experiments was 0.25, 0.75, 1.00, 1.5, 3 and 5µm/s. The tip was held on deposit for 5 seconds.

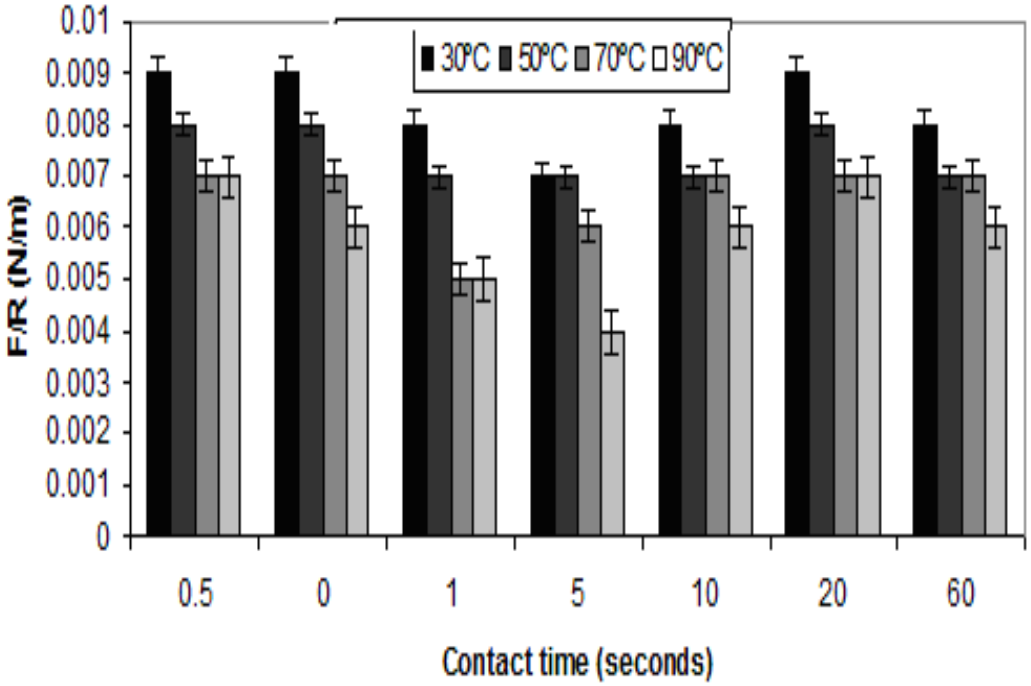

6.5.3: Force measurements of a PTFE microparticle immersed in SCM and then retracted off the deposit, at variable times on SCM. The deposit was spread out between 50µm to 60µm thick on a glass slide, then the SCM was heated for 5 minutes at each temperature and the temperature was monitored and controlled at the required temperature. The waiting times on the deposits for the experiments were 0, 0.5, 1.0, 5.0, 10, 20 and 60 seconds. The approach speed for all experiments was 3µm/s and a rate of retract was 0.25µm/s.

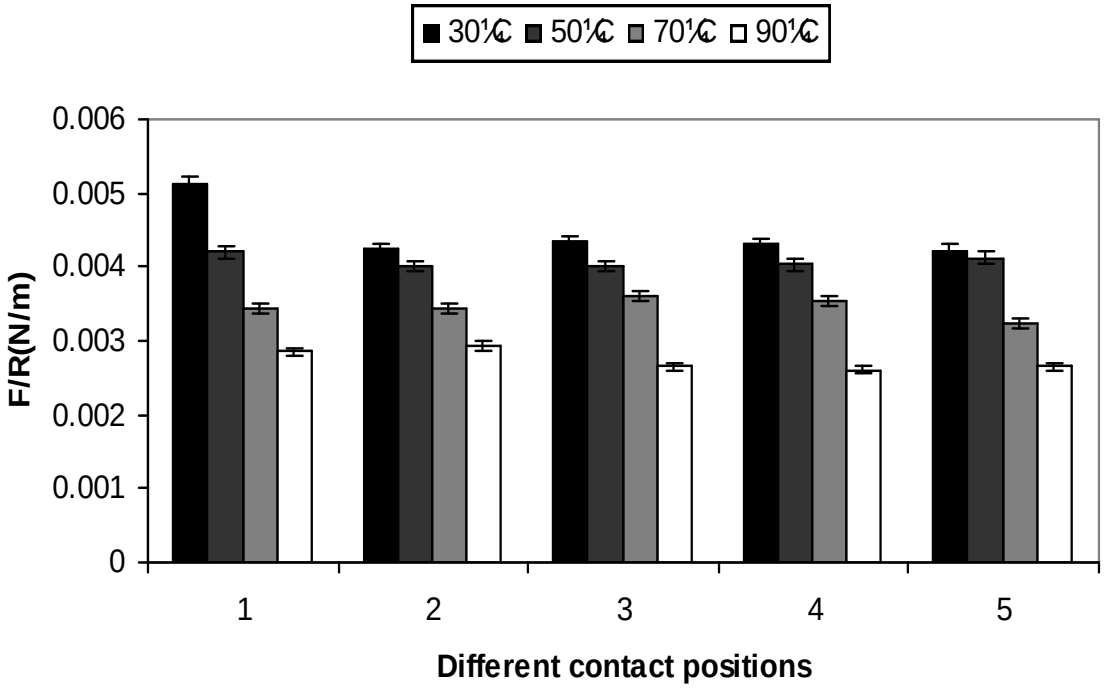

Figure 6.6.1: Force measurements of a stainless steel microparticle immersed in whey protein and then retracted off the deposit. Whey protein was spread out between 50µm to 60µm thick on a glass slide, then the whey protein was heated for 5 minutes at each temperature and the temperature was monitored and controlled at required temperature. Data shows results from five different contact positions on the whey protein deposit. The approach speed for all experiments was 3µm/s, then a 5 second pause on deposit and rate of retract was 0.25µm/s. The data shows a global variation of the mean of the five experiments.

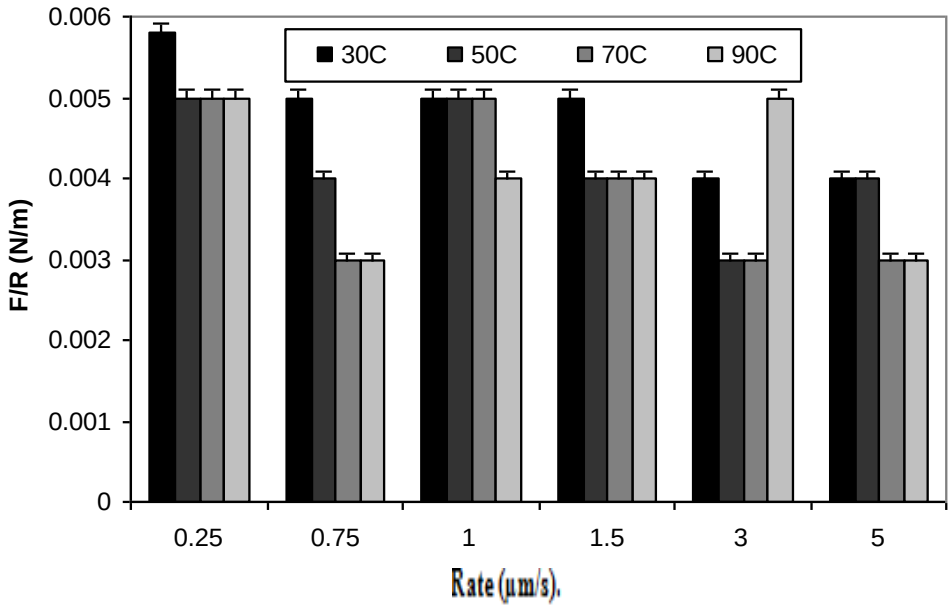

Figure 6.6.2: Force measurements of a stainless steel microparticle immersed in whey protein and then retracted off the deposit, at variable rates on whey protein. The deposit was spread out between 50µm to 60µm thick on a glass slide, then the whey protein was heated for 5 minutes at each temperature and the temperature was monitored and controlled at the required temperature. The retract speed for all experiments was 0.25, 0.75, 1.00, 1.5, 3 and 5µm/s. The tip was held on deposit for 5 seconds.

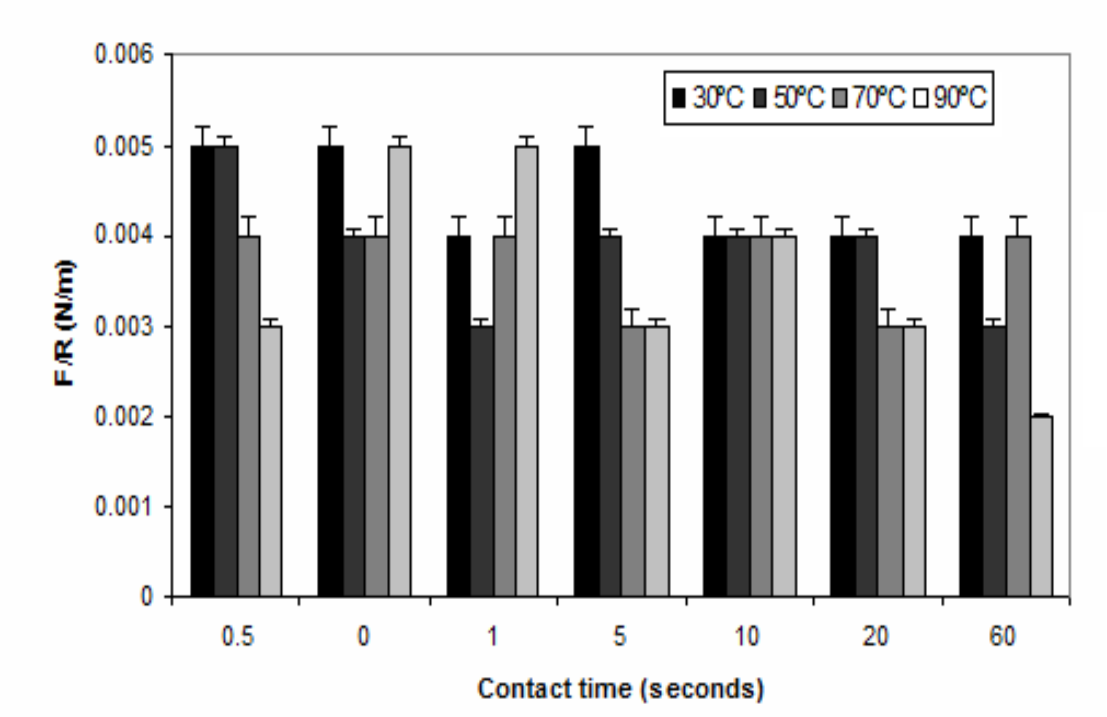

Figure 6.6.3: Force measurements of a stainless steel microparticle immersed in whey protein and then retracted off the deposit, at variable times on whey protein. The deposit was spread out between 50µm to 60µm thick on a glass slide, then the whey protein was heated for 5 minutes at each temperature and the temperature was monitored and controlled at the required temperature. The waiting times on the deposits for the experiments were 0, 0.5, 1.0, 5.0, 10, 20 and 60 seconds. The approach speed for all experiments was 3µm/s and a rate of retract was 0.25µm/s.

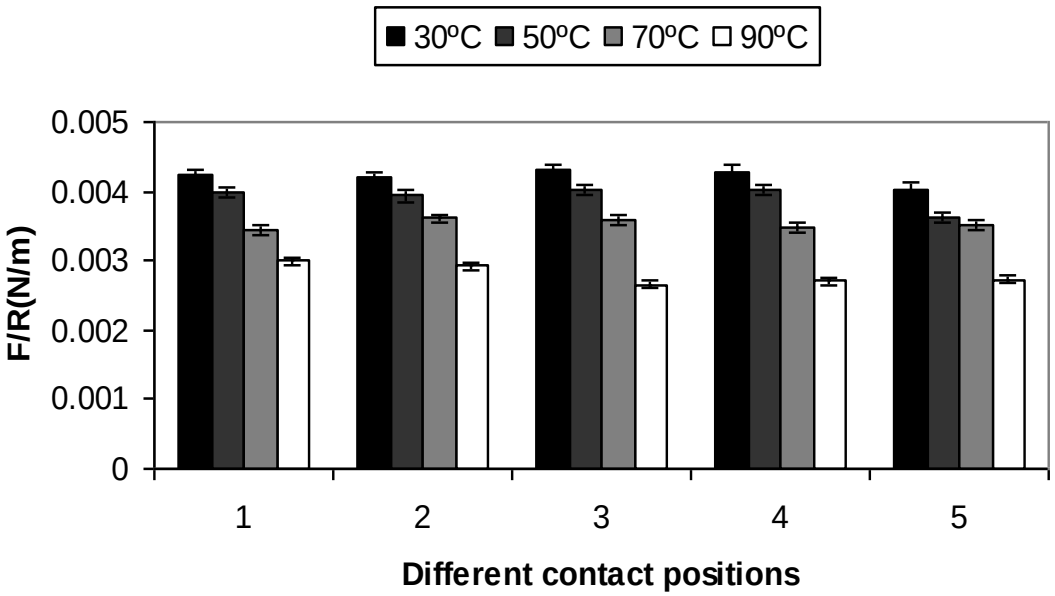

Figure 6.7.1: Force measurements of a PTFE microparticle immersed in whey protein and then retracted off the deposit. Whey protein was spread out between 50µm to 60µm thick on a glass slide, then the whey protein was heated for 5 minutes at each temperature and the temperature was monitored and controlled at required temperature. Data shows results from five different contact positions on the whey protein deposit. The approach speed for all experiments was 3µm/s, then a 5 second pause on deposit and rate of retract was 0.25µm/s. The data shows a global variation of the mean of the five experiments.

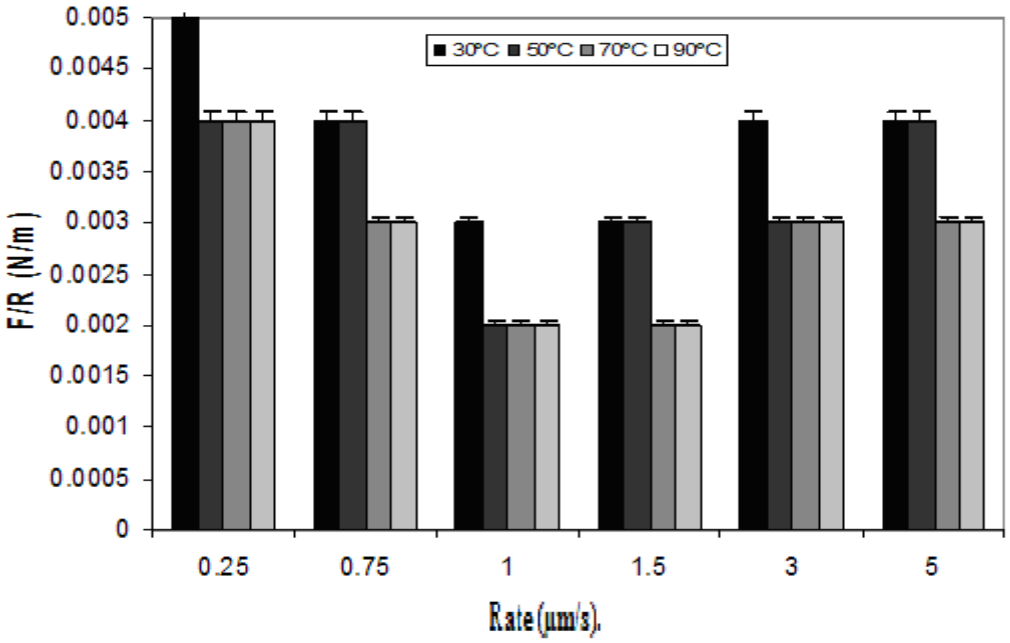

Figure 6.7.2: Force measurements of a PTFE microparticle immersed in whey protein and then retracted off the deposit, at variable rates on whey protein. The deposit was spread out between 50µm to 60µm thick on a glass slide, then the whey protein was heated for 5 minutes at each temperature and the temperature was monitored and controlled at the required temperature. The retract speed for all experiments was 0.25, 0.75, 1.00, 1.5, 3 and 5µm/s. The tip was held on deposit for 5 seconds.

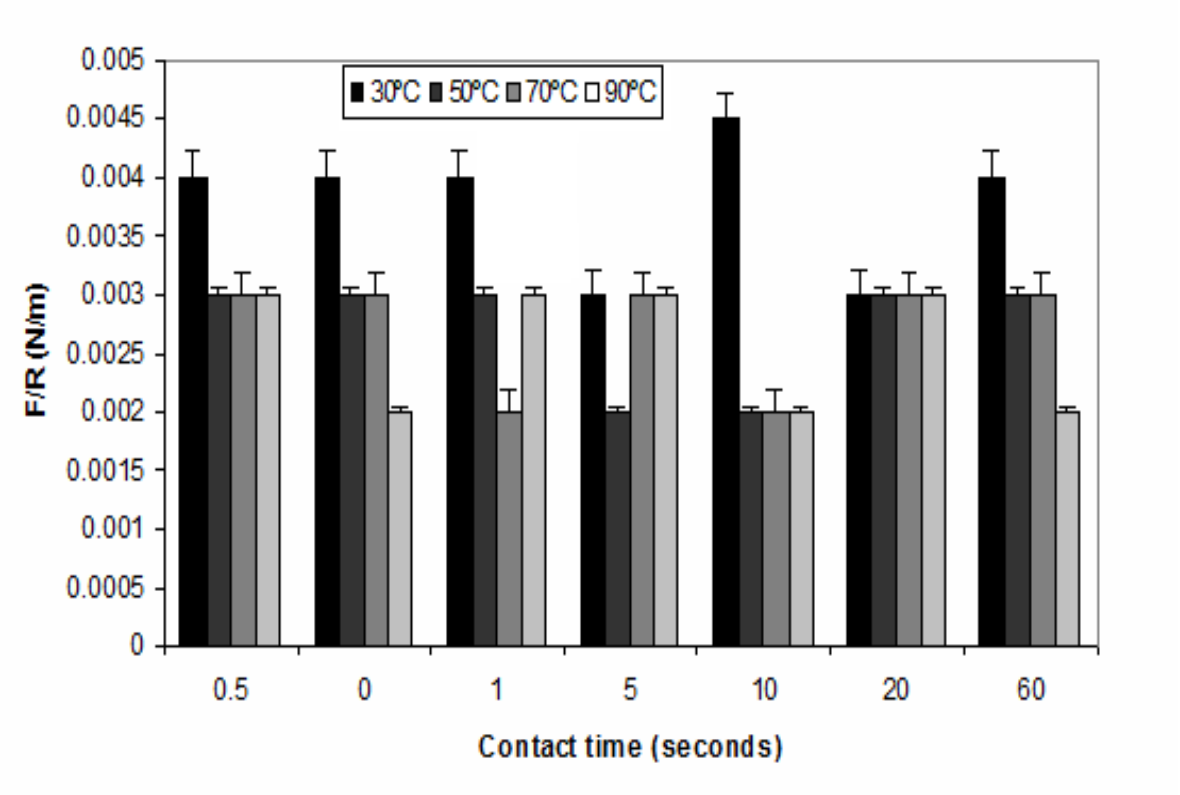

Figure 6.7.3: Force measurements of a PTFE microparticle immersed in whey protein and then retracted off the deposit, at variable times on whey protein. The deposit was spread out between 50µm to 60µm thick on a glass slide, then the whey protein was heated for 5 minutes at each temperature and the temperature was monitored and controlled at the required temperature. The waiting times on the deposits for the experiments were 0, 0.5, 1.0, 5.0, 10, 20 and 60 seconds. The approach speed for all experiments was 3µm/s and a rate of retract was 0.25µm/s.

30°C

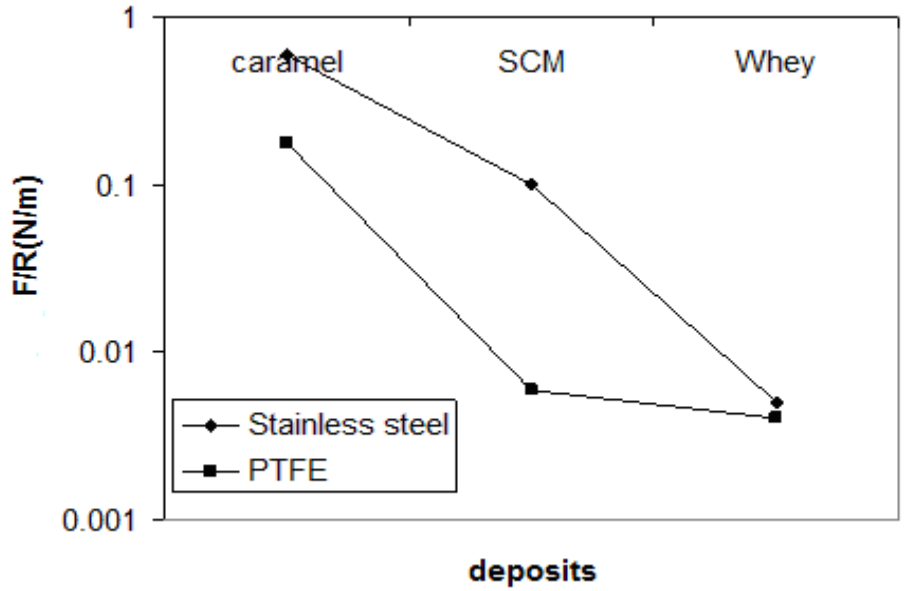

90°C

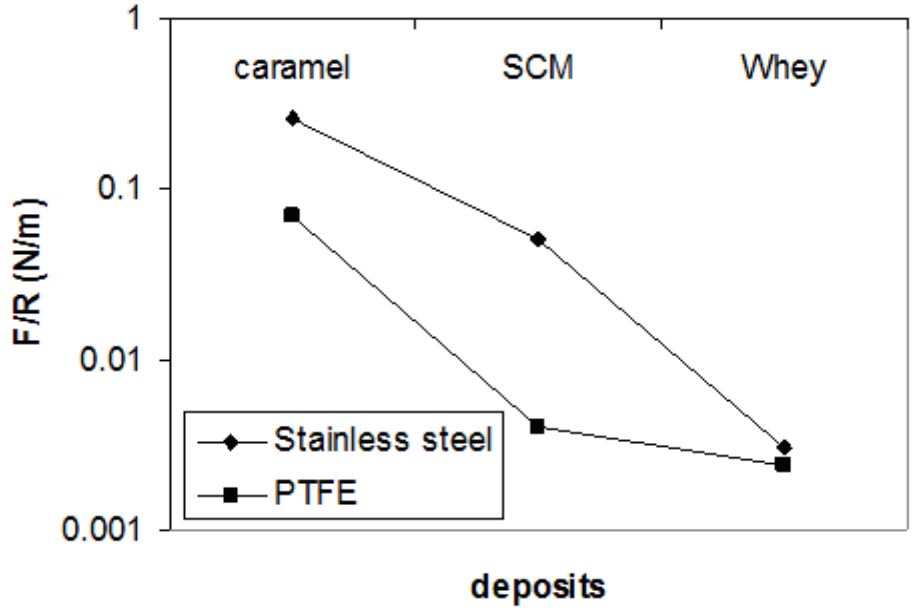

Figure 6.7.4: Summary of Log force measurements of stainless steel and PTFE microparticle immersed in caramel, SCM and whey protein. Data shows results from different contact positions on the deposits. The approach speed for all experiments was 3µm/s, then a 5 second pause on deposit and rate of retract was 0.25µm/s at 30ºC and 90ºC.

CHAPTER 7: CONCLUSIONS AND FURTHER DISCUSSIONS

The contamination of surfaces by fouling and pathogenic micro-organisms is a cause of serious concern within the food industry. The levels of cleanability of material should be addressed when choosing materials for process line equipment, along with their mechanical and anticorrosive properties. A review of previous studies in the literature, largely based on studying the surface interactions and cleaning/fouling processes showed little information on the use of Atomic Force Microscopy (AFM) used in fouling and cleaning. The aim of this thesis is to increase understanding of how interactions between surfaces and deposits may control the cleaning process.

Previous work at Birmingham has led to the classification of cleaning problems into a series of types, of which three are the most difficult to remove in practical terms:

- Fluid mechanical soils; here the bonds between elements of the deposits are such that the deposits can be cleaned with water alone; examples are personal care products such as shampoos, deodorants and toothpaste;
- Biofilms; these can form as thin layers or materials of living organisms, which have to be cleaned using chemical that will kill the organisms as well as remove them from the surface;

- Diffusion-reaction soils; here the bonds between elements of the deposit, and/or deposit and surface are such that the deposit cannot be removed by fluid action alone, so cleaning chemical is needed to react with the deposit to enable removal; examples are the protein or mineral-based deposits which are formed on heat exchanger surfaces during the thermal processing of milk.

Within this project a series of deposits were chosen as representatives of the above problem categories:

- Toothpaste, a soil which can be removed by fluid mechanical action alone;
- As representative of diffusion-reaction soils a series of materials have been used; 'Turkish delight', 'caramel' and sweetened condensed milk give cleaning problems in confectionary processing, whilst whey proteins form the majority of the deposit in milk pasteurisers;

The thesis concentrates on surface interactions between these different food and personal product deposits, using AFM in force mode, to investigate the responses of different surfaces to different foulant materials. This work will help to understand the effects of interfacial surface parameters on the cleaning of different foulant deposits, and may aid in the development of low-fouling and easy-to-clean surfaces.

Four different surfaces were chosen as being representative of surfaces found in industrial practice; stainless steel, glass, ceramic and PTFE. Ceramic and stainless steel surfaces were

substantially rougher than the PTFE and glass surfaces. A number of ‘anti-fouling’ surfaces have been proposed, many of which are based around PTFE.

The AFM provides a method for detecting nanoscale information. Applications of AFM are potentially widespread in food research; it has been used for molecular interaction, molecular manipulation, surface topography, and deposit characterization. AFM analysis could be used to determine physical, chemical and structural mechanisms of fouling and cleaning.

The utility of the AFM has been tested in three different studies:

(iv) To find whether different components of a fluid have significantly different effects on the interactions between particles and surfaces, i.e. to see whether it might be possible to change the surface interactions of a material by changing its composition;

(v) To study whether nano-scale measurements can predict the behaviour at higher length scales, a series of experiments were carried out in which the interaction between deposits and different surfaces was studied using the AFM, as well as using a micromanipulation probe to study the removal of deposits at a micron-mm scale;

(vi) To study the variation of the adhesion forces with temperature; clearly the initial adhesion of deposits occurs at elevated temperature, so it would be useful to understand how the magnitude of the forces change.

7.1.1 Toothpaste ingredients force measurements

. AFM was employed to measure the adhesive interactions between a colloidal silica microparticle and stainless steel, PTFE-coated stainless steel, glass and ceramic surfaces, in the presence of a number of solutions and suspensions of ingredients found in commercially available toothpaste. The purpose was to obtain better understanding of the aqueous environment in which AFM adhesion force measurements were performed and to understand interactions that may occur between the aqueous environment and ingredient solutions

In the presence of most ingredients a repulsive behaviour was observed, indicative of ionic double layer effects, as the silica microparticle will be charged in aqueous solution. A hydrophobic effect-type attraction was observed for the interaction between the silica microparticle and the stainless steel and ceramic surfaces.

In the presence of saccharin solution, sodium lauryl sulphate solution, zinc citrate solution and titanium dioxide suspension, no pull-off forces were measured for the four surfaces and a repulsive interaction was generally observed. The data suggest that the polyanionic charge on the silica surface, which will be deprotonated in aqueous solutions such as zinc citrate and the other solutions mentioned above, dominates the interaction. Stainless steel, glass and ceramic surfaces all have oxygen-rich surface chemistries, in the form of chromium oxide, silicon dioxide and aluminium oxide.

A ‘‘hydrophobic effect’’ deflection-displacement curve is seen, in which an adhesion force is seen to result from the interaction between the silica attached tip and stainless steel surface in presence of HPLC water. This interaction also occurs with the ceramic surface. It has previously been established that for hydrophobic surfaces immersed in water, an attractive

force exists that cannot be accounted for by dispersion forces alone [Mantel, *et al*. 1995]. The origin of the hydrophobic effect is often believed to be changes in water structure adjacent to hydrophobic surfaces, which are entropically unfavourable and impose a new, more ordered structure on the water molecules. This gives rise to an attractive force between silica and surfaces. In water, both ceramic and stainless steel surfaces exhibit a long-range attractive interaction with the silica microparticle and this interaction is indicative of a hydrophobic force. The oxide-terminated stainless steel and ceramic surfaces could give rise to such a force, whereas the glass surface would not be expected to, and indeed does not, as the glass surface is terminated with silicon hydroxide moieties.

One component of the toothpaste, sorbitol solution, shows strong adhesive interactions of 1.70mN/m between stainless steel surfaces discs using the silica microparticle. Sorbitol is used as humectant in many types of products for protection against loss of moisture content, both in oral care products, such as toothpaste and mouthwash, food products such as chewing gums, cookies and cakes, as well as in glues and sticky tapes to help retain adhesive properties. [Britten 1998].

Of the four surfaces only stainless steel exhibited an adhesive interaction with the silica microparticle in sorbitol solution. Conclusions were:

- Contact angle measurements showed that the different surfaces behave differently with a drop of water and sorbitol.
- AFM found different types of behaviour in the presence of saccharin solution, sodium lauryl sulphate solution, sorbitol, zinc citrate solution and titanium dioxide suspension.

7.1.2 Comparison between measurements using Atomic Force Microscopy to those of Micromanipulation.

No previous work has attempted to study the interactions between interfacial measurements at two length scales. It was valuable to do this for a range of reasons, firstly to develop ways of testing surfaces for their fouling potential and cleanability and to identify the smallest scale relevant results that can be obtained.

The soils investigated here generally adhere most strongly to the glass surface with the exception of Turkish delight. The results suggest that the general behaviour with the deposit and microparticle is as follows; glass provides the largest adhesion, then stainless steel and PTFE. The data suggests that PTFE surfaces would in general be better than stainless steel in terms of reducing fouling or cleaning. The use of PTFE-based surfaces in fouling reduction is discussed in Chapter two of the thesis; however there is a difficulty in making reproducible and cheap PTFE coated equipment.. It is clear that this sort of surface can give either reduced fouling or more effective cleaning.

This work has used AFM and micromanipulation equipment to identify adhesive and cohesive effects in the cleaning of food deposit. The caramel deposits are essentially highly cohesive (physical properties of deposits cause intermolecular attraction between like-molecules). On the other hand, SCM, Turkish delight and toothpaste are highly adhesive results suggest that for the SCM, toothpaste and Turkish delight, the cohesive forces between elements of the deposits are weaker (loosely bound) than those of adhesion between surface and deposits, which is opposite to the behaviour of caramel. Thus, it is easier to remove the whole of the caramel deposit than to remove a surface layer. This indicates the AFM and

micromanipulation technique can identify the different mechanical properties of fouling deposits.

In both measurement methods the results show caramel to display adhesive failure and toothpaste, Turkish delight and SCM to show cohesive failure. The PTFE surface generally shows lower adhesion using both AFM and micromanipulation. Both measurement methods measure adhesion forces, however the size of the force is larger with micromanipulation due to the sample contact requiring deformation of the solid as well as contact between deposit and surface. The AFM measures the force at smaller scale length than the Micromanipulation. AFM is a more sensitive measurement method, but significantly more parameters are required to set up experiments, such as the right size of particle and the right cantilever stiffness. Also it is not known until till the experiment is performed how much z-range is required. In comparison the micromanipulation is simple to use and set up. Most deposits are easily compatible, compared to the AFM. The AFM requires more preparation to set up an experiment. Both methods show similar behaviour with each deposit. The micromanipulation and AFM show similarities in adhesion forces with the deposits; however, the range of adhesion is on two different length scales, making it very difficult to compare. It is clear that, as found by other workers, the surface energy affects the force required for removal.

AFM and micromanipulation are both beneficial tools for the measure of adhesion. AFM works at nm-scale whilst micromanipulation measures at μm-mm scale. The aim of this work was to see to what extent the two methods give the same results. The removal technique for the deposits in AFM and micromanipulation is different. AFM measures the vertical force of removal of the particle from a surface, whilst the micromanipulation pulls horizontally to get the adhesion force. A range of results we obtained exhibited that in some cases AFM and

micromanipulation data agree well, for example PTFE shows lowest forces with all deposits with both techniques. However, some effects are seen with AFM and micromanipulation behaviour differs. For example the sizes of the forces are greater with micromanipulation.

7.1.3 Atomic Force Microscopy (AFM) experiments of caramel, whey protein, and SCM deposits at different temperatures.

The effects of temperature on fouling and cleaning of materials, which are known to be thermally labile are studied. Cleaning rates, are known to be temperature-dependent. To identify whether the data would be of value in fouling, AFM force measurements experiments have been conducted over a range of temperatures, approach, retraction rates, contact positions, surfaces and contact times. The following conclusions can be made:

- Temperature changes the food deposits structure as well as increasing the rates of reactions, which create deposits, such as protein denaturation and aggregation. By comparison to the forces found at room temperature, the increase in temperature causes adhesion forces to decrease at different contact points.
- The time the tip sits on the food deposits does not affect adhesion behaviour. The adhesion is similar or consistent at all times, but varies with temperature. This is similar to micromanipulation.
- The rate of retraction on the deposits causes some variability in the adhesion behaviour. The effect on adhesion with approach and retraction rates is not predictable.

The two surfaces used PTFE and stainless steel, show that adhesion occurs with both but is lesser with PTFE than stainless steel. The results show similar effects – micromanipulation and AFM data appears to be comparable, suggesting that it is possible to use AFM to study cleanability.

The experiments show that the forces of adhesion are much less at high temperature than at low temperatures. This is especially interesting as fouling deposits form at high temperatures; such as the 60-100ºC at which caramel is processed, and the 70-90ºC for milk pasteurisation, which causes deposition of Type A protein-rich deposit. Deposits must form at these high process temperatures, but the adhesive forces are very small – much smaller than would be predicted by doing experiments with AFM and micromanipulation at room temperature. It is interesting that the trends of the measurements at room temperature are the same as those at high temperatures. Any effective models for fouling must account for adhesion of deposits onto surfaces with the low adhesion forces seen here, such as for whey protein and stainless steel. The effect of these forces must be greater than the effect of surfaces shear in creating a deposit. The results suggest that equipment or flow regime to resist fouling at temperatures will be overdesigned if data for adhesion at room temperature is considered. This is a potentially important result: data at room temperature for cleaning is much easier to obtain than at high temperature.

The results suggest that only by doing experiments on measuring adhesion at real process temperatures will an accurate measurement be obtained. This is especially important if we are to use computational models for fouling and cleaning, in which the shear stress on the surfaces of plant or deposit can be predicted. The forces measured at room temperature are

a significant overestimate of those, which are found at high temperature. Of course it is well known that cleaning becomes easier at high temperatures but these results allow quantification of it.

It was expected that the adhesion force between particle and surface would increase with time as – for example, whey protein denaturation and aggregation proceeds and bonds form. The data suggests that these reactions have little effect on the adhesion forces, at least as measured by AFM; more work needs to be done to determine what effects, if any, reaction processes have on adhesion at these temperatures.

7.1.4 Future work

The adhesion behaviour of variety of deposits has been investigated on different surfaces. Different ranges of temperatures, rates of removal, positions and at different contact times were tested to investigate AFM in process engineering. Results have provided useful information on the mechanisms involved in cleaning. Further work could be carried out to determine adhesion behaviour over a greater range of surfaces and cleaning conditions and deposit types to increase knowledge of AFM in the processing industry.

It would be useful to develop a technique that could quantify the removal of deposits visually. The image analysis program used could not record all movement of tip to deposit effectively on the AFM. This could help to make better analysis on removal modes, and also to make quantification of the amount remaining on the surface.

Further work can be pursued on chemically treated surfaces and worn surfaces, to see differences in force measurements. However, the limiting factor in applying AFM to food research is the lack of appropriate methodology for different food deposits. Increasing understanding on AFM technology and developing corresponding methodology for complicated food deposit systems, could lead to a more detailed understanding of cleaning at macromolecular and nanometre levels.

The capability of the AFM to provide better understanding of materials structure, surface characteristics and the interactive forces at the meso- and nanoscale level. The AFM will enhance the understanding of large-scale engineering processes, especially as materials are increasingly being designed down to the submicrometre level.

REFERENCES

Adams, E. Kroon, A. Williamson, G. Morris, J. (2003) Characterisation of heterogeneous arabinoxylans by direct imaging of individual molecules by atomic force microscopy. *Carbohydrate Research*, 338, 771–80.

Allen, S. Davies, M. Roberts, C. Tendler, S. Williams, P. (1997) Atomic force microscopy in analytical biotechnology. *Tibtech* 15, 101-105.

Amoudi, A. Robert, W. Lovitt, R. (2007) A Review article Fouling strategies and the cleaning system of NF membranes and factors affecting cleaning efficiency. *Journal of Membrane Science* 303, 4–28.

Asthana, R. Sobczak, N. (2000) Wettability, Spreading, and Interfacial Phenomena in High-Temperature Coatings. *JOM-e*, 52 (1).

Aziz, N. Fryer, P. Zhao, Q. (2006) Effect of electroless Ni-P based composite coating with different surfaces free energies on cleaning of tomato fouling deposit. Fouling, cleaning& Disinfection in Food conference, Cambridge.

Baier, R.E. (1970) Surface properties influencing biological adhesion. In R.S.Manly (Ed) *Adhesion in Biological Systems*. Academic Press, New York, USA. 5, 15-67.

Barnes, L. Lo, F. Adam, R. Chamberlian, L. (1999) Effect of milk protein on adhesion of bacteria on stainless steel surfaces. *Appl EnV Microboil* 67, 2319-2325.

Belmar-Beiny, M. T. Fryer, P. J. (1992). Bulk and surface effects on the initial stages of whey fouling. *Trans IChemE* 70(C) 193-199.

Berdyyeva, C.D. Woodworth, I. Sokolov. (2005) Silica Nanoparticles to Polish Tooth Surfaces for Caries Prevention, *Phys. Med. Biol*. 50, 81.

Beuf, M. Rizzo, G. Leuliet, J. Müller-Steinhagen, H. Yiantsios, S. Karabelas, A. Benezech, T. (2003) Potency of stainless steel modifications in reducing fouling and increasing cleaning of plate heat exchangers processing dairy products. In*: Heat Exchanger Fouling and Cleaning Fundermentals and Applications*, Santa Fe, New Mexico, USA.

Binnig, G. Quate, F. Gerber, C. *Phys. Rev. Lett.*, (1986) 56, 930 – 933.

Blel, W. Legentilhomme, P. Bénézech, T. Legrand, J. Le Gentil-Lelièvre, C. (2008) Application of turbulent pulsating flows to the bacterial removal during a cleaning in place procedure. Part 1: Experimental analysis of wall shear stress in a cylindrical pipe. *Journal of Food Engineering.*

Bott, T.R. (1995) Fouling of heat exchangers, *Elsevier*, New York.

Boulangé-Petermann, L. (1996) Processes of bioadhesion on stainless steel surfaces and cleanability: a review with special reference to the food industry. *Biofouling* 10, 275-300.

Boulange-Petermann, L. Rault, J. Bellon-Fontaine, N. (1997) Adhesion of Streptococcus thermophilus to stainless steel with different surface topography and roughness. *Biofouling* 11, 201-216.

Bowen, R. Lovitt, J. Wright (2000) The influence of ionic strength, nutrients and pH on bacterial adhesion to metals. *J. Colloid Interface Sci.* 228, 428–433.

Boyd, R.D. Cole, D. Rowe, D.L. Verran, J, Coultas, S.J. Paul, A.J. West, R.H. Goddard, D.T. (2000) Surface characterisation of glass and poly(methylmethacrylate) soiled with a mixture of fat, oil and starch. *Journal of Adhesion Science and Technology*. 5, 13-23.

Britten, M. Green, M. Boulet, M. Paquin, P. (1988) Deposit formation on heated surfaces: effect of interface energetic. *Journal of Dairy Research* 55, 551-562.

Burfoot, D. Middleton, K. (2008) Effects of operating conditions of high pressure washing on the removal of biofilms from stainless steel surfaces. *Journal of Food Engineering*. 5, 23-44.

Burgess, J. (1999) Ions in Solution: Basic Principles of Chemical Interactions. 2nd Edition, *Horwood Publishing* (Chichester), 16, 45-89.

Callow, J. Ista, L. Lopez, P. (2007) The Influence of Surface Wettability on the Adhesion Strength of Settled Spores of the Green Alga Enteromorpha and the Diatom Amphora. *Integr. Comput. Biol.* (2002), 42, 1116.

Carambassis, A. Rutland, M.W. (1999) The Charging Properties of Monodisperse Colloidal Silica in Symmetrical Quaternary Ammonium Ion Solutions. *Langmuir*, 15, 5584-5590.

Changani, D. BelmarBeiny, T. and Fryer, J. (1997) Engineering and chemical factors associated with fouling and cleaning in milk processing. *Experimental Thermal and Fluid Science* 14, 392-406.

Chen, Y.L. Helm, C.A. Israelachvili, J.N. (2008) Measurements of the Elastic Properties of Surfactant and Lipid Monolayers. *J. Phys. Chem.* 95, 10736-10747.

Christian, G.K. (2003) PhD: Cleaning of carbohydrate and dairy protein deposits. University of Birmingham, Birmingham, UK.

Clear, S.C. Nealey, P.F. (1999) Chemical force microscopy study of adhesion and friction. *J. Colloid. Interf. Sci*., 213, 238-250.

Cleveland, J.P. Manne, S. Bocek, D. Hansma, P.K. (1996) Choosing AFM Probes for Biological Applications Rev. *Sci. Instrum*. 64, 403-405.

Corrieu, G. (1981) State of the art of cleaning surfaces. Fundamentals and Application of Surface Phenomena Associated with Fouling and Cleaning in Food Processing. Division of Food Engineering, Lund University, Lund, Sweden.

Digital Instruments Veeco Metrology Group, MultiMode™ SPM Instruction Manual Version.

Ducker, W.A. Senden, T.J. Pashley, R.M. (1991) Role of hydration and water structure in biological and colloidal interactions, *Nature*, 353, 239 - 241.

Ducker, W. Tim, J. Senden. (1992) Measurement of forces in liquids using a force microscope, *Langmuir* 8, 1831-1836.

Epstein, N. (1983) Fouling in heat exchangers. *In J.Taborek*, G.F.Hewitt, and N.Afgan (Eds) Heat Exhangers: Theory and Practice. Hemisphere Publishing Corp., Washington, USA.

Fermandez-Torres, M.J. Fitzgerald, A. M. Paterson, W.R. Wilson, D. I. (2001) A Theoretical study of freezing fouling: limiting behaviour based on a heat and mass transfer analysis, *Chemical Engineering and Processing*, 40, 335-344.

Finlay, A. Callow, Ista' K. Lopez**.** (2002) The Influence of Surface Wettability on the Adhesion Strength of Settled Spores of the Green Alga Enteromorpha and the Diatom Amphora School of Biosciences, University of Birmingham. *Integrative and Comparative Biology by* The Society for Integrative and Comparative Biology, 42.

Friis, A. Jensen, B. (2002) Prediction of Hygiene in Food Processing Equipment Using Flow Modelling, *Food and Bioproducts Processing*, 80, 4, 2002, 281-285.

Fryer, P. Asteriadou. K. (2009) A prototype cleaning map: a classification of industrial cleaning processes. *Trends in Food Science & Technology* 20, 6-7, 255-262.

Foster, C. L. Green, M. L. (1990) A model heat-exchange apparatus for the investigation of fouling of stainless steel surfaces by milk II. Deposition of fouling material at 140ºC, its adhesion and depth profouling. *Journal of Dairy Research* 57 339-348.

Gibson, C.T. Smith, D.A. Roberts, C.J. (2005) Calibration of the spring constants of various AFM cantilevers with the small uncertainty level of 2%. *Nanotechnology* 16, 234-238.

Gibson, C.T. Watson, G.S. Myhra, S. (1996) Resonance Response of Scanning Force Microscopy Cantilevers. *Nanotechnology*, 7, 259-262.

Gillham C.R. (1997) Enhanced cleaning of surfaces fouled by whey proteins. University of Cambridge, *Cambridge*, UK. 46, 3, 199-209.

Grandhee. Monnier. V.M. (1991) Mechanism of formation of the Maillard protein cross-link pentosidine. Glucose, fructose, and ascorbate as pentosidine precursors. *J. Biol*. Chem 266 (18): 11649–11653.

Grasshoff, A. (1997) Cleaning of heat treatment equipment. For: IDF monograph, *Fouling and cleaning in Heat Exchangers*. 90, 4, 433-440.

Gotham, S.M. (1990) Mechanisms of protein fouling in heat exchanger. PhD Thesis, University of Cambridge, Cambridge, UK.

Gotham, S.M. Fryer P.J. Pritchard A.M. (1989) Model studies of food fouling. In H.G.Kessler and D.B.Lund (Eds). *Fouling and Cleaning in Food Processing*, Munich University, FRG.

Hankinso, D.J. Carver, C.E. (1968) Fluid dynamic relationships involved in circulation cleaning. *Journal of Dairy Science* 51, 1761-1768.

Hasting (Eds) Fouling, Cleaning and Disinfection in Food Processing. Deparment of Chemical Engineering, University of Cambridge, Cambridge, UK.

Haynes,C.A. Norde,W. (1994) Globular proteins at solid/liquid interfaces. *Colloids and surfaces.B.Biointerfaces* 2, 517-566.

Helalizadeh, A. Müller-Steinhagen, H. Jamialahmadi, A. (2000) Mixed salt crystallisation fouling. Chemical Engineering and Processing 39, 1, 29-43.

Herrmann, P.S.P. Yoshida, C.M.P. Antunes, A.J. Marcondes, J.A. (2004) Surface evaluation of whey protein films by atomic force microscopy and water vapour permeability analysis. *Packaging Technology and Science* 17, 267–273

Hilal, N. Bowen, R. (2009) Atomic force microscopy in process engineering. ISBN-13: 978-1-85617-517-3.

Hodge, R. Rousseau, D. (2003) Flocculation and coalescence in water-in-oil emulsions stabilized by paraffin wax crystals *Food Research International*, 36, 7, 695-702.

Holt, C. Geoffrey, B. Jameson, G. Gillian, E. Norris. (2002) *International Dairy Journal*, 12 4, 2002, 299-310.

Hu, K. Bard, A.J. (1997) Electrochemical Properties of Mixed Self-Assembled Monolayers on Gold Electrodes Containing Mercaptooctylhydroquinone and Alkylthiols. *Langmuir*, 13, 5114-51192

Kane, D. R. Middlemiss, N. E. (1985). Cleaning chemicals- state of the knowledge in 1985. in *Fouling and Cleaning in Food Processing*, eds Lund, D. B. Plett E. and Sandu C., Wisconsin, USA. 312-355.

Iler, R.K. **(**1979) The Chemistry of Silica: Solubility, Polymerisation, *Colloid and Surface Properties, and Biochemistry*, John Wiley and Sons (New York; Chichester). 8,13-67.

Israelachvili, J, (1987) Solvation Forces and Liquid Structure, As Probed by Direct Force *Measurements Acc. Chem. Res*., 20, 415-421.

Jennings, W. G. McKillop, A. A. Luick, J. R. (1957). Circulation cleaning. *J of Dairy Science* 40 1471-1479.

Jullien, C. Benezech, T. Le Gentil, C. Boulange-Petermann, L. Dubois, PE. Tissier, J.P. Traisnel, M. Faille, C. (2008) Physico-chemical and hygienic property modifications of stainless steel surfaces induced by conditioning with food and detergent, *Biofouling*, 24, 163 – 172.

Kanda, Y. Murata, T. Higashitani, K. (1999) Physicochemical and Engineering Aspects, *Colloid Surface A*, 154, 157-166.

Karlsson, A-C. (1999). Fouling and Cleaning of Solid Surface: The influence of surface characteristics and operating conditions. Lund University, Sweden, 5, 28-33.

Kerber, J. S. PhD. (2000) *President of Material Interface*, Inc.

Kerner, R. Phillips, J. C. (2000) Quantitative principles of silicate glass chemistry**,** *Solid State Communications.* 117, 1, 47-51.

Koops, J. Kerkhof, M.F. (1965) Adsorption of euglobulin on agglutinating milk fat globules Biochimica et Biophysica Acta (BBA) - *Biophysics including Photosynthesis, 94, 2, 29,576-578*

Lee, J. Cartwright, R.. Grueser, T. Pascall, M.A. (2007) Efficiency of manual dishwashing conditions on bacterial survival on eating utensils. *Journal of Food Engineering* 80, 885–891.

Lent LE, Vanasupa LS, Tong PS. (1998). Whey protein edible film structures determined by atomic force microscope. *J Food Sci* 63(5):824–7.

Liang, H. (2004). Surface science.*VCH Publishers*, Inc., New York, USA. 565, 173-179

Liu, W, Aziz, N.A. Zhang, Z. Fryer, P.J. (2007) Quantification of the cleaning of egg albumin deposits using micromanipulation and direct observation techniques. *Journal of Food Engineering* 78, 217-224.

Liu, W. Christian, G.K. Zhang, Z. Fryer, P.J. (2002) Development and use of a micromanipulation technique for measuring the force required to disrupt and remove fouling deposits. *Food and Bioproducts Processing* 80, 286-291.

Liu, W. Fryer, P.J. Aziz, Ab. Bridson, N. Zhang, Z. Zhao, Q. Liu, Y. (2005) Cohesion and Adhesion in the Cleaning of Food Fouling Deposits, to be presented at *World Congress of Chemical Engineering*. 61, 6, 2079-2084

Liu, W. Christian, G.K., Zhang, Z., Fryer, P.J. (2006) Direct measurement of the force required to disrupt and remove fouling deposits of whey protein concentrate. *International Dairy Journal* 16, 164-172.

Lower, C.J. Tadanier ,M.F. Hochella, Geomicrobiol. J (2001), Measuring interfacial and adhesion forces between bacteria and mineral surfaces with biological force microscopy. *Int. J. Sys. Bacteriol* 18 63– 76.

Mantel, M. Rabinovich, Y.I. Wightman, J.P. Yoon, R.-H**. (**1995) A Study of Hydrophobic Interactions between Stainless Steel and Silanated Glass Surface Using Atomic Force Microscopy. *Journal of Colloid and Interface Science*, *170*, 203-214.

Martin, H.K. Wickramasinghe, (1987), Optical absorption microscopy and spectroscopy with nanometre resolution. *Appl. Phys. Lett.* 50, 1455.

Morris, V.J., 2004. Probing molecular interactions in foods. *Trends in Food Science and Technology* 15, 291–297.

Morris, V.J. Kirby, R. Gunning, A.P. (1999). Atomic force microscopy for biologists, *London: Imperial College Press*. 21, 4, 617-629.

Morris, V.J. Mackie, A.R. Wilde, P.J. Kirby, A.R. Mills, E.C.N. Gunning, A.P. (2001). Atomic force microscopy as a tool for interpreting the rheology of food biopolymers at the molecular level. *Lebensmittel-Wissenschaft and Technologie* 34, 3–10.

Müller-Steinhagen, H. (2000) Heat Exchanger Fouling, Mitigation and Cleaning Technologies. IChem, ISBN 0 85295 436 0.

Müller-Steinhagen H. Malayeri M.R. Watkinson P. (2005) Heat Exchanger Fouling and Cleaning - Challenges and Opportunities. In H.Müller-Steinhagen, M.R.Malayeri, and Watkinson (Eds) Heat Exchanger Fouling and Cleaning - *Challenges and Opportunities. Engineering Conferences International.*

Myres, D. (1991). Surfaces, interfaces and colloids: principles and applications. *VCH Publishers, Inc*., New York, USA. 5,12-14.

Nakao, H. Hayashi, H. Karasawa H. Hirano K. Sugiyama S. Ohtani T. (2005) Fabricating and aligning π-conjugated polymer-functionalized DNA nanowires: atomic force microscopic and scanning near-field optical microscopic studies. *Langmuir* 21, 7945–50.

Nermen, M.G. Nakhla, W. Wan. (2009) Comparative assessment of hydrophobic and hydrophilic membrane fouling in wastewater applications. *Journal of Membrane Science*, 339, 1-2, 1, 93-99.

Norde,W. (1986) Adsorption of proteins from solution at the solid-liquid interface. *Advances in Colloid and Interface Science* 25, 267-340.

Parbhu A. Danne, M. Hendy, S. (2006) Reducing milk protein adhesion rate: a transient surface treatment of stainless steel, *Fouling, cleaning and Disinfection in food processing conference, Cambridge,* 8-15.

Parbhu, A. Lee, A. N. Thomsen, S. J. Siew, D. C. W. (2002) Atomic force microscopy applied to monitoring initial stages of milk fouling on stainless steel, *Fouling, cleaning and Disinfection in food processing.* 333-239.

Park, D. Koch, R. Cardenas, J. Kas, C.K. Dynamics of cell membranes and the underlying cytoskeletons observed by noninterferometric widefield optical profilometry and fluorescence microscopy *Biophys J.* (2005) 89.

Raghavan, D. Gu, X. Nguyen, T. Vanlandingham, M. (2001). Characterization of chemical heterogeneity in polymer systems using hydrolysis and tapping-mode atomic force microscopy. *Journal of Polymer Science* 39, 1460–1470.

Rankin, B.H, Adamson, W.L. (1973) Scale formation as related to evaporator surface conditions. *Desalination* 13, 63-87.

Rosaninho, R. Rizzo, G. Müller-Steinhagen, H. and Melo, L. F. (2003) The influence of bulk properties and surface characteristics on the deposition process of calcium phosphate on stainless steel. In: *Heat Exchanger Fouling and Cleaning Fundamentals and Applications*, Santa Fe, New Mexico, USA.

Rosmaninho, R. Rizzo, G. Müller-Steinhagen, H. Melo, F. (2005) "Anti fouling stainless steel based surface for milk heating processes in "*Heat Exchanger Fouling and Cleaning*, German Aerospace Centre, Stuttgart, Germany, the University of British Columbia, Canada Eds, ECI Symposium Series, Volume RP2.

Round, N. Rigby, M, MacDougall, J. Ring, G. Morris, J. (2001) Investigating the Nature of branchingin pectin by atomic force microscopy and carbohydrate analysis. *Carbohydrate Reserach* 331, 337–42.

Sader, J.E. Pacifico, J. Green, C.P. Mulvaney, P. (2005) AFM Cantilevers - Calibration.

J. Appl. Phys, 97, 124903.

Sakiyama T., Nagata A., Nagai T., Saeki Y., & Nakanishi K. (1996) Adsorption of β-lactoglobulin onto stainless steel particles and its desorption behaviour in alkaline and

proteolytic enzyme solutions. In P.J.Fryer, A.P.M.Hasting, and J.M.Jeurnink (Eds). *Fouling and Cleaning in Food Processing* 93-100. European Commission, Brussels.

Saygil, G. Ahmali. (2003) Effect of ceramic surface treatment on the shear bond strengths of two resin luting agents to all-ceramic materials, *Journal of Oral Rehabilitation* 30, 758–764.

Schmutz, P. Frankel, G.S. (1998) Corrosion study of AA2024–T3 by scanning Kelvin probe force microscopy and in situ atomic force microscopy scratching. *Journal of the Electrochemical Society* 145, 2295–2306.

Schmidt, D.L. Brady Jr. R.F. Lam, K. Schmidt, D.C. Chaudhury, M.K (2004) Contact angle hysteresis, adhesion, and marine biofouling. *Langmuir* 20, 2830–2836.

Schmutz, P. Frankel, G.S. (1999) Influence of dichromate ions on corrosion of pure aluminium and AA2024–T3 in NaCl solution studied by AFM scratching. *Journal of the Electrochemical Society* 146, 4461–4472.

Schmidt, R.H. (1998) Basic Elements of Equipment Cleaning and Sanitizing in Food Processing and Handling Operations. *Institute of Food and Agricultural Sciences Extension, University of Florida*. 5, 33-79.

Senden, T.J. (2001) Force microscopy and surface interactions *Curr. Opin. Colloid In*., 6, 95-101.

Sharma, A., Garg, D., and Gupta JP. (1982) Solidification fouling of paraffin wax from hydrocarbons, *Letters in heat and mass transfer*, 9, (3): 209-219.

Shaw, Introduction to Colloid and Surface Chemistry. ISBN-13: 978-0750611824

Sheng, X. Yen, P. (2007) Force measurements of bacterial adhesion on metals using a cell probe atomic force microscope, *Journal of Colloid and Interface Science*, 310(2), 661-669.

Simmons, M.J.H. Jayaraman, P. Fryer, P.J (2007) The effect of temperature and shear rate upon the aggregation of whey protein and its implications for milk fouling, *Journal of Food Engineering*, 79, 517-528.

Sokolov, S. Iyer, D. Woodworth, (2006) Nanomed. *Nanotechnol. Biol. Med*. 2, 31.

Somercales, E. F. C. (1988) Fouling of heat transfer surfaces: an historical review. *25th Nat. Heat. Trans. Conf*. ASME. Houston.

Tamime. A (2008) Cleaning-In- Place: dairy, food and beverages, 3rd (Ed) ISBN: 978-1-4051-5503-8

Tadmor, R. (2004). Line energy and the relation between advancing, receding and Young contact angles. *Langmuir,* 20, 7659-7664. ISBN 0743-7463.

Thalhammer, W. Heckl, M. Zink, A. Nerlich, A. G. (2000) Atomic Force Microscopy for High Resolution Imaging of Collagen Fibrils—*A New Technique to Investigate Collagen Structure in Historic Bone Tissues*. 41, 12-46.

Timperley, D. A., Smeulders, C. N. M. (1987). Cleaning of dairy HTST plate heat exchangers: comparison of single- and two-stage procedures. *Journal of the society of Dairy Technology* 40, 1, 4-7.

Torii, A. Sasaki, M. Hane, K. Okuma, S. (1996) Surface Mechanical Property Determination of Soft Materials Through an AFM Nanoindentation Experiment, *Meas. Sci. Technol*., 7, 179-184.

Verran J, (2002) Biofouling in food processing: biofilm or biotransfer potential? *TransIChemE*, 80, 292 – 298.

Verran, J. (2006) The effect of substratum surface topography on the retention of micro-organisms and organic material on defined surfaces. Fouling, Cleaning and Disinfection in Food Processing. Deparment of Chemical Engineering, University of Cambridge, Cambridge, UK.

Watkinson, P. Müller-Steinhagen, H. Malayeri, M.R. (2003) Heat exchanger fouling and cleaning: Fundamentals and applications. *Engineering Conferences International*, USA.

Weiss, A. Bird, M .R. Chukwuemeka, J. K. and Price, Wilson et al, (2002) Effect of surface coating on platelet count drop during cardiopulmonary bypass R. *TransIChemE* 151-164.

Wilson, D.I. Chew, J.Y.M. Fryer, P.J. Hasting A.P.M. (2006) Fouling, Cleaning & Disinfection in Food Processing. Fouling, Cleaning & Disinfection in Food Processing. *Department of Chemical Engineering, University of Cambridge, Cambridge, UK*.

Whitehead, K. Verran, J. (2006) The effect of substratum surface topography on the retention of micro-organisms and organic material on defined surfaces. *TransIChemE* 5,12-19.

Woo, M.W. Daud, W.R.W. Tasirin, S.M. Talib, M.Z.M. (2009) Controlling food powder deposition in spray dryers: Wall surface energy manipulation as an alternative *Journal of Food Engineering*, 94, 2,192-198.

Wu, Z. Hongbing, Chen, Yaming, D, Huiling, M, Jielin, S, Shenfu, C, Vincent, S.J. Craig, J.H. (2008) Cleaning using nanobubbles: Defouling by *Journal of Colloid and Interface Science*, 328, 1.

Victo, J. Alan, R. Wilde, Kirby, E. Clare, N. Mills, A. (2000) Atomic Force Microscopy as a Tool for Interpreting the Rheology of Food Biopolymers at the Molecular Level Gunning Institute of Food Research, *Norwich Research Park*, Colney, Norwich. 29, 44-67.

Yada R.Y. Jackman R.L. Smith J.L. Payie K.G. Tanaka T. (2000) Proteins: Denaturation and food processing. In F.J.Francis (Ed) Encyclopedia of food science and technology. *John Wiley & Sons*, Inc., New York, USA. 4, 45-67.

Yongan, Gu D. L. (1998), A Model for a Liquid Drop Spreading on a Solid Surface Colloids and Surfaces A: *Physicochemical and Eng Aspects* 142, 243-256.

Yoon, J. Lund, D.B. (1994) Magnetic treatment of milk and surface treatment of plate heat exchangers: effects on milk fouling. *Journal of food science* 59, 964-969.

Yun-ren, Q.I.U. Hong, Zhong, Qi-xiu, Zhang, (2009) Treatment of stable oil/water emulsion by novel felt-metal supported PVA composite hydrophilic membrane using cross flow ultrafiltration. *Transactions of Nonferrous Metals Society of China*, 19(3), 773-777.

Zettler, H.U. Weiss, M. Zhao, Q. and Müller-Steinhagen, H. (1999). Modification of heat exchanger plates for reduced fouling deposition. Transactions of the *IMechE*, 6th UK National Heat Transfer Conference, 125-132.

Zhao, Q. Liu, Y. Müller-Steinhagen, H. (2002). Graded Ni-P-PTFE coatings and their potential applications. *Surfaces and Coatings Technology* 155, 279-284.